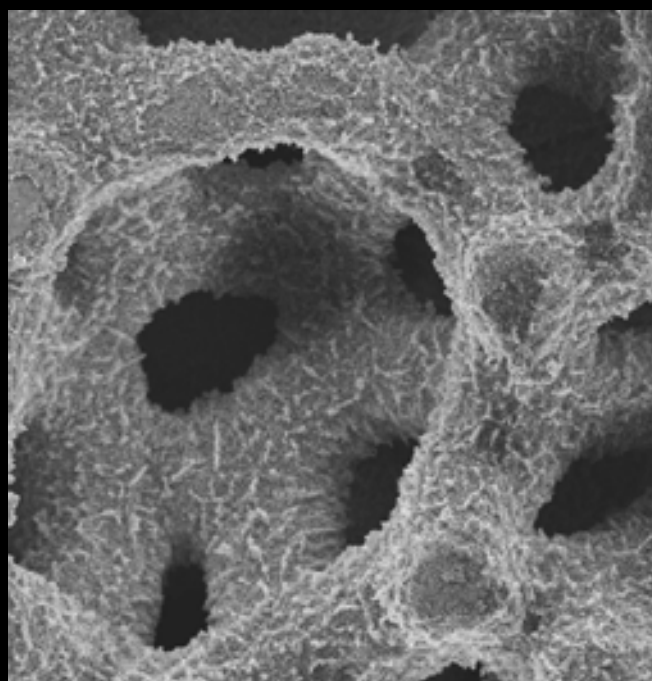
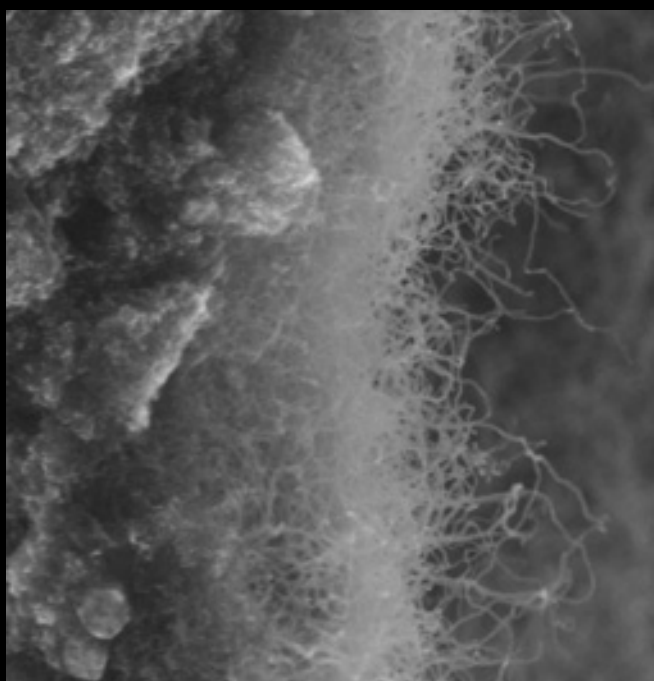


Microstructured Catalyst Support Based on Carbon Nano-Fibers (CNFs)



Nabeel Jarah

MICROSTRUCTURED CATALYST SUPPORT BASED ON CARBON NANOFIBERS

DISSERTATION

to obtain
the doctor's degree at the University of Twente,
on the authority of the rector magnificus,
prof. dr. F. A. van Vught,
on account of the decision of the graduation committee,
to be publicly defended
on Thursday October 28th, 2004 at 15.00 hrs

by

Nabeel AbdulKareem Amin Jarrah

Born on March 12th, 1972

in Irbid, Jordan

This dissertation is approved by the promoter

Prof.dr.ir. Leon Lefferts

and the assistant promoter

Dr.ir. Jan G. van Ommen

To my family

Dissertation committee:

Prof.dr.ir. G. J. Vancso, chairman	University of Twente
Prof.dr.ir. L. Lefferts, promoter	University of Twente
Dr. J. G. van Ommen, assistant-promoter	University of Twente
Prof.dr.ing. D. H. A. Blank	University of Twente
Prof.dr.ing. M. Wessling	University of Twente
Prof.dr.ir. Th. H. van der Meer	University of Twente
Prof.dr.ir J. C. Schouten	Technical University of Eindhoven
Prof.dr. F. Kapteijn	Technical University of Delft
Prof.dr.ir K. P. de Jong	University of Utrecht
Prof. M. J. Ledoux	University of Strasbourg

Publisher:

FEBO b.v.

Postbus 40100, 7504 RC Enschede, The Netherlands

© N. A. K. a. Jarrah, Enschede, 2004

No part of this book may be reproduced in any form of print, photo print, microfilm or any other means without written permission from the author / publisher.

ISBN: 90-365-2109-2

Contents

Summary	1
Samenvatting	5
Summary in Arabic	9
CHAPTER 1	13
GENERAL INTRODUCTION	13
1. Introduction	14
2. Comparison between different types of reactors	16
2.1. Conventional technology	16
2.1.1. Slurry phase reactor	16
2.1.2. Fixed /Trickle bed reactor	16
2.2. Structured catalytic reactors	17
2.2.1. Monolith reactor	17
2.2.2. Foams	18
3. Demands for superior structured catalyst in liquid phase operation	18
4. CNFs as catalyst support	19
4.1. Carbon nano fibers (CNFs)	20
4.2. Immobilization of CNFs on structured supports	22
5. Outline of this thesis	22
References	23
CHAPTER 2	27
DEVELOPMENT OF MONOLITH WITH A CARBON NANOFIBER WASHCOAT AS A STRUCTURED CATALYST SUPPORT	27
Abstract	27
1. Introduction	28
2. Experimental	29

2.1.	Materials	29
2.2.	Catalyst preparation	29
2.3.	Experimental set-up for carbon fiber formation	30
2.4.	Characterization	30
3.	Results and Discussion	30
3.1.	Characterization of the ceramic supports	30
3.2.	Characterization of NiO on monolith	31
3.3.	Carbon fiber formation on the monolith supports	32
3.4.	Characterization of carbon fiber washcoat	32
4.	Conclusions	34
	Acknowledgments	35
	References	35
CHAPTER 3		37
SYNTHESIZING A CARBON NANO-FIBER LAYER ON A MONOLITH SUPPORT; EFFECT OF NICKEL LOADING AND FORMATION CONDITIONS		37
Abstract		37
1. Introduction		38
2. Experimental		39
2.1.	Materials	39
2.2.	Characterization	39
2.3.	Catalyst preparation	40
2.4.	Experimental set-up for CNFs formation	40
3. Results		41
3.1.	Characterization of Ni on monolith	41
3.2.	CNFs formation on the monolith supports	43
3.3.	Structure of the CNFs	45
3.4.	Structure of the monolith	48
4. Discussion		50
4.1.	Parent Ni catalyst	50
4.2.	Formation and structure of CNFs	51
4.3.	Structure of the CNFs-monolith composite	52

5. Conclusions	55
Acknowledgment	55
References	56
CHAPTER 4	57
IMMOBILIZATION OF A LAYER OF CARBON NANOFIBERS (CNFS) ON NI FOAM; A NEW STRUCTURED CATALYST SUPPORT	57
Abstract	57
1. Introduction	58
2. Experimental	59
2.1. Materials	59
2.2. Carbon nanofibers formation	60
2.3. Characterization	61
3. Results	62
3.1. Surface structure of original foam	62
3.2. Carbon nanofibers formation on Ni foam	63
3.3. Structure of the CNFs	63
3.4. Mechanical Stability	66
4. Discussion	68
4.1. Structure of CNFs and the final composite	68
4.2. Stability of the final composite	71
5. Conclusions	74
Acknowledgments	74
References	75

CHAPTER 5	77
EFFECT OF THE SURFACE STATE OF NI FOAM ON CNFS FORMATION	77
Abstract	77
1. Introduction	78
2. Experimental	79
2.1. Materials	79
2.2. Formation of carbon nanofibers	79
2.3. Characterization	80
3. Results	81
3.1. Effect of pre-treatment on the surface morphology of the Ni foam	81
3.1.1. Effect of reduction pre-treatment:	81
3.1.2. Effect of oxidation pre-treatment:	82
3.1.3. Effect of oxidation followed by reduction pre-treatment:	84
3.2. Effect of the pre-treatment on the rate of CNFs formation	85
3.3. Effect of the pre-treatment on the structure of the synthesized CNFs	85
3.4. Effect of the time of formation on CNFs	86
4. Discussion	91
4.1. Effect of the pre-treatment on the morphology of the Ni foam surface	91
4.2. Effect of time of CNFs formation on the structure of the Ni-CNFs composites	92
4.3. Effect of surface morphology of the Ni foam on the texture of CNFs	93
4.4. Effect of surface morphology of the Ni foam on the yield of CNFs	94
5. Conclusions	96
References	96

CHAPTER 6	99
FORMATION OF CARBON NANOFIBERS (CNFS) ON NI –NANO PARTICLES ON SI WAFER	99
Abstract	99
1. Introduction	100
2. Experimental	100
2.1. Materials	100
2.2. Carbon nanofibers formation	102
3. Results	103
3.1. Effect of reduction on the structure of the Ni particle	103
3.2. Effect of reduction temperature on the CNFs formation	105
3.3. Effect of the gas composition on the CNFs formation	105
3.4. Effect of the formation temperature on the CNFs formation	105
4. Discussion	106
4.1. Effect of the reduction temperature on the CNFs formation	106
4.2. Effect of the conditions on the CNFs formation	107
5. Conclusions	108
References	109
CHAPTER 7	111
CONCLUSIONS AND RECOMMENDATIONS	111
1.1. The formation of CNFs on macro-structured supports	111
1.2. Application of the composite materials as structured catalyst support	113
1.3. Catalyst preparations and future outlook	113
1.4. Recommendations on the preparation of these composite materials	115
References	116
Publications	119
Acknowledgement	121
Resume	123

Summary

The work described in this thesis has provided information about the preparation of micro-structured materials based on carbon nano-fibers (CNFs), which were immobilized on macro-structured supports. The CNFs were catalytically produced *via* the decomposition of hydrocarbons (i.e. CH₄ and C₂H₄) over nickel. Two macro-structured materials were used as examples i.e. **ceramic monolith** and **metal foam**. From the perspective of the use of monoliths as structured materials to support catalysts, this work aims on the preparation of improved washcoats based on CNFs, competing the well known relatively dense inorganic washcoats. Metal foams are much less explored as structured catalyst supports and in this case the preparation of stable and uniform washcoats is still a challenge.

Chapters 2 and 3 discuss the results of the immobilization of CNFs on **monolith** support. The detailed microscopic evaluation of the monolith revealed that at the outer surface of the washcoat a hairy layer is formed with a typical thickness of 1 μm containing CNFs exclusively. The structure of this layer is similar to the inverse structure of a traditional alumina washcoat, although much thinner. The hairy layer is supported on a composite layer containing both CNFs and fragments of the alumina washcoat. It turns out that the thickness of the CNFs layer at the outermost surface as well as the diameter of the fibers increases with mean Ni-particle size.

Formation of CNFs on the monolith using methane leads to immediate fragmentation and doubling of the thickness of the washcoat, independent on the amount of CNFs. Thus, a macro-porous composite layer of entangled alumina particles and CNFs is formed. The pore size in the washcoat was 5-20 nm, whereas the typical diameter of the CNFs was 10-30 nm. It is obvious that the formation of a CNF with a diameter larger than that of the pore would result in an immediate fragmentation of the washcoat. The total porosity decreases with the amount of CNF whereas the surface area per gram monolith increases.

Extensive formation of CNFs out of the washcoat results in detachment of the washcoat from the cordierite because a hairy layer of CNFs is formed on the interface between the washcoat and the cordierite, resembling the hairy layer on the outer surface of the washcoat. Furthermore, extended formation of CNFs inside the cordierite body causes disintegration of the monolith body when macro-pores are locally overfilled with CNFs.

Methane is preferred over ethene for the formation of CNFs because ethene forms CNFs rapidly even on relatively large Ni particles, resulting in thick fibers up to 70 nm in the macro-porous cordierite, destroying the monolith.

Chapters 4 and 5 discuss the result of the immobilization of CNFs on **Ni foam**. A rough and hairy layer of entangled CNFs was formed on the surface of the foam. The surface area of the Ni foam increased from less than 1 m²/g to about 30 m²/g. The pore volume of the synthesized CNFs layer is 1 cm³/g. Moreover, the voids between the CNFs are macropores and thus significantly larger than the typical mesopores in conventional inorganic catalyst supports.

The formation of CNFs on polycrystalline Ni started with formation of Ni₃C, which then decomposes into Ni and carbon. As a result, a rough surface with small Ni particles (10-100 nm) is formed when the polycrystalline Ni surface was exposed to ethene at 450°C for 0.5 hour. Some of the Ni particles started to synthesize CNFs with diameters between 10 and 70 nm. The size of the Ni particles is significantly smaller than the size of the grains in the Ni foam (1-10 μm). Thus, fragmentation of the Ni grains into small Ni particles occurs before CNFs start to form.

The formation rate of CNFs on oxidized Ni foam was one order of magnitude higher than the rate on reduced Ni foam. It is concluded that C₂H₄ was able to reduce NiO under the formation conditions forming Ni nuclei. It is suggested that these nuclei are directly converted to small Ni₃C particles, which grow and then decomposes when the size surpasses the window that allow the formation of CNFs. Obviously, the formation of small Ni₃C particles from Ni nano particles, produced by in-situ reduction of NiO will be faster than the Ni₃C formation from large (microns) Ni crystals.

The formation rate of CNFs on pre-shaped small Ni particles supported on monolith takes off with a high rate followed by deactivation exclusively. In contrast, formation rate of CNFs on polycrystalline Ni foam at constant temperature initially increased, reached a maximum value and then decreased. The initial increase in the formation rate of CNFs on polycrystalline Ni is caused by the necessity of fragmentation of Ni grains into small Ni particles.

The integrity of the samples and strong attachment of the CNFs to the Ni foam surface or to monolith are necessary for application of the final composite materials as structured catalyst supports. The monoliths can easily disintegrate when CNFs formation is

excessive, either in the cordierite or on the interface between the cordierite and the washcoat. Thus, having a high Ni concentration at the outer surface of the washcoat and no Ni in the cordierite as well as choosing a low activity of the carbon containing gas (i.e. CH₄) are essential to form CNFs without excessive formation of CNFs in the cordierite.

The integrity of the Ni foam was lost after synthesizing 138 wt% CNFs at 500°C in 3 hours. On the other hand, the foams were stable after synthesizing 50 wt% CNFs at 450°C in 6 hours. The Ni foam collapsed at high temperature because of the increase in the rate of corrosive metal dusting with temperature. As opposed to metal dusting, it seems that dissolution of small amounts of carbon from ethene dissociation in the Ni foam increases the mechanical strength of the foam. In both cases, the CNFs layer can withstand shear forces caused by flowing water (1 m/s) through the composite sample.

Chapter 6 further investigate the formation of CNFs on polycrystalline Ni. Well-ordered, perfectly coordinated polycrystalline Ni particles with different sizes supported on silicon wafer were used to form CNFs. This study allowed us to correlate the properties of individual CNFs formed with the local morphology of the Ni surface. However, the formation of nickel silicide resulted in decreasing the formation rate of CNFs compared to the formation rate on Ni foam. We suggested that lowering of the carbon activity *via* addition of H₂ resulted in homogenous distribution of carbon in the particle. This can explain why the particle fragmented completely into smaller particles.

Finally, in Chapter 7, the composite materials synthesized were qualitatively evaluated and a future research plan was recommended in order to optimise the composite materials as catalyst support in liquid phase.

Samenvatting

Het werk beschreven in dit proefschrift geeft informatie over de bereiding van microgestructureerd materiaal gebaseerd op koolstof nano-vezels (carbon nano-fibres CNF's), welke vast zitten op een macrogestructureerde drager. De CNF's worden katalytisch geproduceerd via de ontleding van koolwaterstoffen (b.v. CH_4 of C_2H_4) over nickel. Twee macro gestructureerde materialen (**een keramische monoliet en een metaal schuim**) werden als voorbeeld gebruikt. Vanuit het perspectief van het gebruik van monolieten als gestructureerde materialen voor katalysator dragers, richt dit werk zich op de bereiding van verbeterde washcoats gebaseerd op CNF's, om te concurreren met de goed bekende relatief dichte anorganische washcoats. Metaal schuimen zijn veel minder goed onderzocht als gestructureerde katalysator dragers en in dit geval is de bereiding van een stabiele en uniforme washcoat nog steeds een uitdaging.

Hoofdstuk 2 en 3 bediscussieert de resultaten van de immobilisering van CNF's op een monoliet drager. De gedetailleerde microscopische evaluatie van de monoliet gaf te zien dat op het buiten oppervlak van de washcoat een harige laag is gevormd met een typerende dikte van 1 μm , die alleen CNF's bevat. De structuur van deze laag is gelijk aan de inverse structuur van een traditionele alumina washcoat, alleen veel dunner. Deze harige laag zit op een composiet laag, die zowel CNF's als fragmenten van de alumina washcoat bevat. Het blijkt dat zowel de dikte van de CNF's in de buitenste laag als de diameter van de koolstof vezels toeneemt met de gemiddelde Ni-deeltjes grootte.

De vorming van CNF's op de monoliet met behulp van methaan, geeft onmiddellijke fragmentatie en verdubbeling van de dikte van de washcoat, onafhankelijk van de hoeveelheid CNF's. Zodoende wordt een composiet laag van verstrengelde alumina deeltjes en CNF's gevormd. De porie grootte in de washcoat was 5-20 nm, terwijl de typerende diameter van de CNF's 10-30 nm was. Het is vanzelfsprekend dat de vorming van een CNF met een diameter groter dan die van de porie, zal resulteren in de onmiddellijke fragmentatie van de washcoat. De totale porositeit neemt af met de hoeveelheid CNF's, terwijl het oppervlak per gram materiaal toeneemt.

Buitensporige vorming van CNF's uit de washcoat resulteert in het loslaten van de washcoat van het corderiet, omdat een harige laag CNF's wordt gevormd op het vlak

tussen de washcoat en het corderiet, die lijkt op de harige laag op het buiten oppervlak van de washcoat. Verder geeft voortgezette vorming van CNF's binnen in het corderiet lichaam, desintegratie van het monoliet lichaam, als de macroporiën lokaal overgevoerd raken met CNF's.

Methaan wordt geprefereerd boven etheen voor de vorming van CNF's, omdat etheen sneller CNF's vormt, zelfs op relatief grote Ni deeltjes, hetgeen resulteert in dikke koolstof vezels tot 70 nm, welke de monoliet vernielen.

Hoofdstuk 4 en 5 behandelen de resultaten van het immobiliseren van CNF's op **nikkel schuim**. Een ruwe en harige laag van verstrengelde CNF's wordt gevormd op het oppervlak van het schuim. Het oppervlak van het nikkel schuim neemt toe van minder dan $1 \text{ m}^2/\text{g}$ tot ongeveer $30 \text{ m}^2/\text{g}$. Het porievolume van de gesynthetiseerde CNF's laag is $1 \text{ cm}^3/\text{g}$. Bovendien is de lege ruimte tussen de CNF's macroporeus en dus aanzienlijk groter dan de typische mesoporiën in conventionele katalysator dragers.

De vorming van CNF's op polykristallijn Ni begint met de vorming van Ni_3C , dat ontleedt in Ni en C. Als resultaat wordt een ruw oppervlak met kleine nikkel deeltjes (10-100 nm) gevormd, wanneer het polykristallijne oppervlak wordt blootgesteld aan etheen bij $450 \text{ }^\circ\text{C}$ gedurende 0,5 uur. Sommige van de Ni deeltjes beginnen CNF's te maken met diameters tussen 10 en 70 nm. De grootte van deze Ni deeltjes is beduidend kleiner dan de grootte van de korrel in het nikkel schuim (1-10 μm). Bijgevolg, treedt er dus fragmentatie van de Ni korrels in kleinere Ni deeltjes voor de CNF's beginnen te groeien.

De vormingssnelheid van CNF's op geoxideerd Ni schuim was een orde van grootte hoger dan de snelheid op gereduceerd Ni schuim. Er wordt geconcludeerd dat C_2H_4 in staat is om NiO te reduceren onder de vormingscondities voor het ontstaan van Ni kernen. Er wordt gesuggereerd dat deze kernen direct worden omgezet in kleine Ni_3C deeltjes, die groeien en dan ontleden, wanneer hun grootte de grens passeert, die de vorming van CNF's toestaat. Ogenschoonlijk is de vorming van kleine Ni deeltjes uit Ni nano deeltjes, geproduceerd door de in-situ reductie van NiO, sneller dan de Ni_3C vorming uit grote (microns) Ni kristallen.

De vormingssnelheid van CNF's op voorgevormde kleine Ni deeltjes gedragen op een

monoliet, start met een grote snelheid, gevolgd door uitsluitend deactivering. In tegenstelling hiermee neemt op polykristallijn Ni schuim de vormingssnelheid van CNF's bij constante temperatuur in het begin alleen maar toe, bereikt dan een maximum en neemt weer af. De initiële toename in de vormingssnelheid van CNF's op polykristallijn Ni wordt veroorzaakt door de noodzaak van de fragmentatie van de Ni korrels in kleinere Ni deeltjes.

De integriteit van de monsters en de sterke hechting van de CNF's aan het Ni schuim of de monoliet zijn nodig voor het toepassen van het uiteindelijke composiet materiaal als een gestructureerde katalysator drager. De monolieten kunnen gemakkelijk uiteen vallen wanneer de CNF's vorming te overdadig is, of in het corderiet of in het tussenvlak van het corderiet en de washcoat. Dus is het creëren van een hoge Ni concentratie aan het buitenoppervlak van de washcoat en geen Ni in het corderiet, alsmede het kiezen van een koolstof bevattend gas met een lage activiteit (b.v. CH_4) van het grootste belang voor de vorming van CNF's zonder excessieve vorming van CNF's in het corderiet.

De integriteit van het Ni schuim ging verloren na het synthetiseren van 138 wt% CNF's bij 500 °C in 3 uur. Anderzijds waren de schuimen stabiel na synthese van 50 wt% CNF's bij 450 °C in 6 uur. Het Ni schuim valt bij hoge temperatuur uit elkaar omdat de snelheid van corrosief metal dusting toeneemt met de temperatuur. Als tegenstelling tot de metal dusting, schijnt het oplossen van kleine hoeveelheden koolstof van de etheen dissociatie, de mechanische sterkte van het schuim te doen toenemen. In beide gevallen kan de CNF's laag de afschuifkrachten van stromend water (1 m/s) door het composiet materiaal gemakkelijk weerstaan.

In hoofdstuk 6 wordt de vorming van CNF's op polykristallijn Ni verder onderzocht. Goed geordend perfect gecoördineerd polykristallijne Ni deeltjes met verschillende grootten gedragen op een silicium wafer, werden gebruikt om CNF's te vormen. Deze studie geeft inzicht in de correlatie van de eigenschappen van de individuele CNF's gevormd met de lokale morfologie van het Ni oppervlak. Jammer genoeg vertraagde de vorming van Ni silicide de snelheid van CNF's vorming vergeleken met de snelheid op nikkel schuim. Wij suggereren dat het verlagen van de koolstof activiteit via het toevoegen van H_2 resulteert in een homogene verdeling van koolstof in het deeltje. Dit kan verklaren, waarom het deeltje volledig fragmenteert in kleinere deeltjes.

Tenslotte wordt in hoofdstuk 7 het gesynthetiseerde composietmateriaal kwalitatief geëvalueerd en toekomstige onderzoeksplannen aanbevolen voor de ontwikkeling van stabiele gestructureerde composietmaterialen als katalysator drager, die gebruikt kunnen worden bij de katalyse van vloeistoffase reacties, met als resultaat minder massatransport limitering en dus een hogere conversie en een betere selectiviteit.

ملخص

تزودنا هذه الأطروحة بمعلومات عن كيفية تحضير مواد تركيبية ميكرومترية من خيوط كربونية نانومترية والتي تم تثبيتها على مواد تركيبية كبيرة الحجم نسبياً. لقد تم انتاج هذه الخيوط الكربونية عن طريق تحطيم غاز الميثان والايثلين بمساعدة محفزات تحتوي على النيكل. تم تثبيت هذه الخيوط على مادتين هما مفاعل المونوليث والفيلتر المعدني. يحتوي مفاعل المونوليث على طبقة رقيقة غير عضوية وذات كثافة عالية نسبياً مثل اوكسيد الألمنيوم. هذه الطبقة هي التي تحمل المحفز في مفاعل المونوليث. الهدف من انتاج هذه الخيوط الكربونية على مفاعل المونوليث هو انتاج طبقة من نوع مطور ينافس الطبقة غير العضوية الموجودة حالياً. الفلتر المعدني لم يتم اختباره لغاية الآن كحامل تركيبية للمحفزات وبالتالي فان تحضير طبقة ذات مساحة واسعة وثابتة على الفلتر ما زال تحدياً.

الفصل الثاني والثالث يناقشان نتائج تحضير وتثبيت الخيوط الكربونية على مفاعل المونوليث. تقييم نتائج الدراسة الميكروسكوبية للمونوليث بينت ان السطح الخارجي للمونوليث يحتوي على طبقة من الخيوط الكربونية بسماكة ميكرومتر واحد تغطي الطبقة العضوية. ان بناء هذه الطبقة الكربونية يحاكي العكس تماماً للطبقة العضوية. ان طبقة الخيوط الكربونية محمولة على طبقة خليط من الخيوط الكربونية وقطع صغيرة من الطبقة غير العضوية. لقد تبين من خلال الدراسة أن سماكة طبقة الخيوط الكربونية وقطر الخيط الكربوني يزدادان بزيادة معدل حجم بلورة النيكل.

لقد أدى تكوين هذه الخيوط الكربونية على المونوليث باستخدام غاز الميثان الى تحطم مباشر للطبقة غير العضوية وبالتالي فان سماكة هذه الطبقة قد تضاعفت بغض النظر عن كمية الخيوط الكربونية التي تم تكوينها وبالتالي تم تكوين الطبقة الخليط المشار اليها سابقاً. ان قطر المسامات في الطبقة غير العضوية كان يتراوح بين ٥ - ٢٠ نانوميتر، بينما كان قطر الخيوط الكربونية يتراوح بين ١٠ - ٣٠ نانوميتر. من الواضح ان تكوين خيوط كربونية بقطر أكبر من قطر المسامات أدى الى التحطم المباشر للطبقة غير العضوية. وبالتالي فان الحجم المسامي لكل غرام من المونوليث كان ينقص بزيادة كمية الخيوط الكربونية المنتجة.

انتاج خيوط كربونية بكميات كبيرة أدى الى انسلاخ الطبقة غير العضوية عن المونوليث وذلك لأن طبقة من الخيوط الكربونية نمت بين المونوليث والطبقة غير العضوية. بالإضافة لذلك فان زيادة انتاج الخيوط الكربونية أدت الى تحطيم كامل للمونوليث، حيث أنه تم تعبئة بعض المسامات الكبيرة في المونوليث بالخيوط الكربونية. ان استخدام غاز الميثان لانتاج الخيوط الكربونية أفضل من استخدام الايثلين لان الأخير يكون خيوط كربونية بشكل سريع ومن حبيبات نيكل كبيرة. وبالتالي فانه يتكون خيوط كربونية سميكة (لغاية ٧٠ نانوميتر) وهذه بدورها تؤدي الى تحطيم المونوليث.

الفصل الرابع والخامس من هذه الأطروحة يناقشان نتائج تثبيت وانتاج الخيوط الكربونية على الفلتر المعدني والذي يتكون من نيكل. لقد تم تكوين طبقة خشنة من الخيوط الكربونية المتشابكة على سطح الفلتر مما أدى الى زيادة مساحة الفلتر من متر مربع واحد الى ٣٠ متر مربع للغرام الواحد. لقد تم تقدير الحجم الفراغي للخيوط الكربونية

بملييلتر واحد لكل غرام. بالإضافة الى ذلك فان الفراغات بين الخيوط الكربونية كبيرة مقارنة بالمسامات الصغيرة في الطبقة غير العضوية.

لقد بدأ تكوين الخيوط الكربونية على سطح فيلتر النيكل بتكوين مركب كربيد النيكل والذي بدوره تحلل الى نيكل وكربون. نتيجة لذلك تكوّن سطح خشن من حبيبات نيكل صغيرة بحجم يتراوح بين ١٠ - ١٠٠ نانوميتر بعد تعريض سطح النيكل لغاز الأيثلين لمدة نصف ساعة عند درجة حرارة ٤٥٠ م. لقد بدأت بعض حبيبات النيكل بتكوين خيوط كربونية بقطر يتراوح بين ١٠ - ٧٠ نانوميتر. ان حجم حبيبات النيكل أصغر بكثير من حجم الجرين للنيكل والتي يتراوح طولها بين ١ - ١٠ ميكروميتر. من خلال ذلك تم استنتاج أن تفكك النيكل الى حبيبات صغيرة قد حدث قبل بداية تكوين الخيوط الكربونية.

لقد تبين أن معدل تكوين الخيوط الكربونية على سطح نيكل مؤكسد هو أعلى بعشرة أضعاف من معدل التكوين على نيكل غير مؤكسد. ان ذلك يعني أن غاز الأيثيلين كان قادراً على تحويل أوكسيد النيكل الى معدن النيكل تحت ظروف التجربة وبالتالي تكوين نواة من النيكلز لقد اقترحنا خلال الدراسة ان هذه النواة تتحول مباشرة الى حبيبة من كربيد النيكل و التي تنمو و تتحلل عندما يصبح حجمها قادراً على انتاج خيط كربوني. من الواضح ان معدل تكوين حبيبات كربيد النيكل, ابتداءً من نواة نيكل صغيرة أسرع من معدل حبيبات من كربيد النيكل من حبيبة كبيرة من النيكل.

لقد ابتداءً انتاج الخيوط الكربونية بمعدل عالٍ من حبيبات النيكل المحمولة على المونوليث ثم بعد ذلك انخفض بشكل مستمر. على العكس من ذلك فان معدل تكوين الخيوط الكربونية على فلتر النيكل ازداد في البداية حتى وصل الى أعلى قيمة ثم انخفض بعد ذلك. ان السبب وراء زيادة معدل انتاج الخيوط الكربونية على فلتر النيكل كان بسبب ضرورة تكوين حبيبات نيكل صغيرة عن طريق تفتيت فلتر النيكل.

ان ضمان سلامة المواد التي تم انتاجها من التفتت و قوة الارتباط بين الخيوط الكربونية و فلتر النيكل أو المونوليث هما عاملان مهمان لتطبيق هذه المواد كحامل للمحفزات. لقد بينا أنه يمكن تحطيم المونوليث عندما تنتج كمية كبيرة من الخيوط الكربونية اما بين الطبقة غير العضوية و المونوليث أو داخل المونوليث نفسه. لذلك يجب أن نتحكم بكمية النيكل الموجودة في هذين المكانين. بالإضافة لذلك فان اختيار غاز ذو تفاعل معتدل مثل الميثان مهم لتكوين الخيوط الكربونية مع عدم تحطيم المونوليث.

لقد تم تحطيم فلتر النيكل بشكل كامل عندما أنتج ١٣٨٪ من الخيوط الكربونية ولمدة ثلاث ساعات تحت درجة حرارة ٥٠٠ م. من ناحية أخرى فان الفاتر لم يتحطم بعد انتاج ٥٠٪ من الخيوط الكربونية لمدة ٦ ساعات تحت درجة حرارة ٤٥٠ م. ان السبب وراء تحطم الفلتر تحت درجة حرارة عالية هو زيادة معدل تآكل المعدن. على العكس من هذا التآكل فانه تبين ان ذوبان كمية قليلة من الكربون في النيكل أدت الى زيادة قوته. في كلتا الحالتين (الفلتر المعدني و المونوليث) فان طبقة الخيوط الكربونية تحملت قوة احتكاك ناتجة عن تدفق ماء بسرعة ١ م/ث خلال هذه المواد.

الفصل السادس يدرس بشكل أعمق تكوين الخيوط الكربونية على النيكل. لقد تم إنتاج الخيوط الكربونية على حبيبات نيكل بأحجام مختلفة و محمولة بشكل مرتب على سيليكون بحيث يمكن تحديد مكان أي حبيبة بسهولة. لقد مكنا هذا الفصل من ربط خصائص كل خيط كربوني مع كل حبيبة نيكل أنتجت ذلك الخيط. للأسف ان تكون سيليسايد النيكل أدى الى انقاص معدل تكوين الخيوط الكربونية. مقارنة بمعدل انتاجها من فلتر النيكل. نحن نفترض ان تخفيض نشاط الكربون باضافة هيدروجين أدى الى وجود متجانس للكربون في حبيبة النيكل. لقد أدى ذلك الى تفتيت الحبيبة بشكل متجانس الى حبيبات صغيرة نسبياً.

أخيراً, لقد تم تقييم أولي للمواد التي تم انتاجها و تم اقتراح خطة مستقبلية لتطوير و تحسين هذه المواد ليتم استعمالها كحامل للمحفزات في تفاعلات السوائل.

Chapter 1

General Introduction

1. Introduction

Catalytic multiphase reactions account for more than 85% of industrial chemical processes and about \$ 1000 billion of chemical sales per annum in USA only [1,2]. Typical processes include the manufacture of petroleum-based products and fuels, production of polymers and other materials and pollution abatement. In most of these processes, a multiphase chemical reactor is the heart of the process [2].

Unfortunately, the rates as well as the selectivity in many industrial catalytic multiphase reactions are affected by the rate of mass transfer. A typical example is converting unsaturated liquid oil to a solid product *via* a multiphase catalytic reaction with H_2 . This hydrogenation is important in industry since the consistency of the melting behavior is improved; resulting is more stable product [3,4]. Gonzalez-Velasco et al. [4] studied in details the catalytic hydrogenation of methyl oleate, which is the main component of olive oil, using a Ni/SiO₂ catalyst in a slurry reactor. The authors concluded that, at 6 bars and 180°C, both activity and selectivity significantly decreased when the size of the catalyst particles is larger than 50 μm and the stirring rate is below 2000 rpm. A second example is heterogeneous catalytic hydrogenation of inorganic salts (e.g. NO₃⁻) dissolved in wastewater or ground water to harmless N₂ [5-7]. However, the undesired by product (i.e. NH₄⁺) is formed. D'Arind et al. [7] studied the effect of support porosity on the selectivity of nitrate reduction. Their results show that the selectivity to N₂ benefits from the use of low surface area and large pores support. The authors concluded that intraparticle diffusion and local buffering in control of the activity and selectivity of the reaction. Therefore, concentration gradients in the catalyst particles need to be avoided, which can be achieved only by limiting diffusion distances to the sub-micron range in both cases

Mass transfer limitation occurs more frequently in industrial catalytic reactions where dissolved species have to react with gaseous compounds (e.g. dissolved H₂) because of two main reasons; First, the solubility of these gases is limited and second, the diffusion coefficients in liquid phase is lower than that in gas phase by a factor of 10⁴ [8].

Figure 1 represents a G-L-S mass transfer model in a slurry phase reactor. First, gas reactants have to dissolve in the liquid phase, transport to the surface of the catalyst particle by diffusion in a stagnant layer of liquid. Then, gas and liquid reactants have to internally diffuse through the porous catalyst particle in order to reach the active site and

react. Similarly, the products of the reaction must diffuse out of the catalyst particle to the surface before being transported to the surrounding bulk of the liquid [9,10].

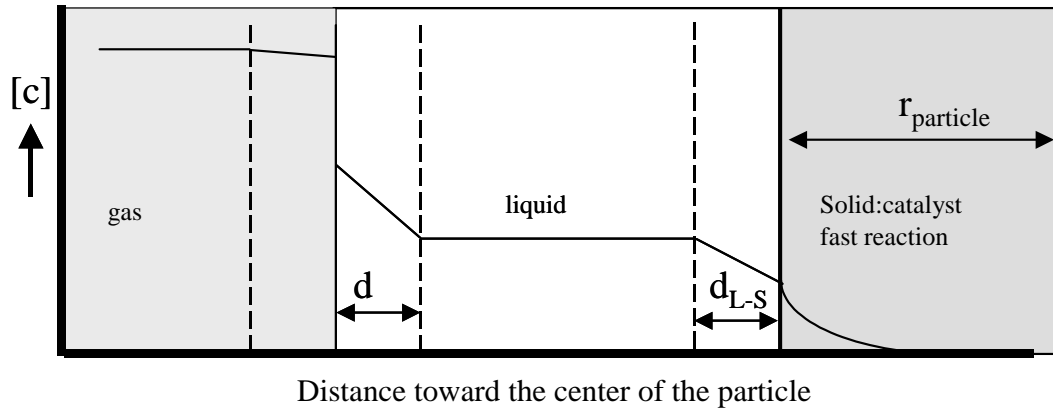


Figure 1: Concentration gradient in and around catalyst particle for a G-L-S fast chemical reaction.

The transfer of reactants from the external surface of catalyst particle to the active sites inside the particle requires a driving force, the concentration gradient, which results in variation of the local concentrations of reactants and products over the active sites. This affects both activity and selectivity and thereby frustrates optimum operation of such catalytic reactors. A measure of the degree of diffusion in the catalytic particle is given by internal effectiveness factor, η , defined as [9,10]:

$$\eta = \frac{\text{Reaction rate with internal diffusion limitation}}{\text{Reaction rate at external surface conditions}}$$

The concentration gradient through the pore volume in a catalyst particle is minimized when the Thiele modulus, ϕ , approaches zero. This can be achieved *via* shortening the diffusion path, L , (i.e. using small catalyst particles) and increasing the porosity of the particles (ϵ), which will result in a decrease in the tortuosity (τ). However, downsizing of catalyst particles is limited due to hydrodynamic constraints (i.e. high pressure drop) in trickle bed reactors and filtration problem in slurry phase reactors. Controlling and increasing the porosity of these small particles is a challenge [9,10].

$$\phi = L \sqrt{\frac{k_v \cdot C^{n-1}}{D_{\text{eff}}}} = L \sqrt{\frac{k_v \cdot C^{n-1} \cdot \tau}{\epsilon \cdot D_{\text{mol}}}}$$

L : diffusion path, k_v : volumetric rate coefficient, C : reactant concentration, n : the order of the reaction, τ : tortuosity, ϵ : porosity and D_{mol} : diffusion coefficient.

2. Comparison between different types of reactors

2.1. Conventional technology

Conventional technologies for heterogeneous catalytic reactions involving both liquid phase as well as gas phase comprise slurry reactors and trickle bed reactors.

2.1.1. Slurry phase reactor

Slurry reactors are three-phase catalytic reactors in which small catalyst particles (1-200 μm) are suspended by mechanical or gas-induced agitation [11]. These small catalyst particles provide a high external surface area as well as a short diffusion path within the catalyst. Thus, this reactor is widely used in hydrogenation and oxidation processes due to effective mass transfer into the catalyst particles. The reactants and the products are well mixed in the slurry phase reactor and therefore the concentration gradient through liquid phase in the reactor is minimized [12].

On the other hand, slurry reactors have some drawbacks. The main drawback is the filtration of the small catalyst particles [12,13]. Filtration units are expensive, complicated and cause operational problems rather frequently. Moreover, the agitation of the slurry causes attrition of the catalyst particles, resulting in a loss of active materials and in even more problematic filtration. The suspended particles can also cause erosion of the equipment [12].

2.1.2. Fixed /Trickle bed reactor

A trickle bed reactor is a fixed bed of catalyst pellets in which gas and liquid flow over the catalyst pellets. The size of the catalyst particles is relatively large (1-10 mm). This type of reactor is widely used in hydrotreatment of petrochemicals [11,13]. Trickle bed reactors usually show plug flow behavior, the catalyst load is high and no filtration is required.

On the other hand, the diffusion path through the catalyst particle is relatively long because of the large size of the catalyst particles. Downsizing the catalyst particles is limited because of increasing pressure drop through the reactor. Moreover, the possibility of creating dry/hot spots is a disadvantage of trickle bed reactors [13].

2.2. Structured catalytic reactors

Quite some research has been performed and is still being performed to develop structured catalyst to combine the advantages of slurry reactors and trickle bed reactors, i.e. create a large liquid-solid surface area as well as short diffusion distances inside the catalysts without needing a separation step. Especially the group of Moulijn and Kapteijn has pioneered the use monoliths [14-18], whereas others used fibers, cloths and gauzes [19-22].

2.2.1. Monolith reactor

A monolith structure consists of parallel channels separated by a thin wall (Figure 2a). The wall normally consists of cordierite, washcoated with a thin layer (10-100 μm) of high surface area material (usually γ -alumina) [12]. The number of channels per square inch (cpsi) depends on the channel diameter (typically 0.8-2 mm). Monolith structures have a large geometric surface area (1890-4790 m^2/m^3) and a high void fraction (0.72-0.84) [23].

The main advantage of the monolith reactor in gas phase operation is the low-pressure drop in the open channel. Based on that, monolith reactors are applied in environmental applications. The most abundant application is as automotive exhaust gas converter (three-way catalyst), but also application in stationary emission control, like deNO_x-ing of power plants [12,24,25].

Hydrogenations have been the most studied gas/liquid reactions in monolith reactors. As an example, the performance of a monolith in the hydrogenation of α -methyl styrene was compared with that of a trickle bed reactor in cocurrent mode under identical conditions of temperature and pressure. The observed reaction rate per unit mass of active metal in the monolith reactor was 13 times higher than that in the trickle bed. The better performance of monolith was attributed to a better mass transfer *via* using Taylor or slug flow [25]. This flow type consists of gas bubbles and liquid slugs flowing consecutively through the monolith channels. The gas bubble fills up the whole space of the channel and only a thin liquid film separates the gas from the catalyst. Thus, gas-solid mass transfer can be enhanced.

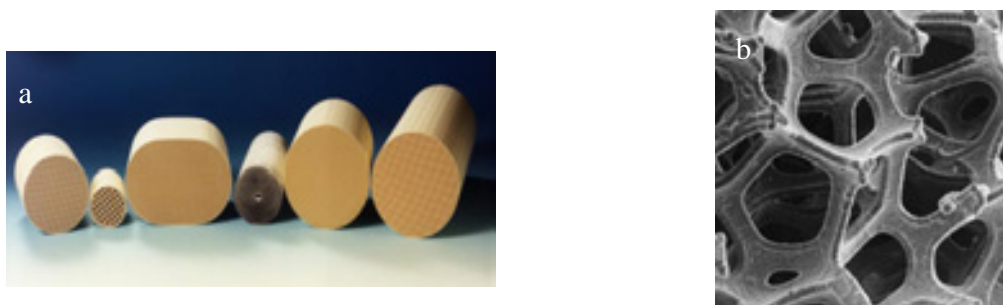


Figure 2: Schematic representation of (a) monolith and (b) metal foam structure

2.2.2. Foams

There are different foam materials described in literature: metallic, ceramic or polymer foams [26]. Catalysis is one area of the foam applications. Only metallic foam will be investigated in this study.

Metal foams have been used as catalysts or catalytic support for highly exothermic reactions in gas phase due to their high thermal conductivity and high mechanical strength. Highly exothermic reactions are typically very fast and the effectiveness factor in porous catalyst is very small. The main advantages of the foam structures are the absence of internal diffusion and the low-pressure drop [12,26]. On the other hand, the surface area of metal foams is very small (less than $1\text{m}^2/\text{g}$), and that limit their use as a catalyst support [26]. To achieve a high surface area, the foam can be coated with a porous high surface area layer. Applying a uniform washcoat on foams is difficult because of poor adhesion of the resulting coating [26-28]. However, Valentini et al. [29] prepared γ -alumina washcoats on alumina foam with good adherence. The detailed information is not yet available, however it is problematic to control the properties of the washcoat as well as the distribution through the foam. However, to our best knowledge, the performance of the foams as catalyst or catalyst supports has been studied for gas phase but not for liquid phase.

3. Demands for superior structured catalyst in liquid phase operation

Slurry phase reactor is still the superior reactor compared to trickle bed reactor because of better mass transfer properties [12]. Even though, there are many examples, as we mentioned above, where the slurry reactor needs extreme small catalyst particles to

achieve high activity and selectivity. Moreover, the mentioned structured catalysts (section 2.2) have been mainly developed for environmental gas applications [24]. In literature there are some examples where gas phase reactions, performed in monolith reactor, were running under mass transfer limitation (e.g. the combustion of methane over a palladium catalyst). It was found that the conversion of methane decreases significantly using the same amount of catalyst dispersed over a thicker washcoat. Even a slight increase in the washcoat resulted in a decrease in the rate significantly [30]. Moreover, Siemund et al. [31] developed a model for a three-way catalytic converter (monolith reactor). The model counts for the hydrocarbons or carbon monoxide oxidation and nitrogen monoxide reduction. It was concluded both experimentally and theoretically that the reaction was running under internal diffusion limitation. From the previous examples it can be concluded that the washcoat of the monolith reactor may be not an optimum for fast gas-phase reactions.

Therefore the washcoat on the monolith reactor would be even less optimum in liquid phase reaction. Moreover, the thickness of the washcoat varies within the channel cross section (e.g. the washcoat is thicker in the corners of the channel). Thus, preparing a new homogenous and highly porous washcoat would improve the performance of the monolith reactor, resulting in an increase in the activity and selectivity. This thesis explores the possibility to prepare such a “washcoat” *via* the immobilization of carbon nano fibers (CNFs) on the wall of the monolith. Moreover, immobilization of CNFs layer on Ni foam will be explored.

4. CNFs as catalyst support

Serp et al. [32] presented in a recent review why CNFs are interesting catalyst supports; They form aggregates that have high surface area ($100\text{-}200\text{m}^2/\text{g}$) combined with a large pore volume ($0.5\text{-}2\text{ cm}^3/\text{g}$) without micro-pores [33]. CNFs aggregates resemble the inverse structure of a traditional catalyst support (e.g. alumina or silica) (Figure 3). Filling the pore volume in a traditional catalyst support with graphite, where after the body of the traditional support is removed would result in formation of a structure resemble the CNFs aggregates. Such a highly porous structure with macropores will decrease the tortuosity in liquid phase applications. Thus, mass transfer rate will be maximized. Moreover, these aggregates have a comparable strength of commercial catalyst supports.

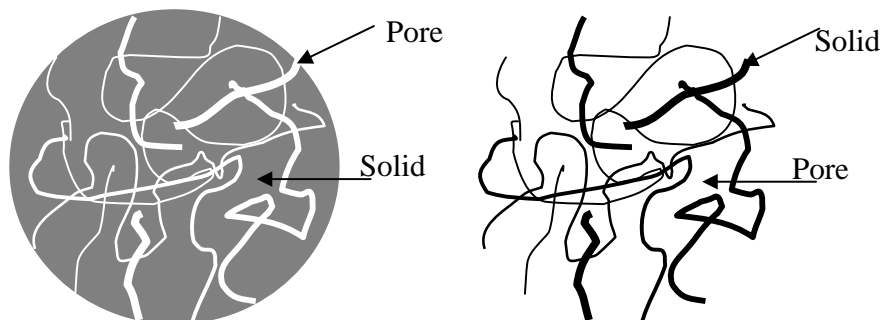


Figure 3: Schematic representation of conventional inorganic catalyst support (left) and CNFs aggregate (right).

Considering the advantages mentioned, CNFs have been used as a catalyst support in gas and liquid phase applications. We will mention a few examples where CNFs were used as catalyst support in liquid phase.

Ledoux et al. [34] used carbon nanofiber supported palladium catalyst for hydrogenation of cinnamaldehyde into hydrocinnamaldehyde. It was shown that both activity and selectivity were enhanced using Pd/CNFs compared to the commercially palladium supported on high surface area activated charcoal. It was concluded that the absence of microporosity in CNFs resulted in an increase in the activity and selectivity of the catalyst *via* maximizing the mass transfer rate.

Ledoux et al. [35] studied the hydrazine decomposition over iridium catalyst supported on CNFs and γ -alumina supports. The authors show that the decomposition rate of hydrazine on Ir/CNFs catalyst was one order of magnitude higher than that on Ir/ γ -alumina. The main reason for this high performance of Ir/CNFs was the fact that CNFs have extremely high external surface area compared to γ -alumina. Moreover, the presence of micropores in γ -alumina trapped some of the hydrazine and limited the conversion. Obviously, The properties of the CNFs aggregates are of interest for kinetic studies in very fast reactions.

4.1. Carbon nano fibers (CNFs)

Until the 1980s, the formation of CNFs was considered a serious problem because they are formed in a temperature range, where many important reactions, such as Fisher-Tropsch synthesis and steam reforming, are carried out. These CNFs are mechanically

strong, so that the formation of these materials does not only destroy the catalyst particles, but even may damage the reactor wall [36].

CNFs are graphite materials can be synthesized by carbon-arc [37], laser vaporization and catalytic methods [33]. From application point of view, the catalytic synthesis is simple, cheap and productive [38].

CNFs can be catalytically produced *via* the decomposition of hydrocarbons or CO over transition metal surface such as Ni, Fe and Co [33,39]. Figure 4 illustrates a mechanism of catalytic formation of CNFs at steady states conditions: First, the hydrocarbon gas decomposes on the surface of the metal particle, resulting in the formation of C and H₂. Second, the C formed dissolves in the metal phase and diffuses through the particle to the interface between the metal and the support, where nucleation of graphite is initiated. Third, the formation of graphite layers continues at the interface, resulting in lifting up the catalyst particle from the support. The formation of CNFs continues until encapsulation of the catalyst particle with a thick layer of carbon takes place.

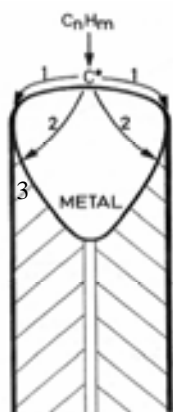


Figure 4: Schematic representation of the mechanism of CNFs formation.

Helveg et al. [40] used *in-situ* TEM to follow the formation of CNFs via the decomposition of CH₄ at 536°C on Ni nanoclusters supported on MgAl₂O₄. The results showed that the formation of CNFs is developed through a reaction induced reshaping of the Ni nanocrystals. Thus, it was concluded that a bamboo-like CNFs are formed.

For unsupported metal particles, Baker et al. [41] proposed, based on TEM results, that more than one CNF can be produced from a metal particle. The authors concluded that distinct crystallographic faces are generated on the particle during reaction. Thus, carbon-

containing gas dissociates on some faces, migrates through the bulk of the metal particle and finally precipitates on the other faces.

4.2. Immobilization of CNFs on structured supports

Despite the pioneering work of Ledoux et al. [35], who immobilized CNFs on graphite felt, CNFs have been mainly used as a catalyst support in the shape of powders [32-34,42-44]. However, porous bodies of CNFs can be formed from porous supported metal catalyst bodies in the size of micrometre to millimetre [33,36]. The main problem encountered is the difficulty of using the powder CNFs in conventional catalytic reactors. Trickle bed reactor will suffer from a high-pressure drop, although the bodies of CNFs in a size of millimetre might be suitable to be used in this type of reactor. On the other hand, agglomeration and filtration are the main problems when these fibers are implemented in a slurry phase reactor [35].

Another reason for the importance of the immobilization of CNFs to structured support is to create functionalised sites on the support. These sites can be used to immobilize Enzymes on the support, resulting in the formation of structured Enzyme bioreactors [46].

The goal of this thesis is to explore the opportunities to immobilize CNFs on macro-structured materials. Two macro-structured materials were used as examples, i.e. ceramic monolith and metal foam. From the perspective of the use of monoliths as structured materials to support catalysts, this work aims on the preparation of improved washcoats based on CNFs, competing with the well known relatively dense inorganic washcoats. Metal foams are much less explored as structured catalyst supports and in this case the preparation of highly porous, stable and uniform washcoats is the challenge.

5. Outline of this thesis

As mentioned before, the goal of this thesis is to synthesis materials with properties that can enhance both activity and selectivity in G-L-S reactions. These materials will be synthesized based on the immobilization of carbon nanofibers on macrostructured supports. Both **Chapter 2 and Chapter 3** discuss the immobilization of CNFs on monolith supports. **Chapter 2** demonstrates the possibility to immobilize a carbon nanofiber layer on a monolith washcoat. It is shown that carbon nanofibers form a

homogeneous and highly open layer with sub-micron thickness, covering the surface of the channels in the monolith. The fibers showed a remarkable attachment to the monolith under ultrasound maltreatment. In **Chapter 3**, a description and explanation of how nickel particle size, the conditions to form CNFs as well as the pore-structure of the wash-coated monolith, determine the structure and properties of CNF as well as the morphology and mechanical strength of the resulting complex composite that contains cordierite, alumina and CNF. In **Chapter 4 and Chapter 5**, we investigate the immobilization of CNFs on nickel foam. **Chapter 4** demonstrates the possibility to synthesize a stable CNFs layer on the foam without separating the grains of Ni *via* corrosive metal dusting. The effect of formation time and formation temperature on the structure of the CNFs and on the final structure of the composite is presented. **Chapter 5** describes and explains how the structure and geometry of the nickel foam surface affects the resulting structure of CNFs as well as the structure of the final composite. It also proposes mechanism of CNFs formation on polycrystalline Ni. In **Chapter 6**, we investigate the effect of formation conditions on well-ordered polycrystalline Ni particles supported on Si wafer. The study in this chapter allows us to correlate the local change in the morphology of Ni surface and the properties of CNFs formed to the formation conditions. Finally, in **Chapter 7** all the results are summarized and some concluding remarks are presented.

References

1. G. Centi and S. Perathoner, *CATTECH*, 7(3), 2003, 78-88
2. M. P. Dudukovic, F. Larachi and P. L. Mills, *Chemical Engineering Science*, 54, 1999, 1975-1995.
3. M. W. Balakos and E. E. Hernandez, *Catalysis Today*, 35, 1997, 415-425.
4. J. I. Gutierrez-Ortiz, R. Lopez-Fonseca, C. Gonzalez-Ortiz de Elguea, M. P. Gonzalez- Marcos and J. R. Gonzalez-Velasco, *React. Kinet. Catal. Lett.*, 70(2), 2000, 341-348.
5. R. Dittmeyer, V.Höllein, K. Daub, *J. Mol. Catal. A.*,; *Chemical* 173, 2001 135-184.
6. M. Hähnlein, U.Prusse, S.Horold, K.D. Vorlop, *Chem. Ing. Tech.*, 69, 1997 93.
7. M. D'Arino, F. Pinna and G. Strukul, *Applied Catalysis B: Environmental*, 53, 2004, 161-168 .
8. W. Teunissen, *Tailoring of carbon fiber and carbon-coated ferromagnetic catalyst supports*, PhD thesis, 2000, Utrecht.

9. H. Scott Fogler, Elements of chemical reaction engineering, Prentice-Hall, Inc., New Jersey, 1999.
10. J. M. Smith, Chemical engineering kinetics, McGraw-Hill, New York, 1981.
11. Y. T. Shah, Recent Advances in Trickle Bed Reactor, Concept and design of chemical reactors, Gordon and Breach science publishers, New York 1986, 299-338.
12. A. Cybulski and J. A. Moulijn, Structured Catalysts and Reactors, Marcel Dekker, New York 1998.
13. J. F. Jenck, Heterogeneous Catalysis and Fine Chemicals II, 1 (1991).
14. M.T. Kreutzr, P. Du, J.J. Heiszwolf, F. Kapteijn and J.A. Moulijn, Chem. Eng. Sci., 56 (2001) 6015.
15. T.A. Nijhuis, M.T. Kreutzer, A.C. Romijn, F. Kapteijn and J.A. Moulijn, Chem. Eng. Sci., 56 (2001) 823
16. T.A. Nijhuis, M.T. Kreutzer, A.C. Romijn, F. Kapteijn and J.A. Moulijn, Catalysis Today, 66 (2001) 157
17. F. Kapteijn, T.A. Nijhuis, J.J. Heiszwolf and J.A. Moulijn, Catalysis Today, 66 (2001) 133.
18. A.E. Beers, R.A. Spruijt, T.A. Nijhuis, F. Kapteijn and J.A. Moulijn, Catalysis Today, 66 (2001) 175
19. L. Kiwi-Minsker, I. Yuranov, V. Holler and A. Renken, Chem. Eng. Sci., 54 (1999) 4785-4790.
20. L. Kiwi-Minsker, I. Yuranov, V. Holler and A. Renken, Catalysis Today, 69 (2001) 175-181.
21. Y. Matatov-Meytal, V. Barelko, I. Yuranov and M. Sheintuch, Applied Catalysis B, 27 (2000) 127
22. Y. Matatov-Meytal, V. Barelko, I. Yuranov, L. Kiwi-Minsker, A. Renken and M. Sheintuch, Applied Catalysis B, 27 (2000) 233
23. Theo Vergunst, Carbon coated monolithic catalysts, PhD thesis, 1999, Delft.
24. G. Centi and S. Perathoner, CATTECH 7(3), 2003, 78.
25. F. Kapteijn, J. J. Heiszwolf, T. A. Nijhuis and J. A. Moulijn, CATTECH 3(1), 1999, 24.
26. Y. Matatov-Meytal and M. Sheintuch, Applied Catalysis A: General 231, 2002, 1.

27. M. F. Zwinkles, S. C. Jaras, P. G. Menon, T. A. Griffin, *Catal. Rev. Sci. Eng.* 35, 1993, 317.
28. W. F. Maier, J. W. Schlangen, *Catal. Today* 17, 1993, 225.
29. M. Valantini, G. Groppi, C. Cristiani, M. Levi, E. Tronconi and P. Forzatti, *Catalysis Today*, 69, 2001, 307-314.
30. R. E. Hayes, S. T. Kolaczowski, P. K. Li and S. Awdry, *Chem. Eng. Sci.* 56, 2001, 4815-4835.
31. S. Siemund, J. P. Leclerd, D. Schweich, M. Prigent and F. Castagana, *Chem. Eng. Sci.* 51, 1996, 3709-3720.
32. P. Serp, M. Corrias and P. Kalck, *Applied Catalysis A: General*, 253, 2003, 337.
33. K. De Jong and J. Geus, *Catal. Rev. – Sci. Eng.* 42(4) (2000) 481.
34. C. Huu, N. Keller, G. Ehret, L. Charbonniere, R. Ziessel and M. Ledoux, *Journal of Molecular Catalysis A: Chemical*, 170, 2001, 155-163.
35. R. Vieira, C. Pham-Huu, N. Keller and M. J. Ledoux, *Chem. Comm.*, 2002, 454-455.
36. M.S. Hoogenraad, *Growth and Utilization of Carbon Fibers*, Ph. D. Thesis, Utrecht (1995).
37. T. Ros, *Rhodium Complexes and particles on Carbon nanofibers*, PhD thesis, Utrecht, 2002.
38. S. Iijima, *Nature*, 354, 1991, 56.
39. B. C. Liu, L. Z. Gao, Q. Liang, S. H. Tang, M. Z. Qu and Z. L. Yu, *Catalysis Letters*, 71(3-4), 2001, 225-228.
40. S. Helveg, C. Lopez-Cartes, J. Sehested, P. L. Hansen, B. Clausen, J. Rostrup-Nielsen, F. Abild-Pedersen and J. Norskov, *Nature*, 427, 426-429.
41. R. T. Baker, M. S. Kim, A. Chambers, C. Park and N. M. Rodriguez, *Studies Surf. Sci. Catal.*, 111, 1997, 99.
42. N. Rodriguez, *J. Mater. Res.*, 8(12), 1993, 3233.
43. A. Chambers, T. Nemes, N. Rodriguez and R. Baker, *J. Phys. Chem. B*, 102, 1998, 2251-2258
44. C. Park and R. Baker, *J. Phys. Chem. B*, 103, 1999, 2453.
45. C. Huu, N. Keller, G. Ehret, L. Charbonniere, R. Ziessel and M. Ledoux, *Chem. Commun.*, 2000, 1871-1872.

46. K. M. de Lathouder, J. J. Bakker, F. Kapteijn, J. A. Moulijn and S. A. Wallin, 5th Netherlands' Catalysis and Chemistry Conference, Noordwijkerhout, The Netherlands, March 2004.

Chapter 2

Development of monolith with a carbon nanofiber washcoat as a structured catalyst support

Abstract

Washcoats with improved mass transfer properties are necessary to circumvent concentration gradients in case of fast reactions in liquid phase, e.g. nitrate hydrogenation. A highly porous, high surface area (180 m²/g) and thin washcoat of carbon fibers, was produced on a monolith support by methane decomposition over small nickel particles. Carbon fibers form a homogeneous layer less than 1 micron thin, covering the surface of the channels in the monolith. The fibers show a remarkable stability against ultrasound maltreatment. The texture of the fibers is independent of both the thickness of the γ -alumina washcoat as well as the time to form carbon fibers.

1. Introduction

Fast chemical reactions can easily cause concentration gradients in reactors and catalysts, when these gradients are necessary to give sufficiently rapid mass transfer rates to keep up with the chemical reaction rates. Gradients occur most easily in liquid phase because of relatively slow diffusion as well as the frequent occurrence of very low concentrations when gasses have to dissolve in the liquid phase before they can reach the catalyst. The consequence is that the local concentrations at the active sites vary, influencing reaction rates as well as selectivity.

Conventional technologies for heterogeneous catalytic reactions involving both liquid phase as well as gas phase comprise slurry reactors and trickle bed reactors. Trickle bed reactors end up easily in diffusion limitations because of the relatively large catalyst particle size that is necessary because of hydrodynamic reasons. Slurry reactors are more suitable for fast reactions because of much smaller catalyst particles sizes, at the expense of additional costs for separation of the catalyst from the products. Also, the lack of robustness of separation technologies, e.g. filtration, is an important concern. Quite some research has been performed and is still being performed to develop structured catalyst to combine the advantages of slurry reactors and trickle bed reactors, i.e. create a large liquid-solid surface area as well as short diffusion distances inside the catalysts without needing a separation step. Especially the group of Moulijn and Kapteijn have pioneered the use monoliths [1-5], whereas others used fibers, cloths and gauzes [6-9].

All structured materials used so far have a relatively small external surface area. Additional surface area needs to be generated to host a sufficiently extended catalytic surface area. This is usually achieved by preparing a porous washcoat on the surface of the structured material, e.g. on monoliths, or by generating pores in the structured material itself, e.g. in carbon fibers. In the rest of this contribution we will use the term washcoat, and the practical work in this contribution is limited to monoliths.

The thickness of washcoats on monoliths as prepared for exhaust application is in the order of tens of microns. This is apparently the optimum for gas-phase conditions in the exhaust; however, the optimum might be different for liquid phase operation. Therefore we will demonstrate in this chapter how to arrive at washcoats with superior properties, i.e. higher porosity and smaller thickness, preserving a significant surface area to support the active phase. New promising supports have been prepared based on carbon-

nanofibers [14-18]. These fibers can be formed catalytically by decomposition of a carbon containing gas over small metal particles like nickel, iron and cobalt. The primary structure and dimensions of the fibers are determined by the temperature, gas composition, active metal, the metal particles size distribution and the support material [19,20]. The secondary structure of the support is determined by the extent of entanglement of the fibers and the extent of orientation of the individual fibers. It has been shown that e.g. nickel particles on oxide supports form an aggregate of carbon fibers shaped identically to the original support, except for an increase in size of typically a factor three [21]. The porosity of these aggregates is very high, e.g. 1cc/g. Therefore, in this study we prepared stable washcoats that consist of carbon nanofibers.

2. Experimental

2.1. Materials

Monolith support samples (600 cells per square inch, obtained from Degussa, Germany) were used with four different average thicknesses of the γ -alumina washcoat; bare cordierite, 9, 13, and 17 μm thick respectively. Nickel (II) nitrate [$\text{Ni}(\text{NO}_3)_2 \cdot 6\text{H}_2\text{O}$] and ammonium nitrate [NH_4NO_3] (pure, Merck, Darmstadt, Germany) were used to prepare the nickel solution. Hydrogen and nitrogen gases with purity 99.999% (INDUGAS, The Netherlands) and methane with purity 99.995% (Hoek Loos, The Netherlands) were used for carbon fibers formation.

2.2. Catalyst preparation

Nickel was deposited on the washcoated monolith by adsorption from a pH-neutral nickel solution (0.1 M) as described else where [22]. The solution contained 29g of $\text{Ni}(\text{NO}_3)_2 \cdot 6\text{H}_2\text{O}$, 80 g NH_4NO_3 and 4 ml of ammonia solution (25 wt%) per liter.

The monolith samples were dipped (20 times/min) in the solution for 3 hours. Free liquid was removed and the samples were dried over-night at room temperature and were then heated (1°C/min) to 120°C for 2 hours, followed by calcination in static air (5°C/min) at 600°C for 2 hours.

2.3. Experimental set-up for carbon fiber formation

Carbon fiber formation was carried out in a quartz reactor with a porous quartz plate at the bottom to support the sample [20,21]. The sample was heated to 700°C (5.5°C/min) in 20% H₂ in N₂ for 2 hours. After cooling to 570°C carbon fibers were formed in 50 % CH₄, 10 % H₂ in N₂ (total flow rate 200ml/min).

Methane conversion was determined with on-line chromatographic analysis (Varian GC model 3700 equipped with a 15 m Q-Plot column). Finally, the sample was cooled down in N₂ to room temperature. The amount of carbon formed on the monolith was determined by weight.

2.4. Characterization

The BET surface area, pore volume and pore size distribution were measured by N₂ adsorption-desorption at 77 K using ASAP 2400 (Micromeritics) instrument.

Nickel loading of the ceramic monolith was measured with Philips X-ray fluorescence spectrometer (PW 1480).

Nickel particle sizes were determined on powdered catalysts with Transmission Electron Microscopy (TEM) (Philips CM30). The morphology of the carbon fibers was studied non-destructively with Scanning Electron Microscopy (SEM) (LEO 1550 FEG SEM) equipped with EDX analysis. The monoliths were broken to allow direct observation of the carbon-fibers on the surface of the wall of one of the inner channels in the monolith.

3. Results and Discussion

3.1. Characterization of the ceramic supports

Table 1 shows the texture of the monolith supports. It is obvious that surface area as well as pore volume is determined almost completely by the γ -alumina phase. The large pores in the cordierite cannot be measured with N₂ adsorption and pore volume of cordierite has been estimated to be 0.5 cc/g based on the bulk density of cordierite (2.51 g/ml) and the apparent density of the monolith [23]. The surface area of all washcoats is 100m²/g. The washcoats contain mesopores only with a total pore volume of 0.33cc/g.

Table (1): Properties of monolith support, NiO and carbon fiber on monolith.

Thickness of γ -alumina washcoat (μm)	No washcoat	9	13	17
Characterization of ceramic support				
BET surface area (m^2/g monolith)	<1	26	35	45
Pore volume (cc/g monolith)	-	0.085	0.116	0.149
Average pore size (\AA)	-	130	128	130
Characterization of NiO on monolith				
NiO wt% (g NiO/100 g monolith)	0.33	1.18	1.44	1.51
NiO monolayers	-	0.31	0.28	0.23
Carbon fiber after 3 hrs of formation				
Amount of carbon fiber (g/g monolith)	0.0085	0.107	0.154	0.157
Amount of carbon fiber (g/g Ni)	3.3	11.5	13.2	13.6
BET surface area (m^2/g monolith)	-	42	55	63
BET surface area (m^2/g carbon fiber)	-	181	179	190

3.2. Characterization of NiO on monolith

Table 1 shows the NiO concentrations in the samples. The relatively low nickel oxide concentration on cordierite is in agreement with estimation of [Ni] assuming introduction of NiO *via* pore-volume-impregnation exclusively. The NiO concentration on the samples with γ -alumina is significantly higher, indicating adsorption of $\text{Ni}(\text{NO}_3)_2$ in the washcoat. The coverage is well below one monolayer in all cases, assuming NiO to cover $8 \text{ \AA}^2/\text{NiO}$ (based on the bulk structure of NiO [24]). The surface coverage decreases with the thickness of the washcoat.

Both visual inspection (greenish color of NiO) as well as local determination of Ni concentration (XRF results) in the monolith proves homogenous distribution of NiO. Particles sized in the range of 6 to 10 nm are observed in all washcoats. Particle sizes in the cordierite without washcoat are obviously much larger because of the extreme low surface area.

3.3. Carbon fiber formation on the monolith supports

The effect of time on stream on the rate of formation of carbon fiber, calculated from the rate of methane conversion, is shown in figure 1. The initial rate per gram nickel is somewhat larger for the thinner washcoats whereas the activity decreases faster.

Table 1 shows the amount of carbon fiber formed on the samples in three hours based on weight. The integral methane conversion calculated from figure 1 is in agreement with these numbers within 20%. The integration of the methane consumption suffers from inaccuracy especially when methane conversion is low.

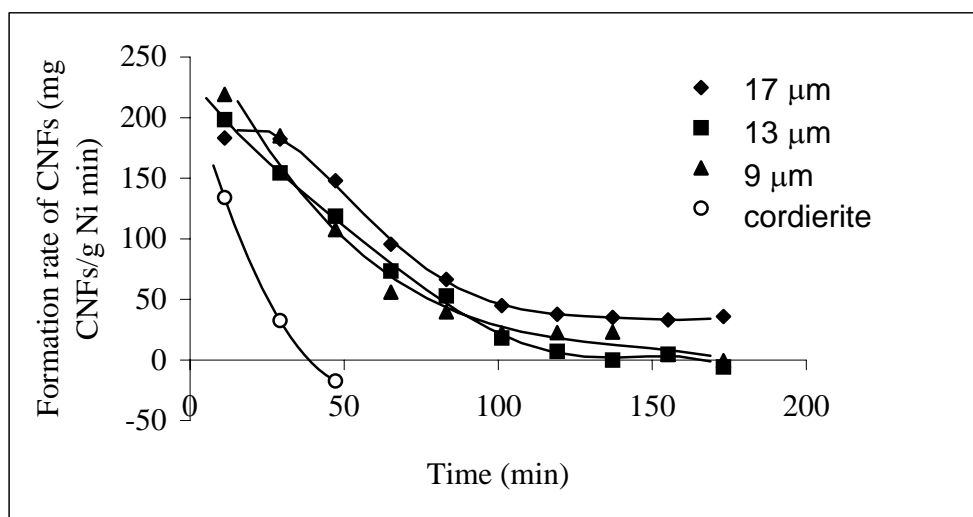


Figure 1: Rate of formation of carbon fiber on nickel loaded monolith with different washcoat thickness.

3.4. Characterization of carbon fiber washcoat

Formation of carbon fibers causes an increase in the total surface area of the samples. Assuming that the surface area of the washcoat remains unchanged and using the carbon concentrations achieved (table 1), the surface area of the carbon fibers was calculated. Also, identical surface areas of the carbon fibers are found when the time of formation was varied. In all cases the surface area is $180 \text{ m}^2/\text{g}$ within 5%. Apparently, the primary structure of the carbon fibers is independent of both the thickness of the washcoat as well as the time of formation.

The secondary structure of the fibers was studied with SEM. Figure 2a shows the typical morphology of carbon fibers formed out of metal particles; the fibers contain metal particles in the top of the fiber exclusively and the diameter of the fibers varies between 10 and 30 nm. Figure 2b shows that carbon fibers cover the surface of the monolith wall homogeneously for all washcoated samples; the side view in figure 2c indicates that this layer is about half a micron thick. It is clear that the layer formed by the carbon fibers is extremely open and thin. However, in some places reminders of the alumina washcoat can be observed (figure 2d) suggesting that the alumina washcoat is fragmented by carbon fiber formation. Finally it was observed that much more carbon fibers are present in the cordierite compared to the nickel impregnated bare cordierite (not shown). From this follows that carbon fibers penetrate from the washcoat into the cordierite. This phenomenon is probably the reason for the strong attachment of the fibers to the monolith.

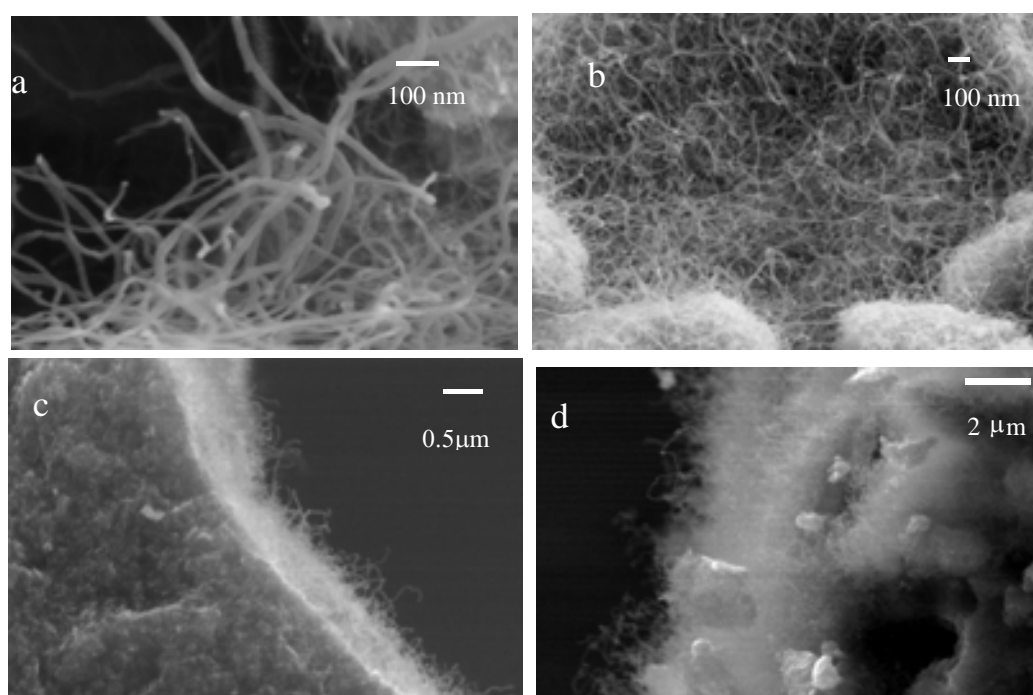


Figure 2: SEM micrographs of carbon nanofibers produced by CH_4 decomposition over nickel particles supported on γ -alumina monolith washcoats; a) High resolution SEM of carbon fiber, b) Top-view on monolith wall covered with fibers, c) Side-view on monolith wall, d) Fragments of γ alumina occluded by fibers.

Extended maltreatment of the sample with 40 KHz ultrasound resulted in limited loss of carbon fibers as shown in figure 3. About 10% of the fibers can be removed and no losses are observed anymore after 40 minutes. Nevertheless, stability under flow conditions applying shear force was demonstrated (Chapter 3).

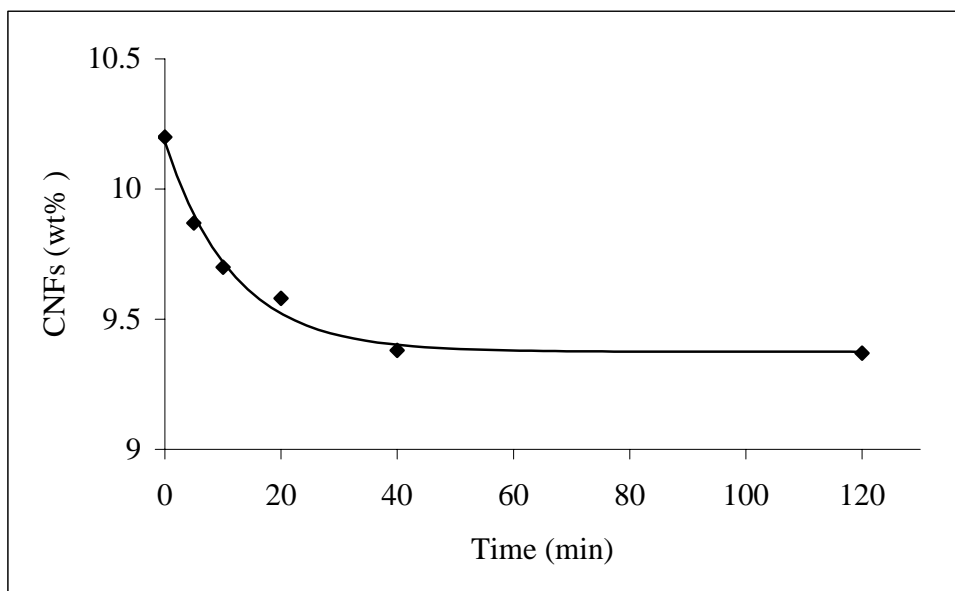


Figure 3: Stability of carbon attachment against ultrasound (40 KHz) treatment; fibers formed during 1 hour on 17 μm washcoat.

4. Conclusions

A highly porous, high surface area ($180 \text{ m}^2/\text{g}$) and thin washcoat, based on carbon fiber, was produced on a monolith support by methane decomposition over small nickel particles. Carbon fibers form a homogeneous layer less than 1 micron thin, covering the surface of the channels in the monolith, provided care is taken to distribute the Ni homogeneously. The fibers showed a remarkable mechanical stability against ultrasound maltreatment.

The structure of the fibers is independent of both the thickness of the γ -alumina washcoat as well as the time used to form carbon fibers.

Acknowledgments

This work was performed under the auspices of NIOK, the Netherlands Institute of Catalysis Research, and the Processtechnology Institute Twente. The authors are gratefully acknowledging Degussa for supplying monoliths, we are grateful to Ing. J. A. M. Vrieling, Ing. V. Skolnik, dr. M. Smithers and dr. R. Keim for XRF, BET, SEM, and TEM measurements respectively. We acknowledge Ing. B. Geerdink for technical support, as well as Prof. K.P de Jong and Dr. M. L. Toebes for an introduction in carbon fiber chemistry.

References

1. M.T. Kreutzr, P. Du, J.J. Heiszwolf, F. Kapteijn and J.A. Moulijn, *Chem. Eng. Sci.*, 56 (2001) 6015.
2. T.A. Nijhuis, M.T. Kreutzer, A.C. Romijn, F. Kapteijn and J.A. Moulijn, *Chem. Eng. Sci.*, 56 (2001) 823
3. T.A. Nijhuis, M.T. Kreutzer, A.C. Romijn, F. Kapteijn and J.A. Moulijn, *Catalysis Today*, 66 (2001) 157
4. F. Kapteijn, T.A. Nijhuis, J.J. Heiszwolf and J.A. Moulijn, *Catalysis Today*, 66 (2001) 133.
5. A.E. Beers, R.A. Spruijt, T.A. Nijhuis, F. Kapteijn and J.A. Moulijn, *Catalysis Today*, 66 (2001) 175
6. L. Kiwi-Minsker, I. Yuranov, V. Holler and A. Renken, *Chem. Eng. Sci.*, 54 (1999) 4785-4790.
7. L. Kiwi-Minsker, I. Yuranov, V. Holler and A. Renken, *Catalysis Today*, 69 (2001) 175-181.
8. Y. Matatov-Meytal, V. Barelko, I. Yuranov and M. Sheintuch, *Applied Catalysis B*, 27 (2000) 127
9. Y. Matatov-Meytal, V. Barelko, I. Yuranov, L. Kiwi-Minsker, A. Renken and M. Sheintuch, *Applied Catalysis B*, 27 (2000) 233
10. C.G. Van de Moesdijk, *The Catalytic Reduction of Nitrate and NO to hydroxylamine; kinetics and mechanism*, Thesis, Eindhoven University of Technology (1979), 134-135.
11. D. Lindner, M. Werner and A. Schumpe, *AIChE Journal*, 34 (1988) 1691.
12. R. Dittmeyer, V.Höllein and K. Daub, *J. Mol. Catal. A; Chemical*, 173 (2001) 135
13. M. Hähnlein, U.Prusse, S.Horold and K.D. Vorlop, *Chem. Ing. Tech.*, 69 (1997) 93.

14. R. Baker, M. Kim and N. Rodriguez, *J. Phys. Chem.*, 98 (1994) 13108
15. S. Shaikhutdinov, L. Avdeeva, B. Novgorodov, V. Zaikovskii and D. Kochubey, *Catal. Lett.*, 47 (1997) 35.
16. R. Baker and C. Park, *J. Phys. Chem. B*, 102 (1998) 5168.
17. R. Baker, A. Chambers, T. Nemes and N. Rodriguez, *J. Phys. Chem. B*, 102 (1998) 2251.
18. R. Baker, C. Park and F. Salman, *Catal. Today*, 53 (1999) 385.
19. K. De Jong and J. W. Geus, *Catal. Rev. – Sci. Eng.* 42(4) (2000) 481.
20. M.S. Hoogenraad, *Growth and Utilization of Carbon Fibers*, Ph. D. Thesis, Utrecht (1995).
21. W. Teunissen, *Tailoring of Carbon Fiber and Carbon-Coated Ferromagnetic Catalyst Supports*, Ph. D. Thesis, Utrecht (2000).
22. J. Paulhiac and O. Clause, *J. Am. Chem. Soc.*, 115 (1993) 11602
23. Cybulski and J. A. Moulijn, *Structured Catalysts and Reactors*, Marcel Dekker, New York, 1998, p.22.
24. R. W. Wyckoff, *Crystal Structures*, Wiley, New York, 1963-1971

Chapter 3

Synthesizing a carbon nano-fiber layer on a monolith support; Effect of nickel loading and formation conditions

Abstract

The work described in Chapter 2 is limited to demonstrate the possibility of immobilization of CNFs on the monolith support. This work describes the influence of the Ni particle size and formation conditions on the properties of the resulting material. It turns out that the thickness of the CNFs layer at the outermost surface (about 1 μm) as well as the diameter of the fibers increases with mean Ni-particle size. The structure of this layer resembles the inverse structure of a traditional inorganic support material, combining high surface area, high porosity and low tortuosity.

Synthesizing CNFs using methane leads to immediate fragmentation and doubling of the thickness of the washcoat independent on the amount of CNFs, forming a macro-porous composite layer of entangled alumina particles and CNFs with a typical diameter of 10-30 nm. Immediate fragmentation is due to the fact that some of the fibers are too thick for the pores in the washcoat. The total porosity decreases with the amount of CNFs whereas the surface area per gram monolith increases.

Large Ni particles are able to grow CNFs for longer times, resulting in detachment of the washcoat from the cordierite, which is caused by extensive formation of CNFs out of the washcoat. Furthermore, extended formation of CNFs inside the cordierite body causes disintegration of the monolith body when macro-pores are locally overfilled with CNF. Methane is preferred over ethene for forming CNFs because ethene forms CNF rapidly even on relatively large Ni particles, resulting in thick fibers up to 70 nm in the macro-porous cordierite, destroying the monolith.

Controlling both Ni particle size and Ni distribution as well as choosing the right activity of the hydrocarbon are essential to form CNFs washcoat without damaging the monolith structure.

1. Introduction

A typical heterogeneous catalyst contains an active component supported on a carrier. Catalyst carriers are high-surface-area materials to facilitate high dispersion of the active catalytic phase, resulting a high activity of the catalyst. However, a high surface area and high intrinsic activity are not sufficient; [1] high porosity of the support and low tortousity are vital to ensure the accessibility of the active sites, and to minimize concentration gradients in the catalyst particles. Gradients occur more easily in liquid phase because of relatively slow diffusion as well as the frequent occurrence of very low concentrations, when gasses have to dissolve in a liquid before they can reach the catalyst. As a consequence, the local concentrations at the active sites through catalyst particles vary, affecting reaction rates and selectivity [2].

Conventional technologies for heterogeneous catalytic reactions involving both liquid phase and gas phase comprise slurry reactors and trickle bed reactors. Reactions in trickle bed reactors easily end up in diffusion limitations because of the relatively large catalyst particle size (mm) that is necessary for hydrodynamic reasons. Catalyst particles for slurry reactors are much smaller (30 μm typically) and thus more suitable for fast reactions, at the expense of additional cost for catalyst separation.

CNFs are graphite materials, which can be catalytically produced by decomposition of a carbon containing gas over small metal particles like nickel, iron or cobalt. CNFs are potentially an alternative catalyst support because of their high surface area, combined with high macro porosity and low tortousity [3,4]. De Jong and Geus introduced the terms primary and secondary structures of CNFs. The primary structure is the bulk structure of the fibers and two variations are well known, i.e. fishbone versus parallel type CNFs. Secondary structure includes both single-fiber properties including diameter, length, shape (straight, bi-directional, twisted, or branched) and surface area, as well as the texture of particles formed out of entangled fibers [3,5]. No detailed study on the texture of the entangled CNFs composite structure is reported in literature.

So far, CNFs have been used as a catalyst support in the shape of powder exclusively [5-7]. The main problems encountered are agglomeration and filtration of CNFs powder [3]. This article reports the synthesis and structural characteristics of CNFs supported on macrostructured materials (e.g. monolith) [8-10] to avoid these problems. The preparation

of a thin and highly porous CNFs layer on monolith, preserving a large surface area to support a catalytically active phase, has been demonstrated in our previous work [11]. This work presents details on the development of CNFs porous ceramic composite materials. We aim on the preparation of a new type of washcoat with superior properties for application as catalyst support in liquid phase. The effect of Ni particle size and the experimental conditions applied to form CNFs on the genesis of the materials as well as the final structure will be revealed.

2. Experimental

2.1. Materials

Ceramic cordierite monolith samples (Length: 10 cm, Diameter: 10 mm, 600 cells per square inch, obtained from Degussa), bare (without washcoat), and with 17 μm average thickness of γ -alumina washcoat, were used. The cordierite monoliths without and with a washcoat are designated cord and Al_2O_3 -cord respectively.

Nickel (II) nitrate [$\text{Ni}(\text{NO}_3)_2 \cdot 6\text{H}_2\text{O}$] and ammonium nitrate [NH_4NO_3] (pure, Merck, Darmstadt) were used to prepare nickel solutions. Hydrogen and nitrogen gases with purity 99.999% (INDUGAS), methane with purity 99.995% (Hoek Loos) and ethene with purity 99.95% (PRAXAIR) were used for CNFs formation.

2.2. Characterization

The BET surface area, pore volume and pore size distribution were measured by N_2 adsorption-desorption at 77 K using ASAP 2400 (Micromeritics) instrument. Cordierite pore volume has been estimated to be $0.37 \text{ cm}^3/\text{g}$, assuming the density of cordierite equals 2.51 g/cm^3 [5,10]. The surface area and pore volume of the washcoat were estimated to be $100 \text{ m}^2/\text{g}$ washcoat and 0.33 cc/g washcoat respectively, neglecting the contribution of the cordierite. Average pore size of the washcoat was $13 \pm 4 \text{ nm}$.

Nickel loading on cord and Al_2O_3 -cord was determined with Philips X-ray fluorescence spectrometer (PW 1480).

Hydrogen chemisorption at 293 K in a home build set-up was used to measure nickel dispersion. Previous to the measurement, the catalyst was reduced at 873 K (5 K/min) for two hours in 20 % H₂, and subsequently evacuated for 1 hour at 873 K. Chemisorption measurements were performed as described in literature [12].

Nickel particle sizes on the γ -alumina washcoat were determined with TEM (Philips CM30), after the washcoat was gently scratched off from the Al₂O₃-cord.

Nickel particle sizes on cord and Al₂O₃-cord as well as the morphology of both CNFs and the support structure were studied with Scanning Electron Microscopy (SEM) (LEO 1550 FEG SEM) equipped with EDX analysis. The samples were cut either along or perpendicular to the channels allowing observation of the cross-section of the monolith walls. CNFs on the surface of the wall, in the γ -alumina washcoat, and in the cordierite along the cross-section of the wall were characterized.

2.3. Catalyst preparation

Nickel was deposited on cord and Al₂O₃-cord from a pH-neutral nickel solution (0.1 M) as described previously [13]. A 0.1 M solution of nickel nitrate was obtained by dissolving 29g of Ni(NO₃)₂·6H₂O and 80 g NH₄NO₃ into 1 L of water and adding 4 ml of ammonia solution (25 wt%). In order to prepare a sample with high nickel loading, a 0.5 M neutral nickel nitrate solution was used.

The monoliths were dipped (20 times/min) in the solution. Samples with different nickel loading were prepared by changing adsorption time and Ni concentration (Table 1). Then free liquid was blown out of the channels and the samples were dried over-night in air at room temperature and subsequently at 393 K for 2hrs with a ramp 1 K/min, followed by calcination in static air at 873 K for 2 hrs.

2.4. Experimental set-up for CNFs formation

CNFs formation was carried out in a quartz reactor with a porous quartz plate at the bottom to support the sample [5,11]. The sample was placed in the reactor, reduced in 20 % H₂ in N₂ (total flow rate 100ml/min). The temperature was raised (5.5 K/min) from room temperature to 973 K (two hours dwell time). Then it was decreased (5 K/min) to the desired temperature and CNFs were formed by a gas mixture containing 50 % CH₄ (or C₂H₄) and 10 % H₂ in N₂ (total flow rate 200ml/min).

Methane conversion was determined by on-line chromatographic analysis (Varian GC model 3700 equipped with a 15 m Q-Plot column). Finally, the sample was cooled down in N₂ to room temperature. The amount of carbon formed on the monolith was determined by measuring the weight increase.

3. Results

3.1. Characterization of Ni on monolith

The nickel concentration along the channels of the Al₂O₃-cord was found to be constant within 5% according XRF analysis. Furthermore, Figure 1 shows the Ni, Al and Si profiles at a cross-section of a wall in Al₂O₃-cord-Ni(3.0) analyzed with Scanning Electron Microscopy-Energy Dispersive X-ray analysis (SEM-EDX). The figure shows that within the alumina washcoat the Ni is evenly distributed because the Ni/Al ratio is constant within the experimental accuracy. The variations in the absolute intensities stem from difference in the surface roughness of the surface of the cross-section. Nickel loading in the cordierite was below the detection limit.

The Ni loading obtained varied from 0.4 to 3.0wt % for Al₂O₃-cord samples (Table 1), whereas Ni loadings on cord samples were much lower. Table 1 also presents average nickel particle diameters, calculated from hydrogen chemisorption. The average diameter of the nickel particles is shown to increase with Ni loading from 8 nm to 14 nm, although the differences for the lower loadings are rather small. The Ni surface area on cord samples was too low to give detectable adsorption of hydrogen, from which it can be estimated that the average nickel particle sizes is larger than 100 nm.

Figure 2.a shows a typical TEM micrograph of Ni particles in the washcoat of Al₂O₃-cord-Ni(3.0). Evaluation of 50 particles in 5 different micrographs revealed a mean particles size of 8 nm with a standard deviation of 3 nm. TEM micrographs did not show a significant difference between nickel particle size on the washcoat of Al₂O₃-cord-Ni(0.4) and Al₂O₃-cord-Ni(3.0). SEM micrograph in figure 2.b shows Ni on the cordierite of Al₂O₃-cord-Ni(3.0). Obviously no statements can be made on the particle size except that the Ni particles here are much larger than in the washcoat. SEM micrograph in figure 2.c shows even larger nickel particle between 20 and 200 nm for cord-Ni(0.8), i.e. in the absence of a washcoat.

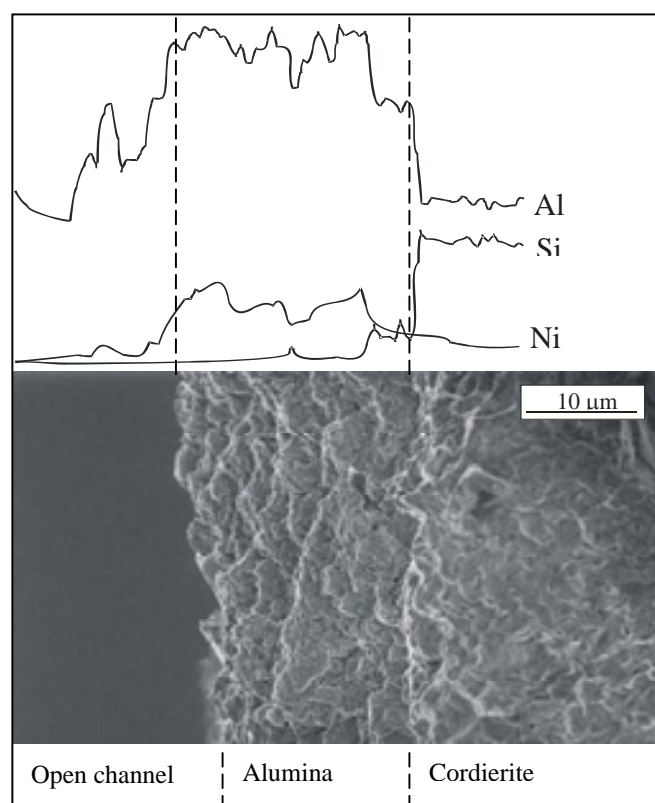


Figure 1: SEM-EDX on Al_2O_3 -cord-Ni(3.0) wall cross section.

Table 1: Amount of carbon nanofiber formed on monolith supports after 3 hrs as a function of nickel loading and hydrocarbon.

Monolith support	$[\text{Ni}^{+2}]$ (M)	Adsorption time (min)	Ni wt %	Avg. Ni particle size (nm)	CNFs wt% (g/g monolith)		Sample name
					CH_4	C_2H_4	
Washcoated cordierite	0.1	2	0.4	8 ± 1	1	11	Al_2O_3 -cord-Ni(0.4)
	0.1	6	0.5	8 ± 1	3		Al_2O_3 -cord-Ni(0.5)
	0.1	30	0.7	9 ± 1	6.4		Al_2O_3 -cord-Ni(0.7)
	0.1	180	1.2	10 ± 1	13.6	23	Al_2O_3 -cord-Ni(1.2)
	0.5	180	3.0	14 ± 1	30	31	Al_2O_3 -cord-Ni(3.0)
Bare cordierite	0.1	2	0.16	-			Cord-Ni(0.16)
	0.1	180	0.16	-			Cord-Ni(0.16)
	0.5	2	0.8	> 100			Cord-Ni(0.8)
	0.5	180	0.8	> 100			Cord-Ni(0.8)

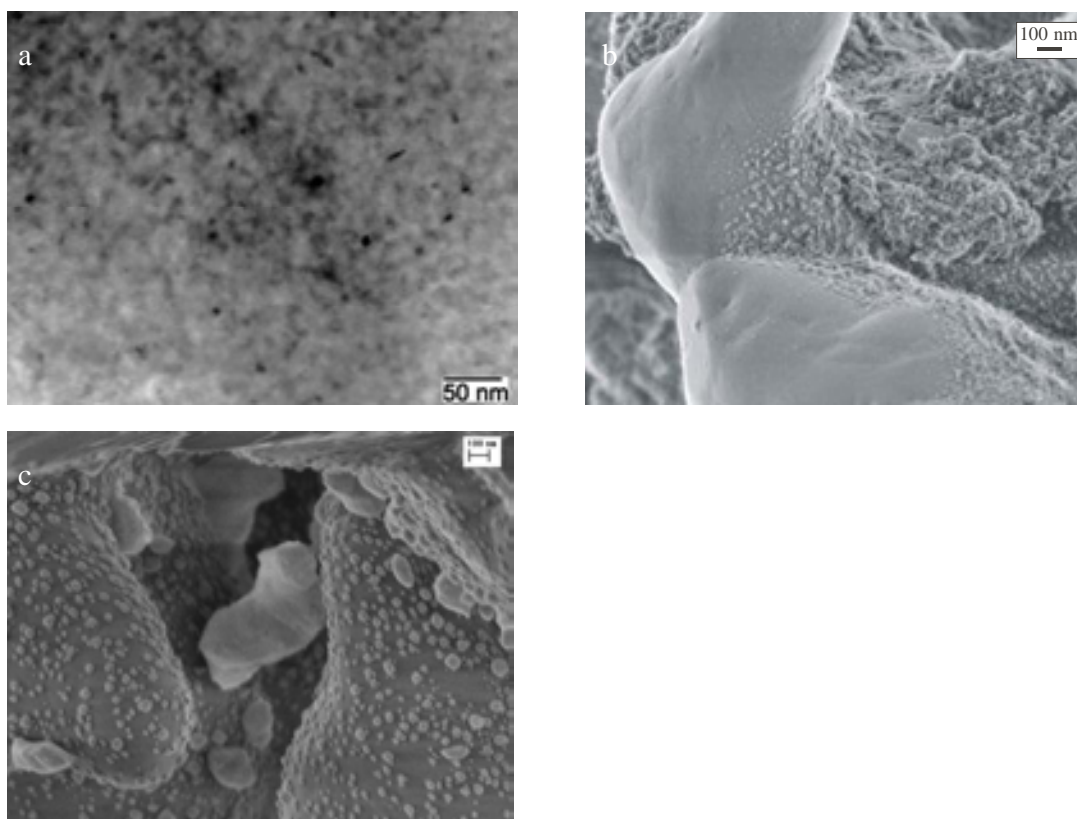


Figure 2: EM micrographs of monolith loaded with nickel, after calcination and reduction at 873 K for 2 hours.

- a: TEM image of alumina washcoat scratched off from Al_2O_3 -cord-Ni(3.0).
- b: SEM image of cordierite of Al_2O_3 -cord-Ni(3.0).
- c: SEM image of cordierite of cord-Ni(0.8).

3.2. CNFs formation on the monolith supports

The influences of three variables, i.e nickel loading, formation time, and hydrocarbon, on the kinetics of CNFs formation have been determined and the results are shown in Figure 3. The formation rates in figure 3a were calculated from the rate of methane conversion. CNFs formation from ethene causes initially complete conversion, followed by rapid deactivation; therefore the rates in figure 3b could only be estimated based on the amount of carbon formed, determined by the increase in weight. The maximum initial methane conversion on Al_2O_3 -cord-Ni(3.0) was not more than 30% and all other samples gave lower conversions. Therefore the transient in the methane concentration through the

reactor is limited and will not significantly influence the rate of formation of CNFs. Figure 3.a shows similar initial rates per gram nickel for all samples with exception of $\text{Al}_2\text{O}_3\text{-cord-Ni(3.0)}$. On the other hand it is clear that the rate of deactivation of the catalysts decrease with Ni loading.

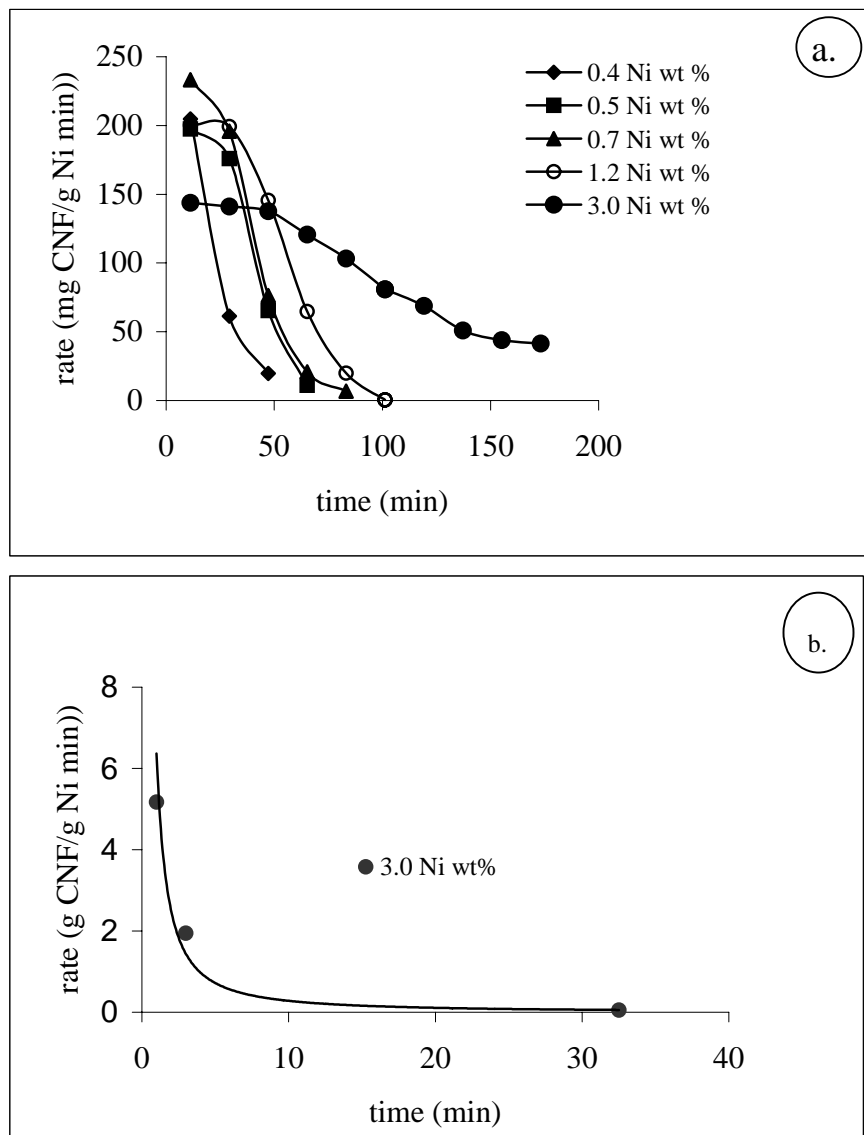


Figure 3: Carbon nanofiber (CNFs) formation rate at 843 K as a function of time on stream from 200 ml/min gas mixture containing 50 % CH_4 (a) or C_2H_4 (b), 10 % H_2 balance N_2 .

3.3. Structure of the CNFs

TEM revealed that the primary structure of all CNFs was fishbone-type (not shown). Both SEM and nitrogen physisorption were used to study the secondary structure of the fibers. Figure 4.a shows that the BET surface area increases monotonously with the CNFs amount, despite the fact that the observations in figure 4.a stem from different Ni loadings and formation-times. Figure 4.b shows that the total (meso and micro) pore volume decreased with the amount of fiber to about half of the original value. On the other hand, the micropore volume was found to increase with the amount of CNFs (figure 4.c). Microporosity is indicated by a positive intercept on the adsorbed volume axis of the t-plot at very low partial pressure [14,15]. Micropore volumes were calculated from the intercept using 0.807 g/ml as the density of liquid nitrogen.

The original values of pore volume, micro-porosity and BET surface area are restored when the carbon fibers are removed by oxidation at 973 K. Table 2 shows the physisorption results of Al₂O₃-cord-Ni(1.2) before and after oxidizing CNFs. It should be remarked that the numbers for the sample after burning the CNFs in table 2 are corrected for an apparent loss in weight of about 7%, caused by loss of some of the washcoat. Besides, removal of CNFs causes the structure of the composite to collapse.

Figure 5a shows that the surface area per gram CNFs slightly decreases with nickel loading for both methane and ethene, calculated from the data in figure 4a. CNFs prepared from methane has significant higher surface area per gram CNFs compared to ethene. Figure 5b shows that the surface area of the CNFs decreases with formation time when ethene was used, while only a weak effect was observed with methane. The surface areas were always in the range from 100 to 200 m²/g, which is typical for CNF's [3,4].

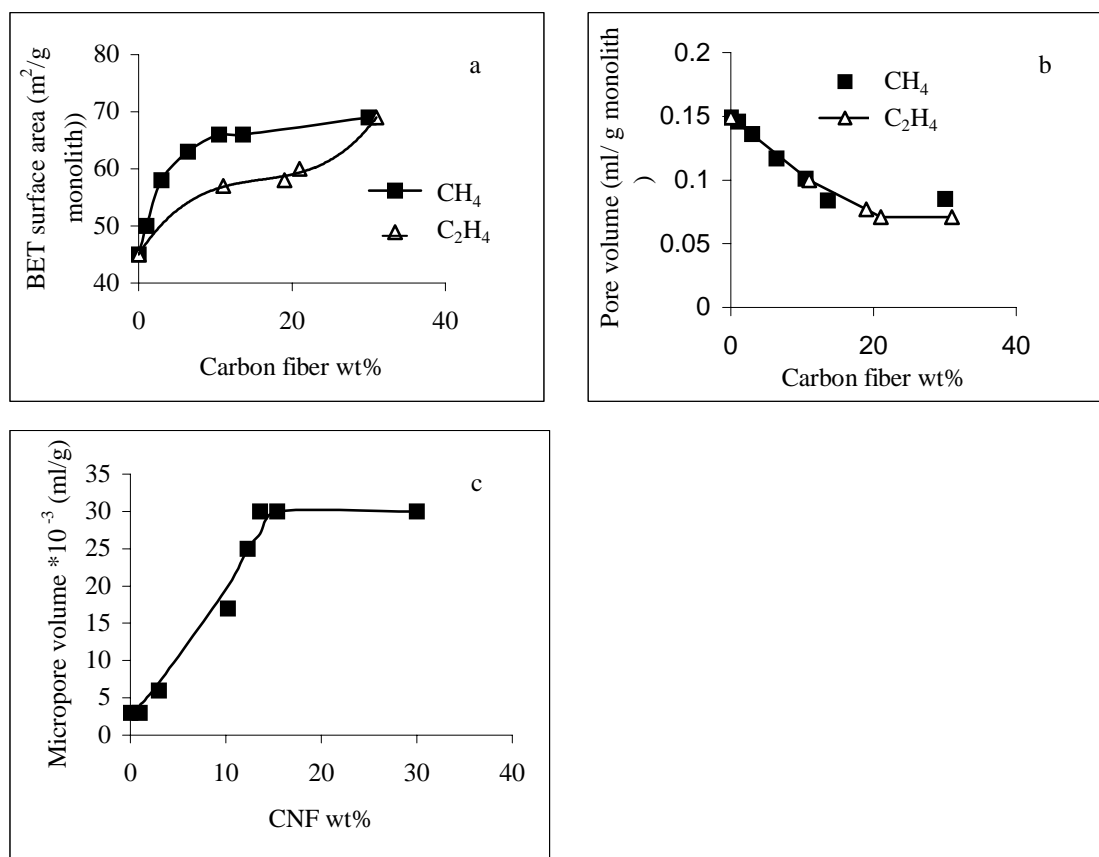


Figure 4: N₂-Physorption results of monoliths containing CNFs as a function of CNFs content. Formation conditions: 200 ml/min gas mixture containing 50 % CH₄ or C₂H₄, 10 % H₂ balance N₂ at 843 K. (a) BET surface area, (b) Pore volume, (c) Micropore volume calculated from t-plot

Table 2 Nitrogen adsorption desorption results of the ceramic support

Sample	BET surface area (m ² /g monolith)	Pore volume (ml/g monolith)	Micropore volume (ml/g monolith)	Average pore size (nm)	Washcoat surface area (m ² /g γ -alumina)
Cord	<1	-	-	-	-
Al ₂ O ₃ -cord (fresh)	45	0.149	.003	13 ± 4	100
Al ₂ O ₃ -cord after burning off the fibers	42	0.143	.003	13 ± 4	100

Growing a carbon nano-fiber layer on a monolith support; Effect of nickel loading and growth conditions

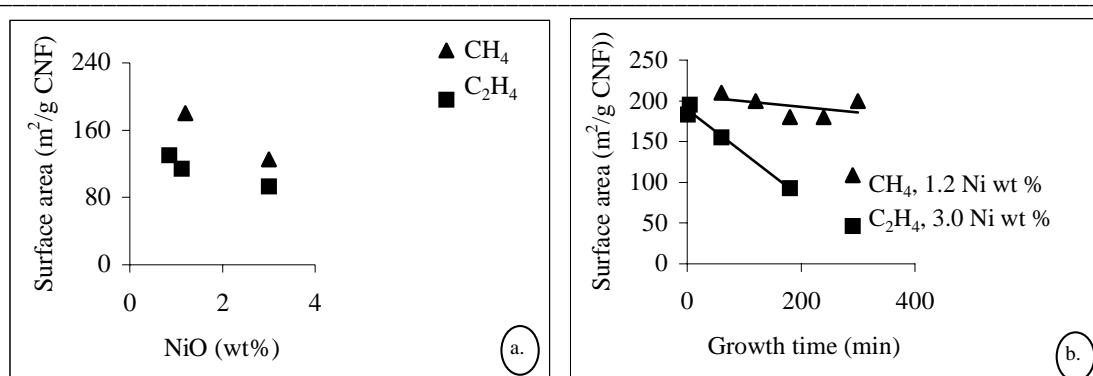


Figure (5) Surface area of CNF's, calculated from the increase in BET surface area of the samples as a function of Ni loading (a) and formation time (b). Formation conditions: 200ml/min gas mixture containing 50 % CH₄ or C₂H₄, 10 % H₂ balance N₂ at 843 K.

Figure 6.a is a typical SEM micrograph of CNF's in the washcoat, sized in the range of 10-30 nm. There is no significant difference in the size of CNF in the washcoat when nickel loading, hydrocarbon and formation time are varied. Also in the cordierite the same diameters of CNF's are observed in all samples, except for Al₂O₃-cord-Ni(3.0) after three hours exposition to ethene, where CNFs up to 70 nm thick were found in the cordierite as shown in figure 6.b.

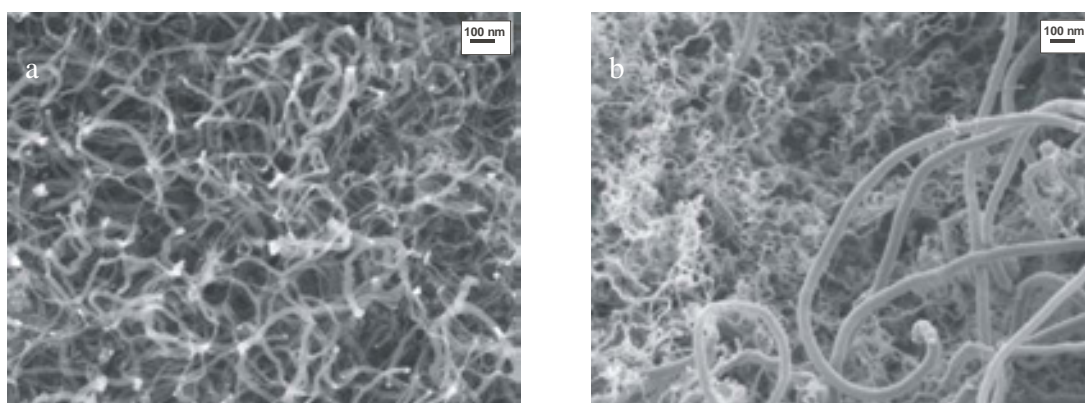


Figure 6: Scanning Electron Micrographs of CNF's on Al₂O₃-cord-Ni(3.0); Formation conditions: 200 ml/min 50 %CH₄, CNFs in the washcoat (a) or C₂H₄, CNFs in the cordierite (b), 10 % H₂ balance N₂ at 843 K for 3 hrs.

3.4. Structure of the monolith

A highly porous, homogenous, and thin layer of CNFs exclusively is always formed at the outside of the washcoat. Micrograph 7.a shows 0.5 μm CNFs layer can be formed when the Ni loading is less than 1 wt%. Micrograph 7.b shows the thickness of this layer increases to about 1 μm , when the Ni loadings in the range of 1.2 to 3 wt%.

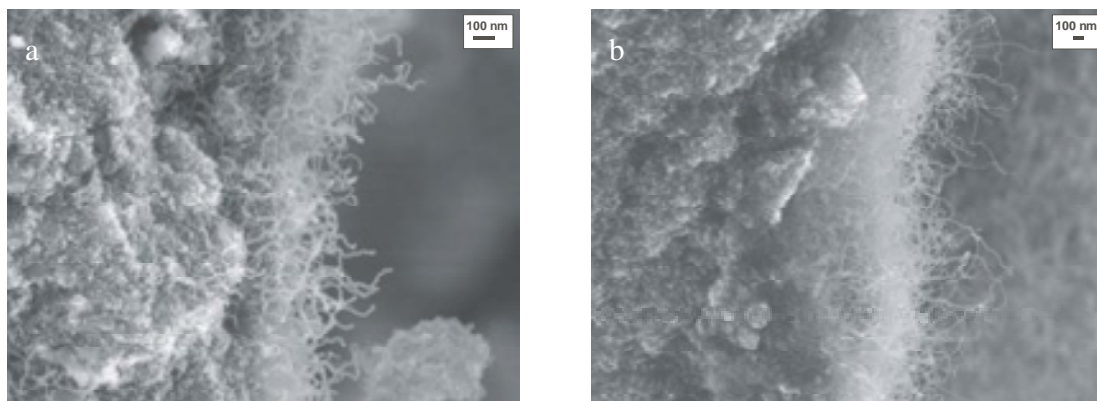


Figure 7: Scanning Electron Micrographs in side-view of the CNFs layer at the outer surface of Al_2O_3 -cord-Ni(0.7) (a) and Al_2O_3 -cord-Ni(1.2) (b); Formation conditions: 200ml/min 50 % CH_4 , 10 % H_2 in N_2 at 843 K for 3 hrs.

It was observed that the apparent thickness of the alumina washcoat always roughly doubled when using methane for three hours, independent of the Ni loading. Figure 8.a gives a typical example, while figure 1 shows the original thickness of the washcoat. It also shows that the washcoat was still attached to the cordierite and there are no cracks visible in the cordierite. Besides, the composite monolith is mechanically stable. The washcoat separated from cordierite only at high nickel loading (Al_2O_3 -cord-Ni(3.0)) using methane as shown in figure 8.b. Moreover, the same sample also contains cracks in the cordierite as shown in figure 8.c. The formation of cracks when using ethene was so extreme that the monoliths powdered completely in every experiment. Some bigger but fragile pieces were studied with SEM. Figure 8.d shows that the alumina washcoat was detached from the cordierite and the cordierite is severely cracked, independent on nickel loading and formation time.

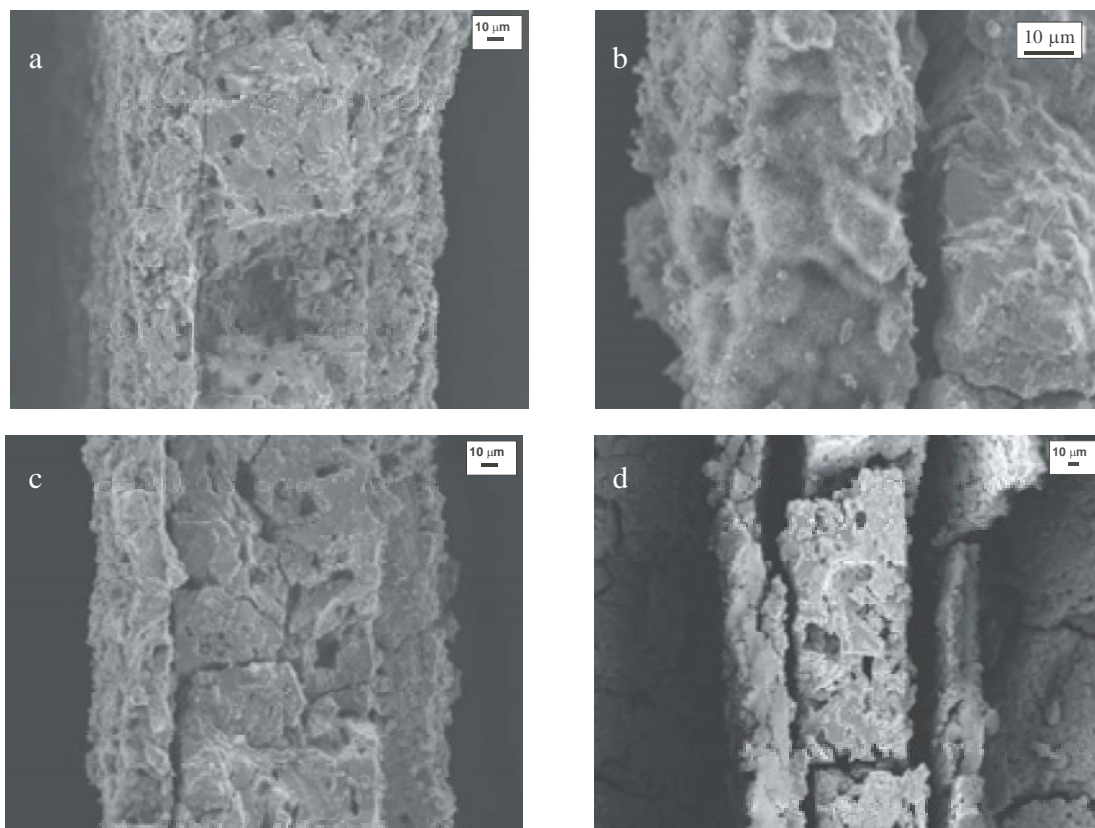


Figure 8: Scanning Electron Micrographs of side-views of a single wall of the monolith after CNFs formation at different formation times and nickel loadings. (200 ml/min 50 % CH₄ or C₂H₄, 10 % H₂ balance N₂ at 843 K). (a) Al₂O₃-cord-Ni(1.2), CH₄, (5 hrs), (b) Al₂O₃-cord-Ni(3.0), CH₄, (3 hrs), (c) Al₂O₃-cord-Ni(3.0), CH₄, (3 hrs) and (d) Al₂O₃-cord-Ni(3.0), C₂H₄, (1 min).

Figure 9 shows SEM micrographs of the cordierite body in Al₂O₃-cord-Ni(1.2) and Al₂O₃-cord-Ni(3.0). Al₂O₃-cord-Ni(1.2) contains much less fibers in the cordierite, as shown in figure 9.a, compared to Al₂O₃-cord-Ni(3.0) both when methane was used (figure 9.b). Ethene caused the presence of large amounts of CNFs in the cordierite even after formation for a short time only (figure 9.c). Moreover, image 6b shows that thick fibers are formed in the cordierite after long time.

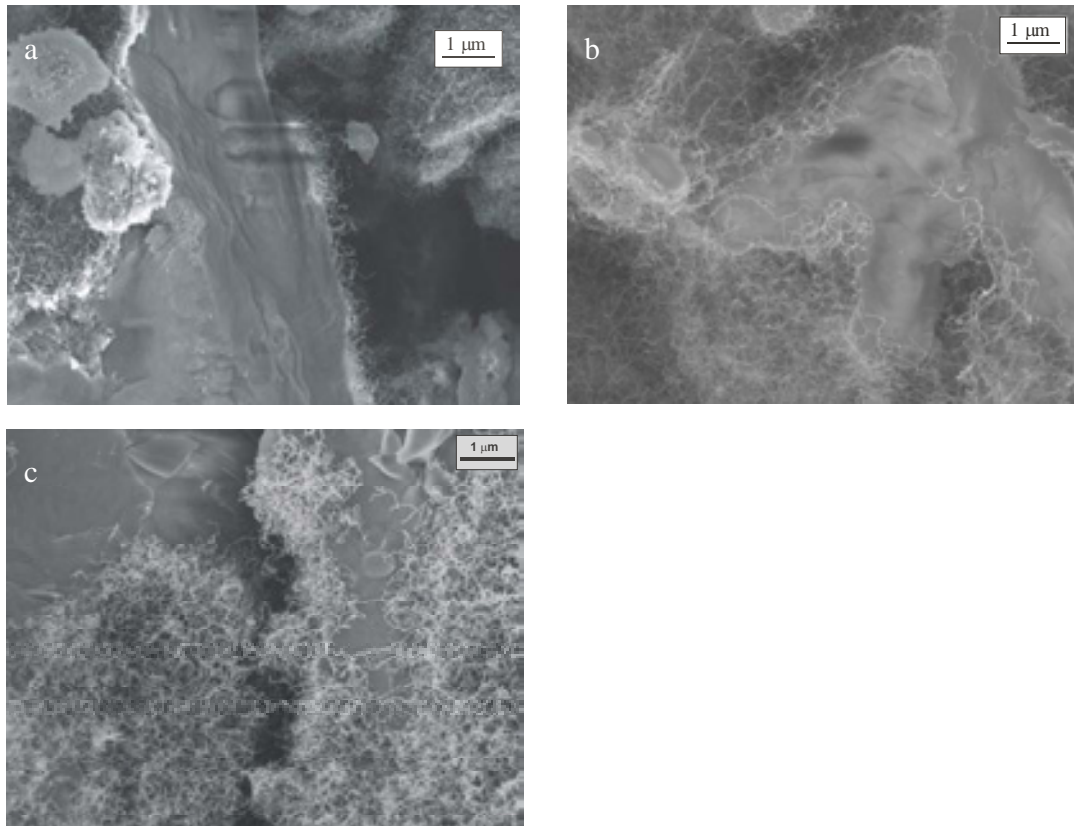


Figure 9: Scanning Electron Micrographs of CNFs in the macropores of the cordierite at different formation times and nickel loading. (200 ml/min 50 % CH₄ or C₂H₄, 10 % H₂ balance N₂ at 843 K). (a) Al₂O₃-cord-Ni(1.2), CH₄ (5 hrs), (b) Al₂O₃-cord-Ni(3.0), CH₄ (3 hrs) and (c) Al₂O₃ cord-Ni(3.0), C₂H₄, (1 min).

4. Discussion

First we will discuss the properties of the parent Ni catalysts and correlate these properties to the dimensions of the resulting CNFs. Finally we will discuss the structure of the CNFs-monolith composite as well as the mechanical integrity of the bodies.

4.1. Parent Ni catalyst

Nickel distribution through the washcoat (figure 1) and along the monolith channel (XRF) were well controlled. This caused formation of equally distributed CNFs along the monolith channel as well.

The mean metal particle size from chemisorption in Al₂O₃-cord-Ni(3.0) is 14 nm (Table 1), which is somewhat larger than the mean particle size observed with TEM (8 ± 3 nm) in the washcoat of this sample (Micrograph 2a). The reason for this is the fact that some of the Ni ends up in the cordierite in much larger particles as seen in figure 2b. The fact that no Ni signal was detected with EDX, as shown in figure 1, is because of the low Ni concentration in the cordierite as the surface area is very low. Nevertheless, Ni deposition on bare cordierite results in even larger Ni particles as can be seen in figure 2c. This suggests that the Ni concentration in the cordierite in the Al₂O₃-cord sample is lower than in the cord sample. This is in agreement with the fact that nickel loading on alumina is mainly controlled by adsorption and not by impregnation. Pore volume impregnation exclusively would have resulted in a Ni loading one order of magnitude lower than the loading obtained.¹¹ On the other hand, nickel loading on bare cordierite was in agreement with what one would expect from pore volume impregnation. Therefore, it is to be expected that during drying of the samples Ni is being transferred from the cordierite pores to the washcoat, as water evaporates for the washcoat exclusively. At the end the small Ni particles in the washcoat dominate.

4.2. Formation and structure of CNFs

From the data on surface area of the fibers in figure 5, one can estimate the mean CNFs diameter, assuming that the density of the fibers equals the density of graphite 2.3 g/cm³ [16]. Sample Al₂O₃-cord-Ni(1.2) with a mean Ni particle size of 10 nm forms CNFs from methane with averaged diameter of 10 ± 2 nm whereas CNFs of 17 ± 2 nm are formed out of 14 nm particles on Al₂O₃-cord-Ni(3.0). Obviously the size of the metal particles determines the diameter of the fibers, in agreement with other studies [17,18]. Correlating the length of CNFs to nickel particle size is less obvious. Simple geometric evaluation shows that $(CNF) \propto nLd^2$ and $(Ni) \propto nd^3$, where $(CNFs)$ and (Ni) are the amounts of CNFs and Ni, respectively; n is number of Ni particles which is assumed to be equal to the number of CNFs, L is the length of the fibers and d is the Ni particle diameter, which is observed to be equal to the diameter of the fibers. It follows that $\frac{(CNF)}{(Ni)} = \frac{L}{d}$. The area under the curves in figure 3 represents the amount of CNFs formed per gram Ni. Thus samples with larger particles (d) produce more $\frac{(CNF)}{(Ni)}$. Obviously, this calculation is a simplification of reality, assuming monodisperse Ni particles and CNFs with identical

length. Nevertheless, it can be qualitatively conducted that the length (L) must increase when the size of the Ni particle increases.

Ethene however produces CNFs with larger diameters compared to methane, especially when fibers were formed during a long period (figure 5b). This is at least partly caused by the formation of very thick CNFs (up to 70nm) in the cordierite under these conditions, as observed in micrograph 6b. However, it is possible that also the mean diameter of the CNFs in the washcoat increases concurrently. The local distribution of fibers with different diameters is unfortunately too inhomogeneous to allow accurate determination of the diameter of the fibers with SEM. Nevertheless, SEM shows typical CNFs diameters between 10 and 30 nm for all samples in the washcoat (figure 6a), which is in the same order as the diameters calculated from the BET surface area for CNF's prepared from both ethene and methane.

The observation that thick fibers in the cordierite are observed only after long times is due to the well known fact that large Ni particles cause slow formation of CNFs whereas they tend to deactivate much slower [3,19,20]. In the case of the more reactive ethene this causes very rapid formation of CNFs initially, followed by a rapid deactivation of small particles, where after only thick fibers continue to form (figure 6b). In the case of methane, the small particles survive longer, but large particles do not form at all. That also explains why the sample with the smallest Ni particle size (8 nm) deactivates relatively fast (figure 3a), leading to the lowest amount of CNFs per gram Ni at the end. Reasonable agreement was found between the amount of CNFs determined both by weight as well as by integrating the methane consumption in figure 2. Moreover, the relatively low initial activity for CNFs formation as well as the low extent of deactivation of sample Al₂O₃-cord-Ni(3.0) is qualitatively explained by the lower dispersion (14 nm) of this sample as well.

4.3. Structure of the CNFs-monolith composite

It was shown before that the formation of CNFs in the γ -alumina washcoat causes fragmentation of this layer, as well an increase in the apparent thickness (figure 8a). It is remarkable that the expansion factor is independent on the amount of CNFs. Apparently, small amount of CNFs causes the fragmentation and expansion, while most of the CNFs fill the created open volume between the fragments. This fragmentation starts at the beginning of the formation process, because CNF's diameter in the washcoat (10-30 nm) is larger than the γ -alumina washcoat pore size (5-20 nm). For example, fragmentation

could not be prevented even on Al₂O₃-cord-Ni(0.4), which has the smallest mean nickel particle size (8 nm) because a few CNFs with diameter larger than the pore diameter will cause fragmentation. This means that the CNFs diameter is controlling the fragmentation process.

Pore volume of the monolith decreased with the amount of CNFs as shown in figure 4b. However, the total volume of the body increased as the wash-coat expanded. One can estimate the pore volume of the composite layer, based on the thickness of the layer and amount of CNFs. For example, the total pore volume of the 1 wt% CNFs composite layer on Al₂O₃-cord-Ni(0.4) was estimated to be 1.3 ml/g. This number decreased to 0.8 ml/g for Al₂O₃-cord-Ni(3.0), which has 30 wt % CNFs. The composite layer is highly macroporous because these newly generated pores are not detected by N₂ adsorption. Moreover, micrograph 6a shows the macroporous properties of the layer. The macro pore volume decreases with the amount of CNFs since the expansion of the thickness of the wash-coat is independent on the CNFs amount. From the fact that the pore volumes and surface areas of the fresh monolith and of a monolith after oxidizing the fibers are close (Table 2), it can be concluded that fragmentation of the alumina wash-coat generates insignificant new surface area. This is in agreement with our observation reported earlier [9] that the fragments are sized in the order of microns at least, orders of magnitude larger than the sizes of the pores in the wash-coat.

The BET surface area of the monolith is found to increase with increasing amount of CNFs (figure 4.a) while the pore volume decreased concurrently (figure 4b). At the same time the micro pore volume increases (figure 4.c), whereas CNFs do not contain micropores [3]. These observations proof that a significant fraction of the CNFs formed fit tightly in the pores of the wash coat without fragmentation occurring. The fit is so tight that the remaining space between fibers and pore-walls introduces micro-porosity in the composite material.

From the point of view of application of these materials as catalyst support, the quest is to maximize the surface area as well as the total pore volume. These properties vary in opposite way with the amount of CNFs, implying the need to optimize the amount of CNFs. However, the amount of CNFs also needs to be limited in order to arrive at mechanically stable materials as will be discussed below.

Detachment of the composite alumina-CNFs layer from the cordierite occurs when the amount of CNFs is too high (Micrograph 8.b). Close inspection of the interface reveals the presence of a CNFs layer of 1 μm on the washcoat, identical to the CNFs layer at the outside surface of the composite washcoat layer. The detached face of the cordierite contains much less carbon fibers. Thus, CNFs formed out of the washcoat are responsible for the detachment of the composite washcoat from the cordierite.

Fragmentation of the cordierite occurs only after extensive formation of CNFs, in contrast to fragmentation in the washcoat, starting more or less instantaneously. This is caused by the large difference in pore sizes. The cordierite contains macro pores only implying that a single CNFs will never cause fragmentation because the diameter of the fibers is by far smaller than the size of the pores. In the cordierite, on the other hand, the pores are on average even slightly smaller than the fibers observed, as discussed before. Therefore, fragmentation in the cordierite will occur only when locally too many fibers are formed that cannot be hosted anymore in the macro-pores. Ethene therefore causes much faster fragmentation of the cordierite, independent of the Ni loading (Micrograph 8d), because the rate of formation of CNFs with ethene is extremely high (Table 1). Moreover, large Ni particles present in the cordierite can form CNFs only from ethene and not from methane. Therefore ethene results not only in faster formation of CNFs, it also causes formation of relatively more CNFs in the cordierite (Figure 9c) instead of in and on the surface of the alumina washcoat. Therefore, CNFs formed with methane destroy the cordierite only when a high Ni loading is combined with a long time to form CNFs (Micrograph 8c), which again is contributed to relatively large amounts of CNFs in the macro-pores in the cordierite (Figure 9b).

Finally, the thickness of the homogenous and thin CNFs layer at the outer surface along the monolith seems to increase with nickel loading. Micrograph 7a and 7b show that density of fibers (number/area) decreases with the thickness of the layer. The increase in the thickness is tentatively explained by the fact that length of the CNFs increases with increasing nickel particle size (section 4.2). The structure of this layer of entangled CNFs can be regarded as the inverse structure of a theoretical inorganic support material. In other words, it increases porosity and decreases tortuosity without compromising the surface area. Therefore this layer holds the most promise when used as washcoat for catalysts in liquid phase.

5. Conclusions

In this study we describe and explain how nickel particle size, the conditions to form CNFs as well as the pore-structure of the wash-coated monolith determine the structure and properties of CNFs as well as the morphology and mechanical strength of the resulting complex composite that contains cordierite, alumina and CNFs.

It turns out that the thickness of the CNFs layer at the outermost surface (about 1 μm) as well as the diameter of the fibers increases with the mean Ni-particle size.

Formation of CNFs using methane leads to immediate fragmentation and doubling of the thickness of the washcoat independent on the amount of CNFs, forming a macro-porous composite layer of entangled alumina particles and CNFs with a typical diameter of 10-30 nm. Immediate fragmentation is due to the fact that some of the fibers are too thick for the pores in the washcoat. The total porosity decreases with the amount of CNFs whereas the surface area per gram monolith increases.

Large Ni particles are able to form CNFs for longer times, resulting in detachment of the washcoat from the cordierite, which is caused by extensive formation of CNFs out of the washcoat. Furthermore, extended formation of CNFs inside the cordierite body causes disintegration of the monolith body when macro-pores are locally overfilled with CNFs. Methane is preferred over ethene for synthesizing CNFs because ethene forms CNFs rapidly even on relatively large Ni particles, resulting in thick fibers up to 70 nm in the macro-porous cordierite, destroying the monolith.

Controlling both Ni particle size and Ni distribution as well as choosing the right hydrocarbon are essential to form CNFs washcoat without damaging the monolith structure.

Acknowledgment

This work was performed under the auspices of NIOK, the Netherlands Institute of Catalysis Research. The authors gratefully acknowledge Degussa for supplying monoliths, we are grateful to Ing. J. A. M. Vrieling, Ing. V. Skolnik, dr. M. Smithers and

dr. R. Keim for XRF, BET, SEM, and TEM measurements respectively. We acknowledge Ing. B. Geerdink for technical support.

References

1. J. F. Le Page, Applied heterogeneous catalysis, TECHNIP, Paris, 1986, p. 3.
2. J. F. Jenck, Heterogeneous Catalysis and Fine Chemicals II Amsterdam, 1991, 1.
3. K. De Jong and J. Geus, Catal. Rev. – Sci. Eng., 2000, **42(4)** 481.
4. N. M. Rodriguez, J. Mater. Res., 1993, **8(12)** 3233.
5. M.S. Hoogenraad, Growth and Utilization of Carbon nano fibers, 1995, Ph. D. Thesis, Utrecht.
6. C. Pham-Huu, N. Keller, G. Ehret, L. Charbonniere, R. Ziesel and M. Ledoux, Journal of Molecular Catalysis A: Chemical, 2001, **170**, 155-163.
7. J. M. Planeix, N. Coustel, B. Coq, V. Brotons, P. S. Kumbhar, R. Dutartre, P. Geneste, P. Bernier and P. M. Ajayan, J. Am. Chem. Soc., 1994, **116**, 7935-7936.
8. M.T. Kreutzr, P. Du, J.J. Heiszwolf, F. Kapteijn and J.A. Moulijn, Chem. Eng. Sci., 2001, **56**, 6015.
9. T. A. Nijhuis, A. E. Beers, T. Vergunst, I. Hoek, F. Kapteijn and J. Moulijn, Catalysis Reviews, 2001, **43(4)**, 345-380.
10. A. Cybulski and J. A. Moulijn, Structured catalysts and reactor, 1998, Marcel Dekker, Inc. New York.
11. N. Jarrah, J. G. van Ommen and L. Lefferts, Catalysis Today, 2003, **79-80**, 29-33.
12. M. Pilar Gonzalez-Marcos, J. I. Gutierrez-Ortiz, C. Gonzalez-Ortiz de Elguea, J. A. Delgado, J. R. Gonzalez-Velasco, Applied Catalysis A: General, 1997, **162** 269-280.
13. J. Caillerie, M. Kermarec and O. Clause, J. Am. Chem. Soc., 1995, **117**, 11471.
14. R. A. van Santen, P. W. N. M. van Leeuwen, J. A. Moulijn and B. A. Averill, Catalysis: An Integrated Approach, Second, revised and enlarged edition, 1999, Elsevier, Amsterdam 550-565.
15. P. D. Mercera, Zirconia as a support for catalysts, preparation characterization and properties, 1991, Ph.D. Thesis, Twente.
16. Weast, R., CRC Handbook of Chemistry and Physics, 64th edition, CRC, Florida.
17. A. Oberlin, M. Endo and T. Koyama, J. Cryst. Growth, 1976, **32**, 335.
18. N. M. Rodriguez, A. Chambers, R. T. K. Baker, Langmuir, 1995, **11**, 3862.
19. M. L. Toebes, J. H. Bitter, A. J. van Dillen and K. P. de Jong, Catalysis Today, 2002, **76**, 33-42.
20. R. T. Baker, P. S. Harris, R. B. Thomas and R. J. Waite, J. Catal., 1973, **30**, 86.

Chapter 4

Immobilization of a layer of carbon nanofibers (CNFs) on Ni foam; a new structured catalyst support

Abstract

The work described in Chapters 2 and 3 is limited to CNFs attached to porous ceramic materials. This work describes the preparation of new materials with the required properties based on immobilizing carbon nanofibers (CNFs) on the surface of Ni foam.

CNFs were catalytically synthesized by decomposition of ethene over the Ni foam. The influence of formation conditions on the morphology of the CNFs, on the mechanical stability of the CNFs-Ni-foam composite structures and on the attachment of the CNFs to the Ni foam is discussed.

The surface area of the Ni-CNFs-foam composite increased with the loading of CNFs, from less than 1 m²/g to 30 m²/g for 50 wt% CNFs on the foam. The layer of the CNFs was highly open with a pore volume of 1 cm³/g CNFs.

Stable Ni-CNFs-foam composite structures can be obtained under the conditions that the extent of corrosive metal dusting of Ni is limited, via decreasing the temperature and/or the formation time. Some metal dusting is however needed to form small Ni particles that allow formation of CNFs.

The extent of corrosive metal dusting determines to what extent CNFs are weakly attached. The remaining CNFs, at least 80%, are remarkably strongly attached. Every single CNF is bonded to the Ni structure, probably via penetration of the CNFs into the polycrystalline Ni foam.

Controlling the conditions of CNFs formation is vital in order to optimize the mechanical stability of the CNF-Ni-foam composite structures as well as the strong attachment of the CNFs to the surface of the Ni foam.

1. Introduction

Carbon materials are frequently used as catalyst support because of high surface area and chemical inertness [1]. Recently, new graphitic materials, i.e. carbon nanofibers (CNFs), received increasing interest because highly porous aggregates can be formed. These aggregates have high surface area (100-200 m²/g) and high pore volume (0.5-2 cm³/g) without the presence of micropores [1,2]. These properties are favourable for a catalyst support material because sufficient surface area is provided in combination with high porosity and low tortuosity, thus maximizing the effective diffusion coefficient. This is particularly important in the application of heterogeneous catalysts in liquid phase. CNFs can be synthesized catalytically by decomposing hydrocarbon or CO over small metal particles like Ni [3].

So far CNFs have been mainly applied as catalyst support in powder form [1,2,4-6]. Application of such a fluffy powder in conventional catalytic reactors in liquid phase is problematic. Trickle bed operation will result in a high-pressure drop in the reactor, while slurry phase operation will encounter agglomeration of the fibre-particles as well as the need for filtration step [2].

Immobilization of CNFs on a support would overcome the disadvantages of agglomeration and tedious filtration. A structured support material is to be preferred in order to optimise hydrodynamics for operation in liquid phase. In our previous work, a washcoat of CNFs was synthesized on a monolith support [7,8]. Ledoux et al. [9] have synthesized CNFs on graphite felt. The graphite felt with the fibres was used to support iridium catalyst. This catalyst showed better performance for the extreme fast decomposition of hydrazine, compared to iridium on γ -alumina, due to the high external surface area of the fibers. In this work, Ni foam will be used as a structured support to immobilize the CNFs.

Ni foams are highly porous structured materials. Their structure resembles the inverse structure of a packed bed of dense spheres; the empty space between the spheres is filled with Ni, where after the spheres are removed thus creating the new macro-pores. The main disadvantage of metal foams is the low surface area (<1 m²/g), which limits their applicability as catalyst supports. Applying a uniform ceramic washcoat on Ni foams is difficult because of poor adhesion of the resulting coating [10]. However, Valentini et al. [11] prepared γ -Al₂O₃ washcoats on aluminium foam with good adherence. Detailed

information is not yet available, however it is clear that controlling the properties of the washcoat as well as the distribution through the foam is problematic. Therefore it is important to find alternative methods to create a highly porous layer on the surface of metal foams.

Synthesizing CNFs on Ni foam would be a new method to increase the surface area of the foam. On the other hand, it is well known that exposition of Ni to hydrocarbons at temperature between 400 and 800°C results in corrosion *via* metal dusting, i.e. fragmentation of polycrystalline Ni into small Ni particles [12-14]. To the best of our knowledge this is the first attempt to synthesize CNFs on Ni foams without destroying the foam. Huang et al. [15] have synthesized CNFs from Ni foam at temperatures between 550 and 700°C using acetylene, in an attempt to optimize the amount of CNFs per gram of Ni and thereby completely destroying the foam.

The aim of the present work is to explore the immobilization of CNFs on the surface of Ni foam. Therefore we studied the influence of the conditions used for CNFs synthesis on three critical properties: the surface area and the porosity of the CNFs layer, attachment of the CNF to the Ni-foam and the mechanical properties of the CNFs-Ni-foam composite.

2. Experimental

2.1. Materials

Figure 1 shows the typical morphology of the Ni foam (RECEMAT) applied in this study; it is a three dimensional network of connected strands. Each strand is shaped like a prism. The foams were sheets with a size of 20×10 cm² and a thickness of 5 mm. Cylindrical samples of Ni foam (10 mm in diameter) were prepared using wire-cut Electrical-Discharge Machining (AGIECUT CHALLENGE 2). It appeared that the apparent density of the foam varied ($\pm 25\%$) within the sheet, although the pore size was found to be constant. The variation in density is caused by variation in the thickness between 11 and 15 μ m of the Ni walls of the hollow strands. The geometric surface area per gram Ni was estimated to be less than 1 m²/g, based on the morphology of the foam described above and the bulk density of Ni metal (7.78 g/cm³).

Hydrogen and nitrogen (99.999%, INDUGAS), and ethene (99.95%, PRAXAIR) were used for CNFs formation without further purification.

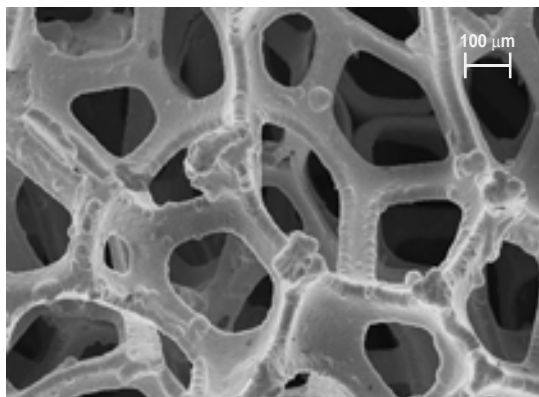


Figure 1: SEM micrograph of Ni foam (RECEMAT) as received.

2.2. Carbon nanofibers formation

CNFs formation was carried out in a quartz reactor with a porous quartz plate at the bottom to support the Ni foam [7,8]. A sample of about 0.4 g was reduced in 20 % H₂ in N₂ with total flow rate of 100ml/min. The temperature was raised (5.5°C/min) from room temperature to 700°C (two hours dwell time), where after temperature was decreased (5°C /min) to the desired temperature to form CNFs. Finally, CNFs were synthesized using a gas mixture containing 25 % C₂H₄ in N₂ (total flow rate 107 ml/min) at temperatures between 450 and 500°C.

Ethene conversion was determined with on-line chromatography (Varian GC model 3700 equipped with a 15 m Q-Plot column). The formation rate was calculated from the production rate of hydrogen, which was the only product in the gas phase. The maximum conversion of ethene in most cases was below 5 %. Therefore the ethene concentration does not vary significantly through the reactor and homogeneous formation of CNFs is to be expected.

Finally, the sample was cooled down in N₂ to room temperature. The amount of carbon formed on the foam was determined by measuring the increase in the weight caused by the formation of CNFs.

2.3. Characterization

After CNFs formation, each sample was blown with 100 L/min air stream for one minute, in order to clean the samples from any loose fibers before characterization.

Surface concentration of carbon on the fresh and reduced metal foam was studied using X-ray photoelectron spectroscopy (XPS, Physical Instruments Φ Quantum 2000).

BET surface area of CNFs was calculated from the N₂-adsorption isotherm, obtained at 77 K (ASAP 2400 Micromeritics).

The samples were studied (without destruction) with Scanning Electron Microscopy (SEM) (LEO 1550 FEG SEM) equipped with EDX analysis. The morphology of the CNF was studied using an in-lens detector. An SE2 detector, which is more sensitive to the higher energy secondary electrons, was used to detect areas rich in Ni.

The amount of loose CNFs was determined from the decrease in the weight of the foam when blowing the foam with air. The stability of the CNFs towards shear forces, which would be necessary when applied as catalyst support in liquid phase, was tested by flowing water through the foam at room temperature with a linear velocity of 1 m/s. The extent of loss of CNFs was calculated from the difference between the initial and final weight of the foam.

Temperature programmed hydrogenation (TPH) of the Ni foam after carbon deposition was performed in order to identify the type of the synthesized carbon. The temperature was raised (5°C/min) from room temperature to 1000°C. TPH was done using 50-vol% H₂ in Ar at a total flow rate of 50 ml/min. The products were continuously recorded using quadrupole mass spectrometer (Balzers QMG 420).

The mechanical stability (deformation) of the final composite structures was determined in a mechanical testing machine (Zwick 1 kN) with constant cross speed at 0.25 mm/min.

3. Results

3.1. Surface structure of original foam

The Ni foam was reduced with H_2 to convert any NiO on the surface of the foam into Ni metal, because metal oxides inhibit carbon deposition [16]. Micrograph 2a shows the surface of the Ni foam before reduction, while micrograph 2b shows the surface of the foam after reduction, both at two magnifications. The low magnification micrographs show grain sizes of 1 to 10 μm , which did not change significantly during reduction. The surface of the Ni foam before reduction was rough, showing the presence of some black spots. The black spots were analyzed with EDX to be carbon. The carbon is a remainder of the polymer, which was used to prepare the foam. Only Ni was detected with EDX on the rough surface. Micrograph 2b shows that the carbon spots have disappeared and that the surface was smoothed after reduction at 700 °C for 2 hours.

XPS analysis showed that the C/Ni atomic ratio decreased from 7 to 1 during reduction. This means that the reduction pre-treatment removed most of the original carbon from the surface of the foam.

Some facets appeared on the Ni surface after reduction (micrograph 2b). The restructuring of the Ni foam surface may be due to the fact that metal surfaces show adsorbate-induced restructuring when exposed to a chemisorbing gas like H_2 , or due to the removal of carbon, as it is known that 0.25 monolayer of carbon on Ni induces restructuring of the topmost Ni atoms [17].

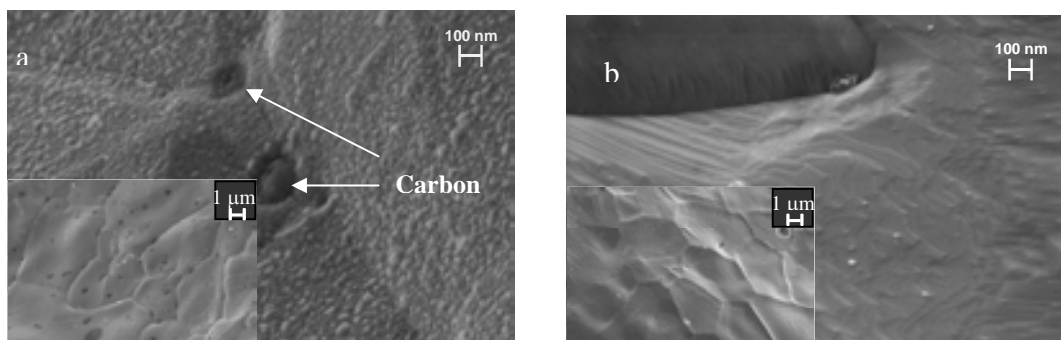


Figure 2: SEM micrographs of Ni foam. (a) As received, (b) reduced in 20 % H_2 in N_2 (100 ml/min) at 700 °C for 2 hour and passivated by 5 % air in N_2 at room temperature.

3.2. Carbon nanofibers formation on Ni foam

Figure 3 shows the formation rate of CNFs on Ni foam at different temperatures between 450 and 500 °C. The rate increased with time till a maximum value and then decreased. The maximum formation rate of CNFs was higher and was achieved faster at higher temperature. However, the formation rate of CNFs also decreased relatively fast at high temperature. The area under the curves in Figure 3 represents the amount of CNF (g CNF/ g Ni) formed at different temperatures. The amount of CNFs, calculated from figure 3, was in reasonable agreement ($\pm 15\%$) with the weight increase of the samples. However, the rates of CNFs formation were reproducible only with a typical variation of $\pm 25\%$, which is due to the inhomogeneity of the Ni foams as was mentioned in the material section.

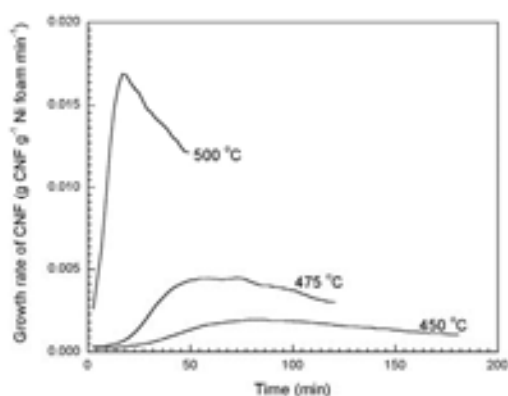


Figure 3: Formation rate of CNFs on Ni foam at different formation temperatures.

3.3. Structure of the CNFs

Micrograph 4a shows the structure of the Ni foam after synthesizing 25wt% CNF at 450°C for 2 hours. The mean characteristic width of the strand was $170 \pm 5 \mu\text{m}$, calculated from statistical analysis of 30 strands using micrograph 4a, as well as three other micrographs at different positions on the sample. Micrograph 4b is a typical micrograph showing the details of the CNF layer. A highly porous CNF layer with relatively thick fibers (40-70 nm) was observed.

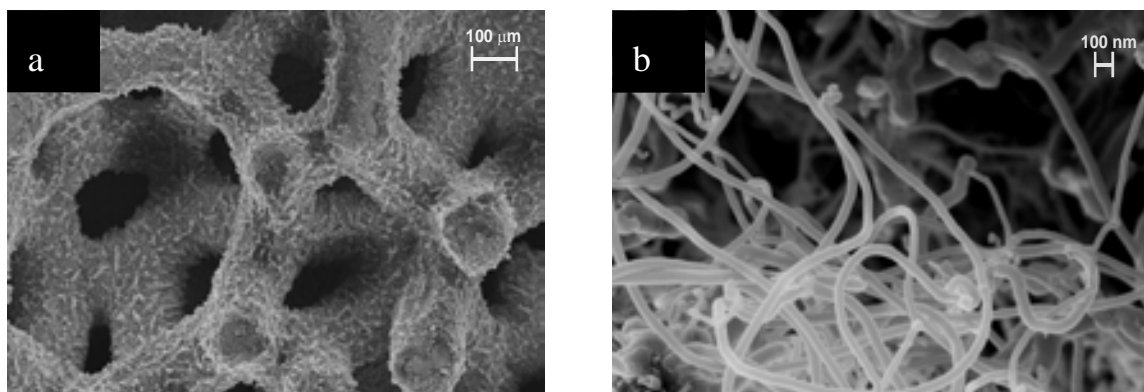


Figure 4: SEM micrographs of CNFs-Ni foam (a) loaded with 25 wt% CNF synthesized at 450°C after 2 hours (b) Details of the CNFs layer.

Figure 5 shows the temperature programmed hydrogenation (TPH) profile of the CNFs-Ni foam loaded with 25wt% CNFs (micrograph 4a). The only product observed was CH₄ (m/e = 16). Figure 5 shows a clear methane peak at 550°C and a very small peak at 330°C. Samples with lower CNFs loading (e.g. after 30 min of CNFs formation, see Figure 7) showed a small methane peak was observed at 550°C only and no peak could be observed at 330°C.

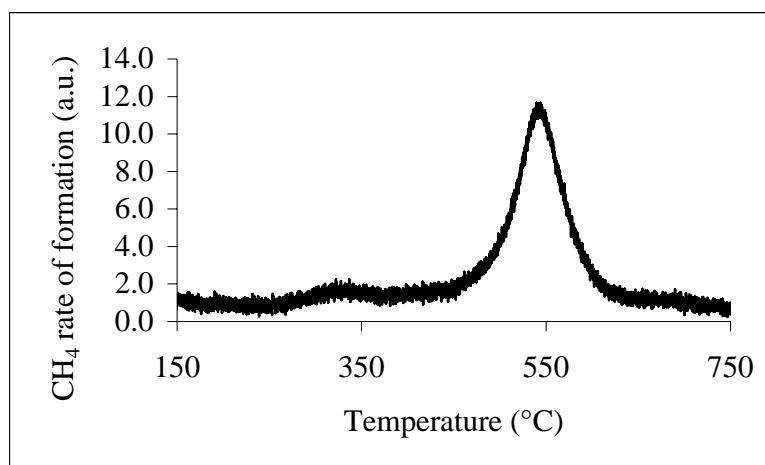


Figure 5: Temperature-programmed hydrogenation profile of CNFs-Ni composite, after 2 hours of CNFs formation at 450 °C. Heating rate: 5°C/min, flow rate: 50ml/min, 50vol% H₂/Ar.

Nitrogen physisorption and SEM were used to study the structure of the CNFs. From the BET surface area of the foam after formation of CNFs and the amount of CNF on each sample, the surface area per gram CNF can be calculated. Figure 6 shows that the BET

surface area of CNFs was $90 \pm 10 \text{ m}^2/\text{gCNFs}$, independent of the amount of CNF on the foam. However, the error margins of the surface areas of the three samples with CNFs less than 10wt% (Figure 6) is larger than $\pm 10 \text{ m}^2/\text{gCNFs}$ because the surface area of the whole sample is too low to be measured accurately. The amount of CNFs was varied either by using different formation temperatures (450, 475 and 500°C) for 0.5 hour, or by changing the time at 450°C .

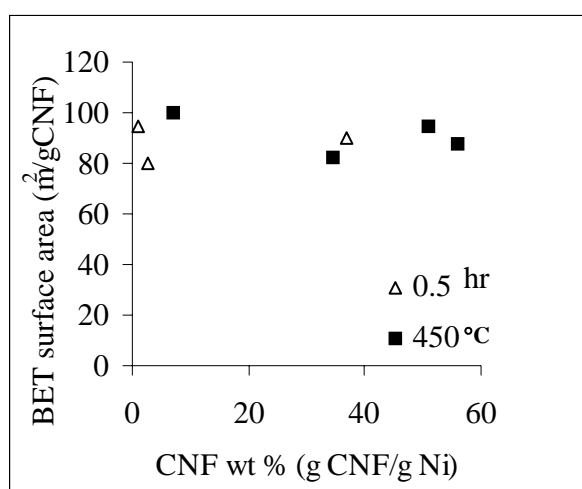


Figure 6: BET surface area of CNFs synthesized on Ni foam (!) at 450°C for different formation time, (8) at different formation temperature ($450\text{-}500^\circ\text{C}$) for 0.5 hr formation time.

Micrographs 7a and 7b represent the Ni surface after formation of CNFs for 0.5 hour at 450°C . The left hand side of micrograph 7a was taken using the in-lens detector, while the right hand side of the micrograph was taken using the SE2 detector. The left hand side of the micrograph shows a very rough surface with limited numbers of thick fibers (40-70 nm). The right hand side shows small features (20-100 nm) on the surface of the foam. The fact that these features look bright with the SE2 detector implies that these features are rich in Ni on a surface that contains a lot of carbon. Some of these features were found at the top of a CNF (1) or incorporated in a CNF (2); only a few of these particles are indicated in micrograph 7a. Micrograph 7b represents the same sample with higher magnification, showing the presence of very fine CNFs (10-20 nm) as well. Unfortunately, it was not possible to estimate the mean diameter of the CNFs and the mean size of the Ni features because of the heterogeneity of the surface structure of the samples.

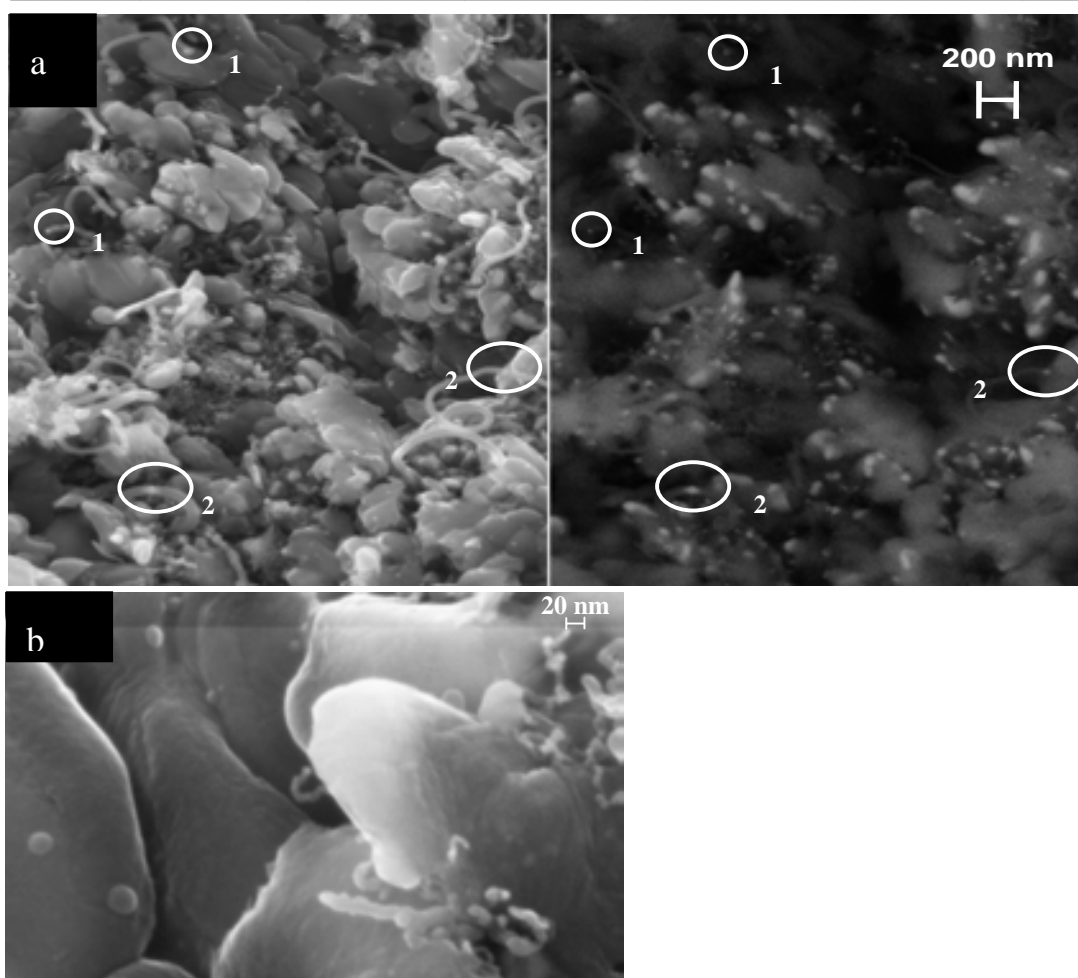


Figure 7: HRSEM micrographs of Ni foam after synthesizing CNFs for 0.5 hour at 450°C. (1) Ni particles at the top of CNFs, (2) Ni particles within the structure of CNFs.

3.4. Mechanical Stability

Mechanical integrity of the samples and strong attachment of the CNFs to the Ni surface are necessary for application of the CNF-Ni foam composite as structured catalyst support.

The foam collapsed completely when too many CNFs (138wt %) were synthesized, e.g. after 3 hours at 500 °C. Collapse of the foam could be circumvented by decreasing the amount of CNFs to 50 wt% (450 °C, 6 hours).

Mechanical properties of the integral foams were determined by measuring the critical compression stress, defined as the minimum pressure required to initiate deformation.

The samples showed plastic deformation. Figure 8 shows that the critical compression stress increased with the CNFs content.

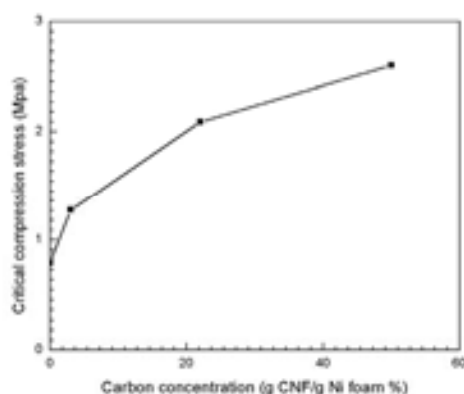


Figure 8: Critical compression stresses of CNF-Ni foam composite at 0.25 mm/min constant cross speed for different CNF contents, synthesized at 450 °C.

The initial loss of CNFs during cleaning with compressed air increased with CNFs loading and formation temperature (Figure 9). After the removal of the loose fibres, the attachment of the fibres against shear force was tested by flowing water through the foam with a linear velocity of 1m/s. No further loss of CNFs could be detected during 4 hours of applying the shear force to the composites after formation of 2, 8, 22 and 31wt% CNFs. Moreover, the composite with 22wt% CNFs was exposed to shear forces during 96 hours and no loss of CNFs could be detected.

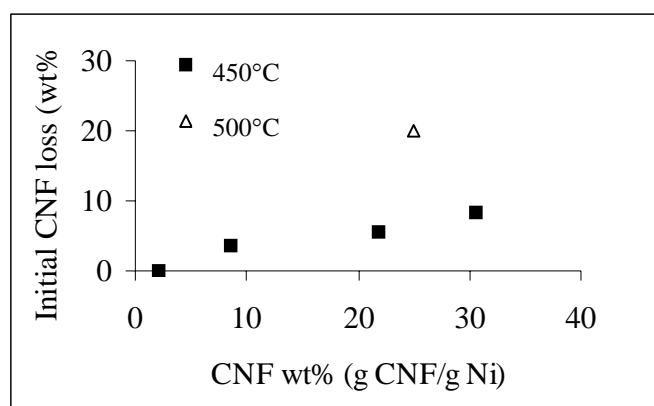


Figure 9: Initial losses of CNF (relative change in CNFs wt%) against shear forces caused by blowing the foam with 100 L/min air stream for 1 min.

4. Discussion

4.1. Structure of CNFs and the final composite

A catalyst support should have a high surface area to maximize the number of accessible active sites. Moreover, a high pore volume and large pore sizes of the support are particularly important in the application of heterogeneous catalyst in liquid phase reactions to decrease the tortuosity. Unfortunately, the surface area of a catalyst support increases when pore size decreases, which increases tortuosity and as a result mass transfer will be retarded. Thus, maximizing the surface area as well as the porosity of the CNFs layer is essential for applying these composite materials as catalyst supports. The surface area of the foam increased up to 30 m²/g in the case of 50 wt% CNFs. One can estimate the pore volume of the CNFs layer from the increase in the characteristic width of the strands, the CNF wt% and the densities of both graphite (2.3 g/cm³) and Ni (7.78 g/cm³). Thus, the pore volume was estimated to be 1 cm³/gCNF for the sample with 25 wt% CNFs shown in Figure 4.

The pore volume of the synthesized CNFs layer is in the higher range of the pore volume of γ -alumina, which ranges typically from 0.5 to 1 cm³/g [18]. Moreover, the voids between the CNFs (Micrograph 4b) are macropores and thus significantly larger than the typical mesopores that dominate in γ -alumina (3-12 nm) [18].

The initial morphology of the surface of the Ni foam, used to synthesize CNFs, is shown in Figure 2b. The morphology is typical for polycrystalline Ni, showing grains sized between 1 and 10 μ m. A rough surface with small Ni particles, sized in the range of 10-100 nm, formed (micrograph 7a) when the polycrystalline Ni surface was exposed to ethene at 450°C for 0.5 hour. Some of the Ni particles started to synthesize CNFs with diameters between 10 and 70 nm (micrographs 7a and 7b). The size of the Ni particles is significantly smaller than the size of the grains in the Ni foam. Thus, fragmentation of the Ni grains into small Ni particles occurs before CNFs start to form. Similarly, Kim et al. [19] have synthesized CNFs with diameters between 25 and 100 nm, starting with 1 μ m Ni particles using ethene. The authors concluded that fragmentation of the 1 μ m Ni particles into smaller Ni particles occurred prior to CNFs formation. The Ni particles observed in Figure 7 are probably involved in the formation of CNFs, despite the fact that some of the Ni particles are too large compared to the diameter of CNFs. We suggest that the relatively large Ni particles are fragmented further at a later stage, followed by the formation of CNFs. Park et al. [20] showed that thin CNFs with diameter less than 20 nm

were formed using ethane from Ni particles with a diameter larger than 60 nm supported on activated carbon. The authors also concluded that fragmentation took place of the large particles into smaller particles.

Figure 3 shows that the formation rate of CNFs at constant temperature initially increased, reached a maximum value and then decreased. In contrast, formation of CNFs using supported pre-shaped small Ni particles with a suitable size to form CNFs immediately, takes off with maximum rate immediately followed by deactivation [8]. The initial increase in the formation rate of CNFs on polycrystalline Ni is caused by the necessity of fragmentation of Ni grains into small Ni particles as shown in Figure 7. The rate of formation of Ni particles is apparently higher than the rate of deactivation of Ni particles, until the maximum rate of formation of CNFs is achieved. Then, deactivation of Ni particles dominates. The maximum formation rate of CNFs was achieved when the rate of formation of Ni particles and the rate of deactivation of Ni particles are equal.

Figure 3 also shows that the maximum rate of CNFs formation was higher and was achieved faster at higher temperature. On the other hand, also the deactivation was much faster at higher temperature. The overall rate of CNFs formation on polycrystalline Ni is determined by two factors: first, the number of Ni particles that allow CNFs formation and second, the intrinsic rate of CNFs formation for each Ni particle. The number of Ni particles contributing to the formation of CNFs is determined by the rate of generation of Ni particles *via* the fragmentation of Ni grains, as well as by the rate of deactivation of Ni particles due to encapsulation with carbon. It is generally agreed in metal dusting literature that the fragmentation rate of Ni grains into small Ni particles increases with temperature [21-23]. On the other hand, the deactivation rate of the Ni particles also increases with temperature during CNFs formation on pre-shaped Ni particles supported on γ -alumina [24]. It is known that the apparent activation energy of CNFs formation is 145 kJ/mol [3]. Despite the fact that the mentioned activation energy was measured for the decomposition of acetylene over Ni catalyst, it is generally agreed that the intrinsic rate of CNFs formation is controlled by diffusion of carbon through the Ni particle. This means that we can assume that the activation energy of CNFs formation using ethene is also 145 kJ/mol. The apparent activation energy using the maximum formation rates (Figure 3) at different temperatures was 200 ± 20 kJ/mol, which is significantly higher than 145 kJ/mol. Thus, the maximum formation rate of CNFs increases with temperature not only because of the increase in the intrinsic rate, but also because the number of active Ni particles at the maximum rate apparently increases with temperature.

The TPH of the CNFs that were synthesized on the Ni foam for two hours resulted in two peaks in the formation of methane at 330 and 550°C, respectively (Figure 5). The two methane peaks indicate that two types of carbon species were formed during the formation of CNFs. De Box et al. [26] studied the TPH of CNFs formed on 50wt% Ni/SiO₂ catalyst using 10vol% H₂/N₂. The author reported a main methane peak at 550 °C and a shoulder at 425°C. The main peak was attributed to CNFs, while the shoulder was attributed to amorphous carbon. Similarly, we may attribute the main methane peak at 550°C as shown in Figure 5 to CNFs, while the peak at 330°C is due to hydrogenation of amorphous carbon. The ratio of the area under the peak at 550°C to the area under the peak at 330°C was 25:1. Moreover, carbon formed after 30 min (Figure 7) could not be detected at all. Thus, it can be concluded that the amount of CNFs synthesized is by far dominating over the amount of amorphous carbon.

Micrographs 4 and 7 show that CNFs are formed with diameters varying between 10 and 70 nm, which is in the usual range of CNFs [2]. Ni particles are observed both at the top as well as within the CNFs, as indicated in micrograph 7a by (1) and (2), respectively. It is obvious that the diameter of the CNFs are controlled by the size of the Ni particles from which the CNFs are formed, similar to the formation of CNFs from pre-shaped Ni nano-particles supported on alumina [8].

SEM micrographs 7a and 7b showed the presence of both thin (10-20 nm) and thick fibers (40-70 nm) after 0.5 hour of CNFs formation, while mainly thick fibers (40-70 nm) were observed after 2 hours of CNFs formation (micrograph 4b). The mean diameter of the CNFs was calculated using the BET surface area per gram CNFs (Figure 6), assuming the density of the CNFs equals the density of graphite 2.3 g/cm³ [2]. The mean diameter of the CNFs was 22 ±2 nm, which is in the range of the smallest diameters observed with SEM. However, the mean diameter was constant, independent of the formation time and formation temperature. Obviously, the observations with SEM (Figure 7) and the BET data for samples with low CNFs loading, are not in conflict, despite the limited accuracy of the BET data. This implies that the layer of thick CNFs shown in Figure 4 must contain also thin CNFs, despite the fact that exclusively thick CNFs were observed in SEM micrographs. Moreover, it follows that the ratio between the amount of thin CNFs and the amount of thick CNFs is independent of time and temperature. As the thin CNFs are not observable with SEM (micrograph 4b), we suggest that the thin CNFs are located exclusively deep in the CNFs layer, close to the Ni surface. This explanation is reasonable under the assumption that the fast deactivation of small particles overrules the fast rate of formation of thin CNFs, as this would result in thin CNFs located close to the

Ni surface exclusively. It is known that small Ni particles form CNFs faster and also deactivate faster than large Ni particles [3,27]. On the other hand, the relatively large Ni particles grow slowly but steadily, thus generating long and thick CNFs that determine the morphology of the outer layer observed with SEM.

4.2. Stability of the final composite

The integrity of the Ni foam was lost after synthesizing 138 wt% CNFs at 500°C in 3 hours. On the other hand, the foams were stable after synthesizing 50 wt% CNFs at 450°C in 6 hours. The Ni foam collapsed at high temperature because of the increase in the rate of corrosive metal dusting with temperature as discussed above [21-23]. It is known that carbon precipitates and accumulates at defects (e.g. grain boundaries) in the Ni [28]. Accumulation of carbon in the grain boundaries may separate the grains and as a result the foam collapses. Similarly, Huang et al. [15] found that the amount of CNFs per gram Ni can be maximized by synthesizing at 550°C, completely destroying the foams.

Unexpectedly, the strength of the integral CNF-Ni-composite foams against deformation increased with CNFs loading below 50wt% (Figure 8). Moreover, the composites were not brittle and showed plastic deformation. Similarly, Olurin et al. [29], who studied the effect of the carbon content on the strength and ductility of nickel foams, have found that carbon migrates to the grain boundaries of Ni and increases the cohesive forces, resulting in an increase in the fracture strength. As opposed to metal dusting, it seems that dissolution of small amounts of carbon from ethene dissociation in the Ni foam increases the mechanical strength of the foam.

The other necessary feature for application is strong attachment of the CNFs to the surface of Ni foam. Figure 9 shows that the initial loss of CNFs during air cleaning increased with the amount of CNFs per gram Ni and with temperature. As mentioned above, the extent of metal dusting of Ni increases with temperature and with the amount of CNFs formed [21-23]. We suggest that this increase in the initial loss of CNFs is mainly due to increased metal dusting corrosion. However, more than 80% of the CNFs were stable during air cleaning. Moreover, no further loss could be detected when a shear force was applied by flowing water through the samples with a linear velocity of 1m/s. It was reported in literature that graphite fibers can penetrate through the Ni [12,13] and we suggest that this effect is responsible for the strong attachment. The fact that CNFs are strongly attached at very low CNFs loading formed at 450°C for 0.5 hour (micrograph

7a) is a strong support for the hypothesis that every CNF is attached to the Ni foam. This means that the entanglement between the CNFs is not responsible for the attachment of CNFs to the Ni surface.

We propose that carbon dissolution and segregation, Ni fragmentation and formation of CNFs proceed as schematically shown in Figure 10. Initially (a) carbon is deposited from ethene. This carbon (b) diffuses into the Ni grains and precipitates in the grain boundaries. This apparently increases the resistance of the Ni foam against deformation. Fragmentation of the Ni grains into small Ni particles started and CNFs start to form (c). Each CNF is attached to the Ni structure, probably *via* penetration of the CNF into the Ni foam. The formation of CNFs continues and new small Ni particles are formed, partly close to the connection of the early CNFs with the foam. As a result, the early CNF loses its attachment to the foam, so that these CNFs can be blown out (d). Even longer exposition to ethene causes extensive accumulation of carbon at the grain boundaries, which finally result in total disintegration of the grains *via* corrosive metal dusting (e).

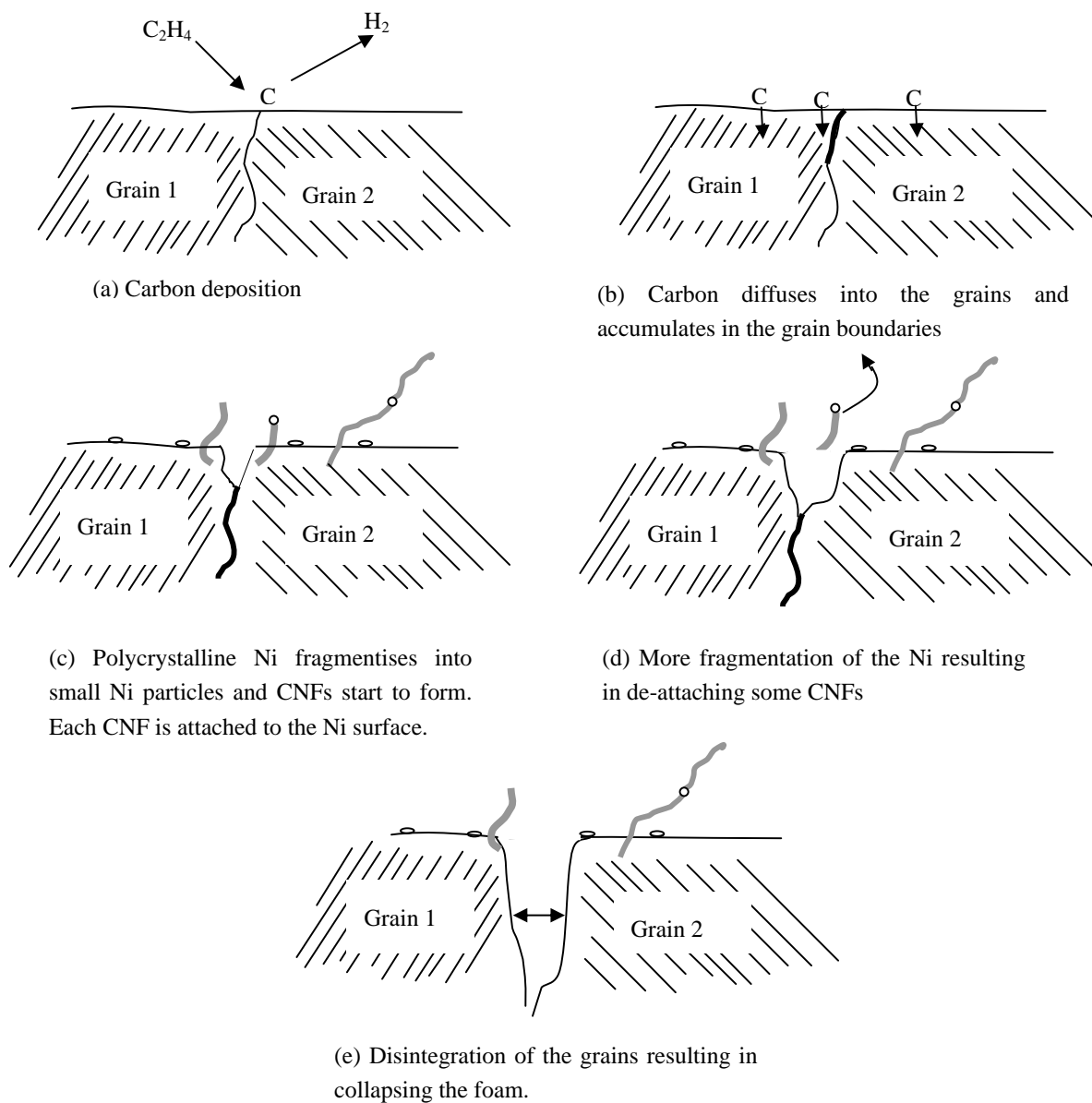


Figure 10: Proposed mechanism for the synthesis of CNFs on polycrystalline Ni.

5. Conclusions

In this study we describe and discuss a new method to increase the surface area of Ni foam by synthesizing an immobilized layer of CNFs on the foam surface using ethene. We studied the effects of formation conditions on three properties; the morphology of the CNFs layer, the mechanical properties of the CNF-Ni-foam composite and the attachment of the CNF to the Ni foam.

The surface area of the Ni-CNFs-foam composite increased with the loading of CNFs, from less than 1 m²/g to 30 m²/g for 50 wt% CNFs on the foam. The layer of the CNFs was macroporous with a pore volume of 1 cm³/g CNFs.

Stable Ni-CNFs-foam composite structures can be obtained under the conditions that the extent of corrosive metal dusting of Ni is limited, *via* decreasing the temperature and/or the formation time. Some metal dusting is however needed to form small Ni particles that allow formation of CNFs.

The extent of corrosive metal dusting determines to what extent CNFs are weakly attached. The remaining CNFs, at least 80%, are remarkably strongly attached. Every single CNF is bonded to the Ni structure, probably *via* penetration of the CNFs into the polycrystalline Ni foam.

Controlling the conditions of CNFs formation is vital in order to optimize the mechanical stability of the CNF-Ni-foam composite structures as well as the strong attachment of the CNFs to the surface of the Ni foam.

Acknowledgments

This work was performed under the auspices of NIOK, the Netherlands Institute of Catalysis Research. The authors gratefully acknowledge RECEMAT for supplying Ni foams, we are grateful to Ing. J. A. M. Vrieling for BET measurements, to Mr. A. van denBerg for XPS measurement and to dr. M. Smithers for SEM measurement.

References

1. P. Serp, M. Corrias and P. Kalck, *Applied Catalysis A: General*, 253, 2003, 337.
2. K. De Jong and J. Geus, *Catal. Rev. – Sci. Eng.*, 42(4), 2000, 481.
3. N. Rodriguez, *J. Mater. Res.*, 8(12), 1993, 3233.
4. A. Chambers, T. Nemes, N. Rodriguez and R. Baker, *J. Phys. Chem. B*, 102, 1998, 2251-2258.
5. C. Huu, N. Keller, G. Ehret, L. Charbonniere, R. Ziessel and M. Ledoux, *Journal of Molecular Catalysis A: Chemical*, 170, 2001, 155-163.
6. C. Huu, N. Keller, G. Ehret, L. Charbonniere, R. Ziessel and M. Ledoux, *Chem. Commun.*, 2000, 1871-1872.
7. N. Jarrah, J. van Ommen and L. Lefferts, *Catalysis Today*, 79-80, 2003, 29-33.
8. N. Jarrah, J.G. van Ommen and L. Lefferts, *Journal of Material Chemistry*, 14(10), 2004, 1590-1597.
9. R. Vieira, C. Huu, N. Keller and M. Ledoux, *Chem. Commun.*, 2002, 954-955.
10. Y. Matatov-Meytal and M. Sheintuch, *Applied Catalysis A: General* 231 (2002) 1-16.
11. M. Valentini, G. Groppi, C. Cristiani, M. Levi, E. Tronconi and P. Forzatti, *Catalysis Today*, 69, 2001, 307-314.
12. E. Pippel, J. Woltersdorf and R. Schneider, *Materials and Corrosion* 49, 1998, 309-316.
13. R. Schneider, E. Pippel, J. Woltersdorf, S. Strauß and H. Grabke, *Steel Research* 68 (7), 1997, 326-332.
14. C. M. Chun, T. A. Ramanarayanan and J. D. Mumford, *Materials and Corrosion*, 50, 1999, 634-639.
15. W. Huang, X. Zhang, J. Tu, F. Kong, Y. Ning, J. Xu and G. van Tendeloo, *Phys. Chem. Chem. Phys.*, 4, 2002, 5325-5329.
16. Holstein, W., *Ind. Eng. Chem. Res.*, 33, 1994, 1363-1372.
17. G. A. Somorjai, *Introduction to Surface Chemistry and Catalysis*, Wiley, New York 1994, p. 55.
18. R. L. Augustine, *Heterogeneous Catalysis for the Synthetic Chemist*, Marcel Dekker, Inc., New York, 1996.
19. M. Kim, N. Rodriguez and R. Baker, *J. Catal.*, 131, 1991, 60-73.
20. C. Park and M. A. Keane, *J. Catal.*, 221, 2004, 386-399.
21. H. Grabke, *Materials and Corrosion*, 49, 1998, 303-308.

22. H. Grabke, *Materials at high temperatures*, 17(4), 2000, 483-487.
23. C. Chun, J. Mumford and T. Ramanarayanan, *Journal of the electrical society*, 147(10), 2000, 3680-3686.
24. M. S. Hoogenraad, *Growth and Utilization of Carbon Nano Fibers*, Ph.D. Thesis, Utrecht University, The Netherlands, 1995.
25. J. G. McCarty, P. Y. Hou, D. Sheidan and H. wise, *ACS Symposium Series* 202, 253, 1982.
26. P. K. De Boks, A. J. H. M. Kock, E. Boellaard, W. Klop and J. W. Geus, *J. Catal.*, 96, 1985, 454.
27. R. T. Baker, P. S. Harris, R. B. Thomas and R. J. Waite, *J. Catal.*, 30, 1973, 86
28. Z. Zeng and K. Natesan, *Chem. Mater.*, 15, 2003, 872-878.
29. O. B. Olurin, D. S. Wilkinson, G. C. Weatherly, V. Paserin and J. Shu, *Composites Science and Technology*, 63, 2003, 2317-2329.

Chapter 5

Effect of the surface state of Ni foam on CNFs formation

Abstract

The work described in Chapter 4 was limited to the preparation of CNFs on the surface of polycrystalline Ni at different temperatures. This work describes in detail the effect of the morphology and surface properties, i.e. the Ni grain size, the coverage with NiO as well as the grain size of the NiO, on the formation of CNFs.

The formation of CNFs on polycrystalline Ni starts with the formation of meta-stable Ni₃C, which later decomposes into Ni and C. As a result, nano Ni particles are created with dimensions suitable for CNFs formation. Therefore, the rate of formation of CNFs on polycrystalline Ni becomes significant after the decomposition of the Ni₃C, thus forming the Ni nano particles.

The presence of a NiO layer increases the formation rate of CNFs one order of magnitude. NiO is apparently reduced in-situ and facile conversion of Ni nuclei to Ni₃C particles is responsible for the rapid formation of CNFs, as opposed to sluggish formation of Ni₃C particles from large (1-10 μm) Ni crystals.

1. Introduction

Carbon nanofibers (CNFs) are graphite materials that can be formed *via* catalytic decomposition of hydrocarbons or CO over small metal particles such as Ni [1]. The mechanism of CNFs formation and the properties of these materials have attracted great interest in different research areas. CNFs display unique mechanical and chemical properties that have motivated the search for applications in composite materials. Adding CNFs to the polymer materials induces electrical conductivity [2]. For catalytic applications, CNFs are attractive materials because these materials form aggregates with high surface area ($100\text{-}200\text{m}^2/\text{g}$), high pore volume ($0.5\text{-}2\text{ cm}^3/\text{g}$) without the presence of micropores [3]. These properties are favourable for a catalyst support material because sufficient surface area is provided in combination with high porosity and low tortuosity, thus maximizing the effective diffusion coefficient. This is particularly important in the application of heterogeneous catalysts in liquid phase.

On the other hand, the formation of CNFs was considered a serious problem because they are formed in a temperature range, where many important metal-catalyzed reactions are carried out, such as Fisher-Tropsch synthesis and steam reforming. CNFs are mechanically strong, so that the formation of these materials does not only destroy the catalyst, but may even damage the reactor wall [4]. Moreover, the formation of the CNFs cause an increase in the pressure drop and reduction of heat transfer properties due to fouling in reactors and heat exchangers, respectively [5-7].

Mechanistic studies have indicated that the formation of CNFs is catalyzed by transition metals or metal carbides, but not by transition metal oxides [8,9]. The inactivity of metal oxides was postulated to be due to either the lack of activity of metal oxides for cleavage of carbon-carbon bonds [10], or to the low solubility of carbon in several metal oxides [11]. However, reduction pre-treatment of metal oxides might not be necessary, as the oxides might be reduced in-situ with the hydrocarbons under the conditions of CNFs formation. Baker et al. [12] concluded that FeO, which was reduced using ethane and acetylene during CNFs formation, was one order of magnitude more active than Fe in the formation of CNFs.

In our previous study [13], we have shown that the formation of CNFs on polycrystalline Ni foams started with fragmentation of the Ni grains into small nano sized particles. We also have shown that the rate of CNFs formation increased when the number of active Ni

particles increased. In this study we explore the possibility to manipulate the yield, the stability and the morphology of CNFs *via* modifying the surface morphology of the Ni foam. Moreover, we studied the initiation of CNFs formation by following the changes in the surface morphology of the Ni foam with the time of formation in order to understand the mechanism of CNFs formation on polycrystalline Ni.

2. Experimental

2.1. Materials

The Ni foam (RECEMAT) applied in this study is a three dimensional network of connected strands. The foams were sheets with a thickness of 0.5 mm. The apparent density of the foam varied within the sheet ($\pm 25\%$) because of variation in the thickness of the walls of the hollow strands (section 2.1, Chapter 4). The geometric surface area per gram Ni was estimated to be less than $1 \text{ m}^2/\text{g}$ as described in Chapter 4.

Hydrogen and nitrogen (99.999%, INDUGAS), and ethene (99.95%, PRAXAIR) were used for CNFs formation without further purification.

2.2. Formation of carbon nanofibers

CNFs formation was carried out in a quartz reactor with a porous quartz plate at the bottom to support the Ni foam. Cylindrical samples of Ni foam (10 mm in diameter and 5 mm height) were prepared using wire-cut Electrical-Discharge Machining (AGIECUT CHALLENGE 2). A sample of about 0.4 g was used to form CNFs. Three pre-treatment procedures were done on the samples. First, samples were reduced at 500 or 700°C in 20 % H_2 in N_2 with total flow rate of 100ml/min. The temperature was raised (5.5°C/min) from room temperature to the reduction temperature (two hours dwell time). The reduced samples are designated as (red- reduction temperature in °C). Second, samples were oxidized in stagnant air at temperature range between 300 and 700°C. The temperature was raised (10°C/min) from room temperature to the oxidation temperature (one hour dwell time). The oxidized samples are designated as (oxid- oxidation temperature in °C). Third, a sample was oxidized in stagnant air at 700°C for one hour as described above and then was reduced in 20 % H_2 in N_2 with total flow rate of 100ml/min at 700°C for two hours dwell time. This sample was designated as (oxid- 700°C - red- 700°C). After the pre-treatment, the temperature was increased or decreased in the same gas mixture

used for the pre-treatment (5°C /min) to 450°C to form CNFs using 25 % C₂H₄ in N₂ (total flow rate 107 ml/min).

Ethene conversion was determined with on-line chromatography (Varian GC model 3700 equipped with a 15 m Q-Plot column). The formation rate was calculated from the production rate of hydrogen, which was the only product in the gas phase. The maximum conversion of ethene was always below 10%, unless a higher conversion is reported.

Finally, the sample was cooled down in N₂ to room temperature. The amount of carbon formed on the foam was determined by measuring the increase in the weight caused by the formation of CNFs.

2.3. Characterization

After CNFs formation, each sample was blown with 100 L/min air stream for one minute, in order to clean the samples from any loose CNFs before characterization.

Surface concentration of C on the fresh and reduced Ni foams was measured with X-ray photoelectron spectroscopy (XPS, Physical Instruments Φ Quantum 2000).

The structure of the samples was studied with X-ray diffraction (XRD) using a PANalytical X'pert-APD powder diffractometer system equipped with a position-sensitive detector with a 2 θ range of 120° using Cu K $_{\alpha 1}$ ($\lambda=1.78897$ Å) radiation.

BET surface area of CNFs was calculated from the N₂-adsorption isotherm, obtained at 77 K (ASAP 2400 Micromeritics).

The samples were studied with Scanning Electron Microscopy (SEM) (LEO 1550 FEG SEM) equipped with EDX analysis. The morphology of the CNFs was studied using an in-lens detector. An SE2 detector, which is more sensitive to the higher energy secondary electrons, was used to detect the distribution of Ni in the surface of the foam.

3. Results

3.1. Effect of pre-treatment on the surface morphology of the Ni foam

3.1.1. Effect of reduction pre-treatment:

Micrograph 1a shows the surface of the Ni foam before reduction, while micrographs 1b and 1c show the surface of the foam after reduction in H₂ for 2 hours at 500 and 700°C, respectively. The low magnification micrographs in 1a and 1c show grain sizes of 1 to 10 μm, which did not change significantly during reduction. The surface of the Ni foam before reduction was rough with carbon spots present as indicated in micrograph 1a [12]. The surface of the Ni foam after reduction at 500°C (micrograph 1b) is smoother than the surface of the fresh sample (micrograph 1a). However, reduction at 700°C resulted in further smoothening of the surface, although also some faceting could be observed (micrograph 1c). Moreover, carbon spots disappeared during reduction at 700°C.

XPS analysis showed that the C/Ni atomic ratio decreased from 7 to 1.4 after reduction at 500°C, while C/Ni ratio dropped to 1 after reduction at 700°C.

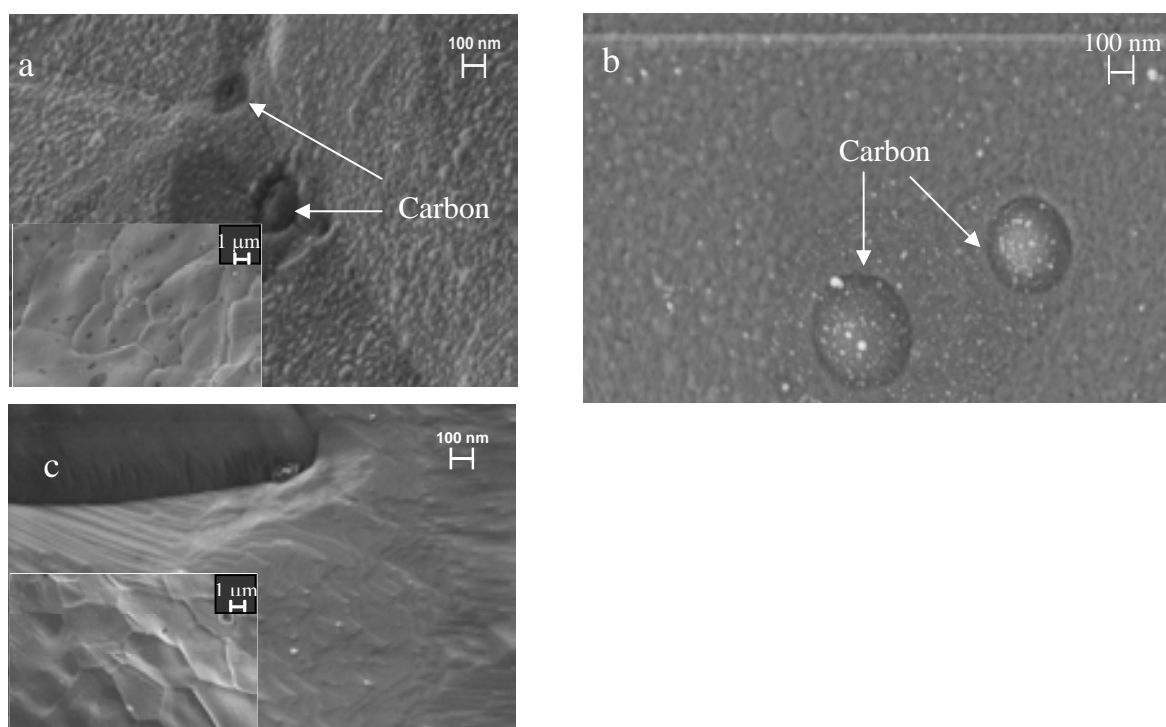


Figure 1: SEM micrograph of the surface of Ni foam: (a) as received, (b) after reduction at 500°C and (c) after reduction at 700°C.

3.1.2. Effect of oxidation pre-treatment:

The micrographs in Figure 2 represent the surface morphology of the Ni foam after oxidation in stagnant air for 1 hour at different temperatures. Three-dimensional features were created on the Ni surface during oxidation at 300°C as shown in micrograph 2a. Some of these features are small (20 to 40 nm) as pointed by (1), while also much larger features in the order of microns are observed, as pointed by (2). Micrograph 2b shows that most of the surface of the Ni foam is covered with a rough layer after oxidation at 500°C, whereas some areas of the Ni foam seem bare as pointed in (1). Micrographs 2c and 2d show that the rough layer is covering the surface completely at higher oxidation temperatures. However, oxidation of Ni foam at 700°C resulted in a smoother surface (micrograph 2d) compared to the surface of Ni foam oxidized at 600°C (micrograph 2c). Ni and oxygen were detected with EDX on the surface of every sample in Figure 2.

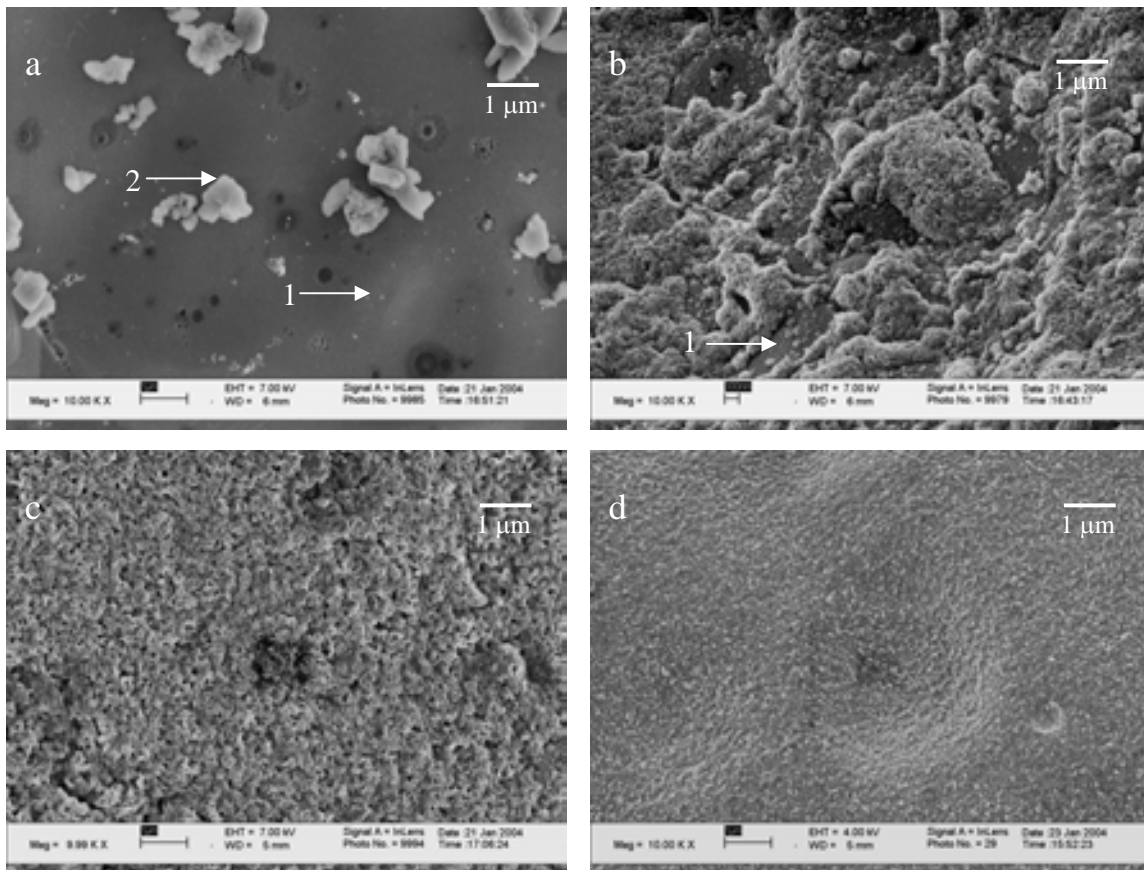


Figure 2: SEM micrographs of the surface of Ni foam after oxidation in static air for 1 hr. (a) oxid- 300°C, (b) oxid-500°C, (c) oxid-600°C and (d) oxid-700°C.

Figure 3 shows the XRD patterns of the Ni foam oxidized at different temperatures. Three Ni metal peaks were detected at 2θ positions of 44.5, 51.9 and 76.4 degrees. Three main NiO peaks were detected at 2θ positions of 37.3, 43.3 and 62.9 degrees. The intensities of the NiO peaks increased with oxidation temperature. NiO wt% was estimated using the reference intensity ratio (RIR) method [14], whereas NiO grain sizes were estimated using the Scherrer equation on the diffraction peak at 43.3°. The data in Table 1 show that the calculated NiO wt% from XRD data was in reasonable agreement with the NiO wt% calculated from the weight increase of the samples during oxidation. Moreover, It shows that both the weight percentage of NiO and the average size of the NiO grains increased with the oxidation temperature. It appeared impossible to estimate both the amount and the grain size of NiO formed at 300°C, as the intensity of the NiO peak was too low.

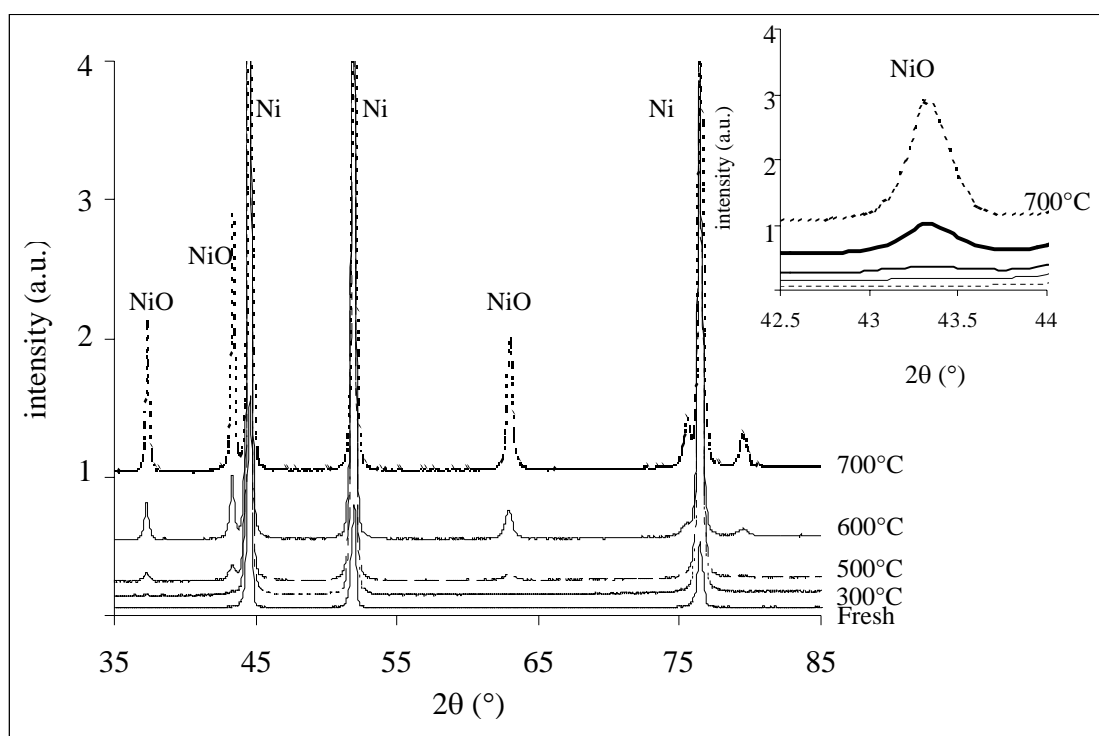


Figure 3: X-ray diffraction patterns of Ni foam at different oxidation temperatures.

Table 1: Amount of NiO and the average size of the NiO grains, estimated from XRD data using the NiO peak at 43.3° and the NiO wt% calculated from the weight increase of the foam.

Sample	NiO wt% (XRD)	NiO wt% (Weight increase)	Average size of NiO grains (nm)
Oxid-300°C	-	-	-
Oxid-500°C	1	2 (± 0.6)	28
Oxid-600°C	4	3 (± 0.3)	41
Oxid-700°C	18	15 (± 0.05)	76

3.1.3. Effect of oxidation followed by reduction pre-treatment:

Micrograph 4a shows a rough Ni surface containing holes after oxidation at 700°C and subsequent reduction at 700°C. Micrograph 4b shows a typical hole, which was full of carbon as analyzed by EDX. The size of the Ni grains around the hole shown in micrograph 4b was in the range of 0.5 to 3 μm and only Ni was detected outside the hole by EDX. It is clear that reduction of the NiO layer resulted in the formation of new grains of Ni, sized smaller than the original grains (1-10 μm) before pre-treatment (micrograph 1a).

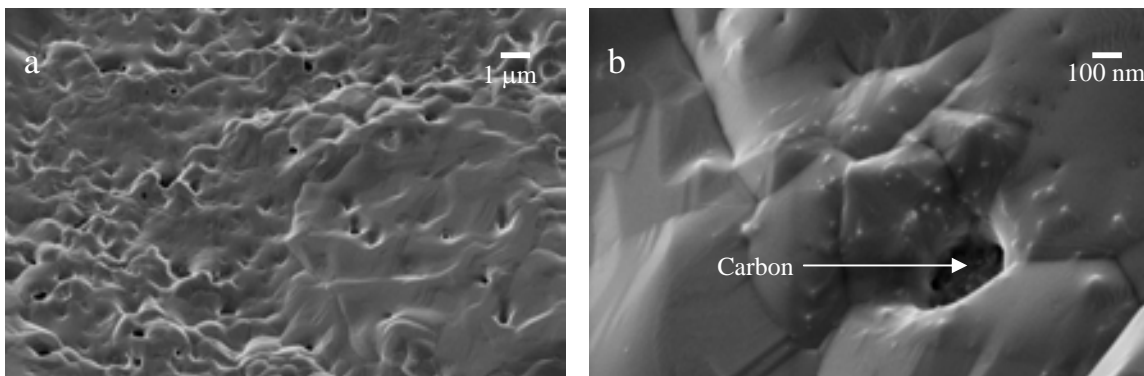


Figure 4: SEM micrographs of the surface of the Ni foam after oxidation at 700°C and reduced at 700°C. (a) low magnification, (b) high magnification.

3.2. Effect of the pre-treatment on the rate of CNFs formation

Figure 5a shows that the formation rate of CNFs decreased with increasing reduction temperature. Moreover, the rate of formation of CNFs took off earlier after reduction at lower temperature. Figure 5 also shows that the formation rate of CNFs was higher on the sample oxidized before reduction compared to the sample that was reduced at 700°C without prior oxidation.

Figure 5b shows that the formation rate of CNFs increased with oxidation temperature; the foam was not pre-reduced with H₂ in these experiments. The initiation of CNFs on the oxidized samples (Figure 5b) was faster than on the pre-reduced ones (Figure 5a). The formation rate of CNFs on the oxidized samples (Figure 5b) was one order of magnitude higher than the rate on the pre-reduced samples (Figure 5a).

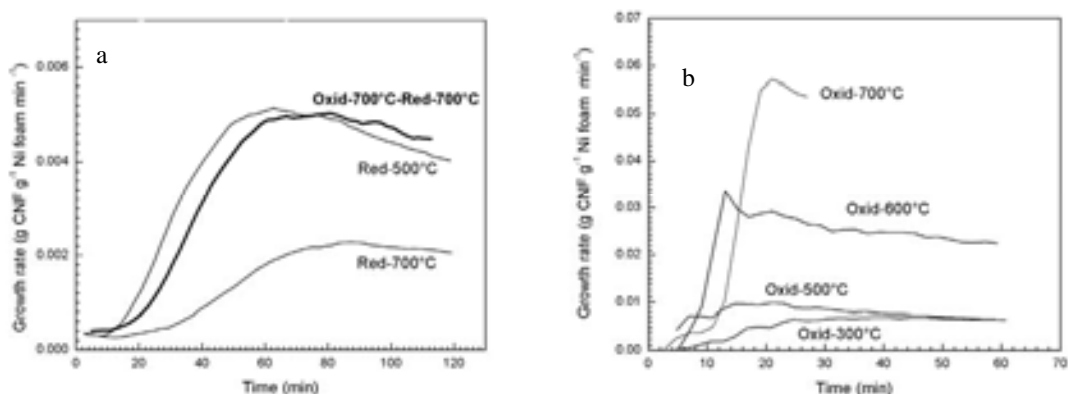


Figure 5: The formation rates of CNFs on Ni foam (a) reduced, (b) oxidized at different temperatures. Formation conditions: 25 % C₂H₄ in N₂ (total flow rate 107 ml/min) at 450°C.

3.3. Effect of the pre-treatment on the structure of the synthesized CNFs

The foams oxidized at 600 and 700°C without pre-reduction with H₂, collapsed completely after the formation of CNFs for 2 hours and 1 hour, respectively. On the other hand, all the other samples did not collapse. Micrograph 6a is a typical micrograph showing the details of the CNFs formed on these samples. The diameter of the CNFs was between 40 and 70 nm. On the other hand, micrograph 6b is a typical micrograph of CNFs formed on a collapsing foam. Obviously, again CNFs with diameters between 40 and 70 nm are observed, but additionally much smaller CNFs were present as indicated in the circle in micrograph 6b.

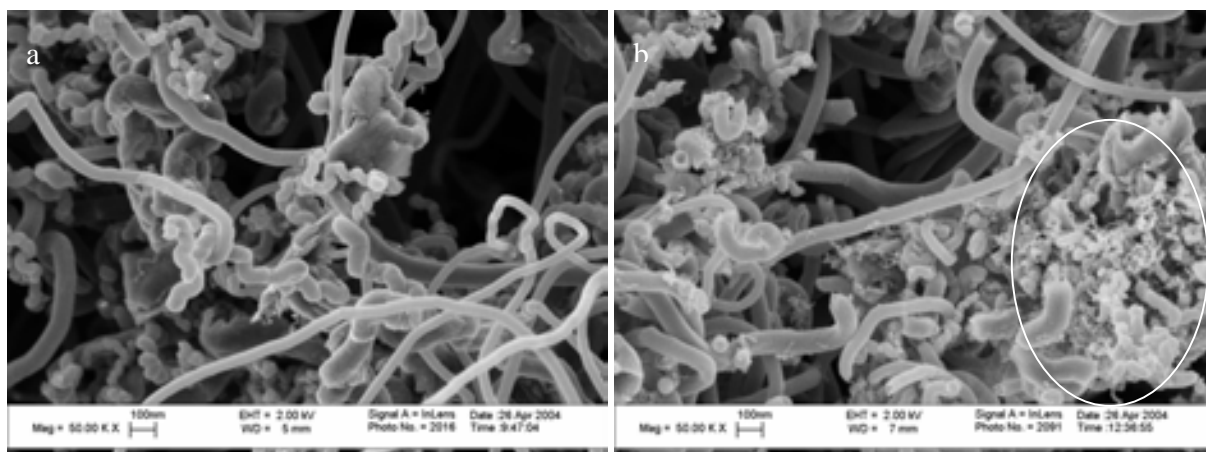


Figure 6: SEM micrographs of CNFs formed on Ni foam at 450°C. (a) oxidized at 500°C (Ni foam did not collapse) and (b) oxidized at 700°C (Ni foam collapsed).

The BET surface area of the CNFs was calculated using the BET surface area of the foam after formation of CNFs and the amount of CNFs on each sample, assuming exclusively CNFs were formed. We have shown that this assumption is reasonable (Chapter 4). Figure 7 demonstrates that the BET surface area of the CNFs was $90 \pm 10 \text{ m}^2/\text{g}$ CNFs, independent on the pre-treatment conditions.

3.4. Effect of the time of formation on CNFs

The initiation of the formation of CNFs on Ni foam was investigated by exposing the Ni foam to the gas mixture for short periods of time, where after the changes in the surface morphology of the foam were characterized. The Ni foam reduced at 700°C was chosen for this part of the study because of the slow kinetics of the CNFs formation in the first 30 minutes as shown in Figure 5a. The slow kinetics allows following the changes on the Ni surface before the surface of the Ni foam is completely covered with CNFs.

The micrographs in Figure 8 show the changes in the surface morphology of the Ni foam after different times of reaction. Micrograph 8a shows that strips with a dimension of $100 \times 200 \text{ nm}$ were formed on the surface of the Ni foam after 1 min of reaction at 450°C. After 5 minutes of reaction, limited numbers of CNFs were formed on the surface of the Ni foam as pointed in micrograph 8b. The morphology of the Ni surface did not change significantly after 10 minutes of reaction (not shown). More CNFs were formed and accumulated on the surface of the foam after 20 min (micrograph 8c). Micrograph 8d represents the surface of Ni foam after 30 minutes of reaction. The left hand side of

micrograph 8d was taken using the in-lens detector, while the right hand side of the micrograph was taken using the SE2 detector. The left hand side of the micrograph shows a very rough surface with some CNFs. The right hand side shows small Ni particles (20-100 nm) on the surface of the foam, as discussed in Chapter 4. CNFs and fragmented Ni particles were observed on the surface of the Ni foam after 1 and 2 hours of CNFs formation, as micrographs 8e and 8f show.

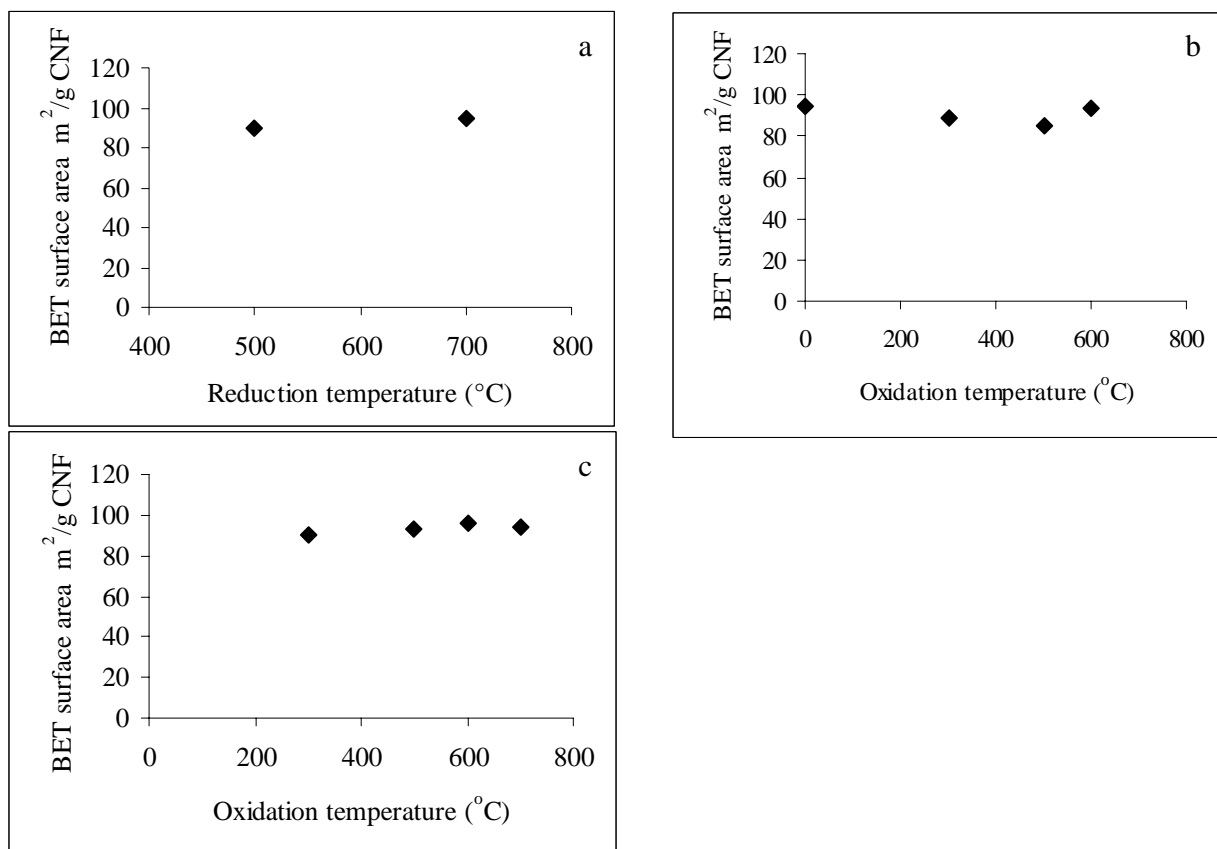


Figure 7: BET surface area of CNFs synthesized on Ni foam after (a) reduction, (b) oxidation and reduction 700°C and (c) oxidation at different temperatures.

Figure 9a shows a series of XRD patterns of Ni foams reduced at 700°C and after formation of CNFs for 10 and 120 minutes. The patterns in Figure 10a show five Ni metal diffraction peaks at 2θ positions between 40 and 100 degrees. Neither the shape nor the intensity of these peaks varied with the formation time. A graphite peak was recorded after 120 minutes of CNFs formation at 2θ position of 26 degrees. Figure 9b shows that the graphite peak can be observed only after at least one hour of formation. On the other hand, four peaks with low intensities were detected at 2θ positions of 39.3, 41.6, 58.6 and

72.3 degrees after 10 min of CNFs formation, as pointed in rectangles in figure 9c. These diffraction peaks are assigned to Ni_3C that started to form after 1 min of reaction as pointed in the circles in Figure 9c. The intensity of the Ni_3C peaks continues to increase in the first 10 minutes of CNFs formation, where after the Ni_3C peaks totally disappeared after 20 minutes of reaction.

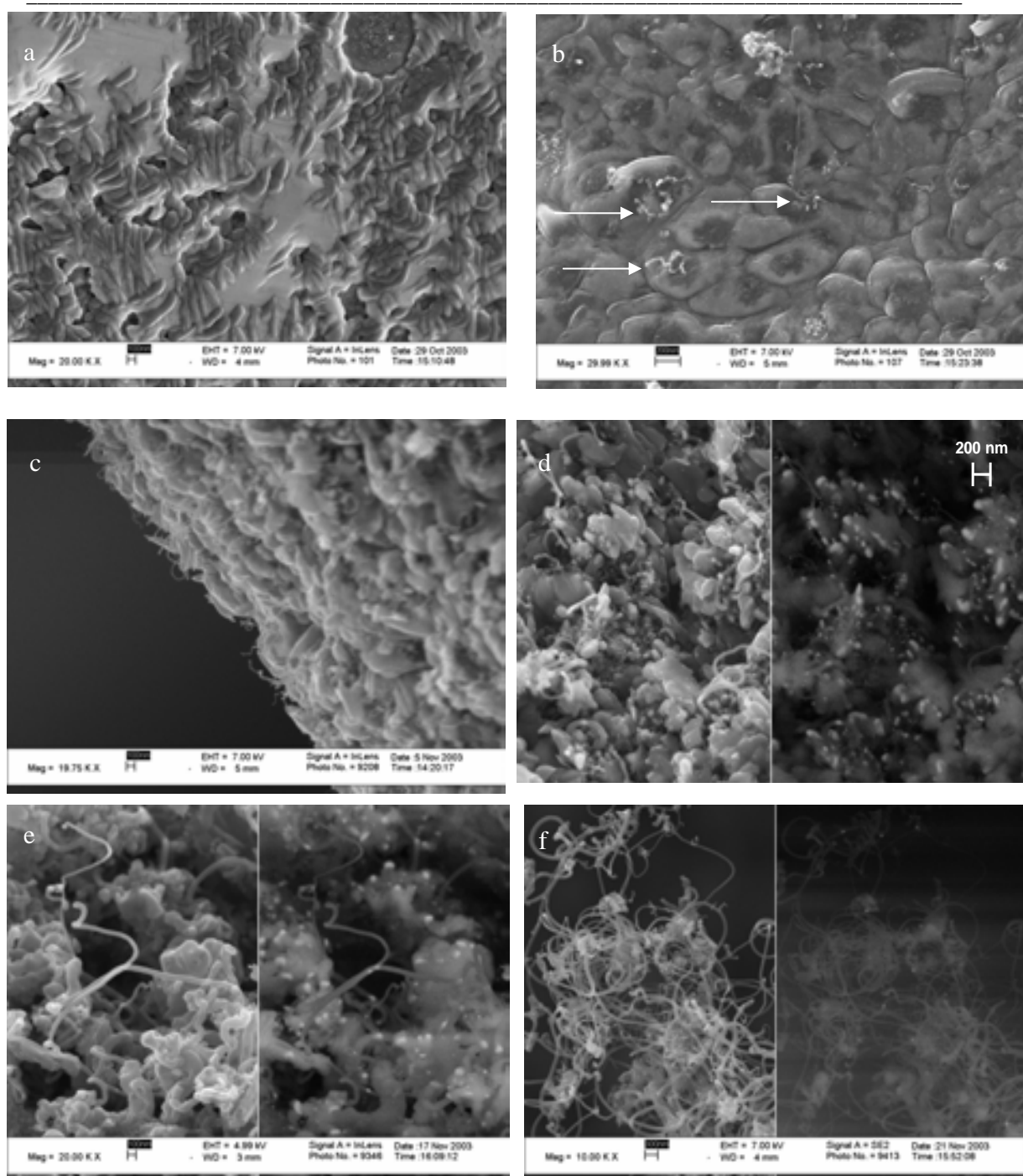


Figure 8: SEM micrographs of the surface of Ni foam after exposure to 25 % C₂H₄ in N₂ (total flow rate 107 ml/min) at 450°C for (a) 1 min, (b) 5 min, (c) 20 min, (d) 30 min, (e) 60 min, (f) 120 min. Pretreatment conditions: reduced at 700°C.

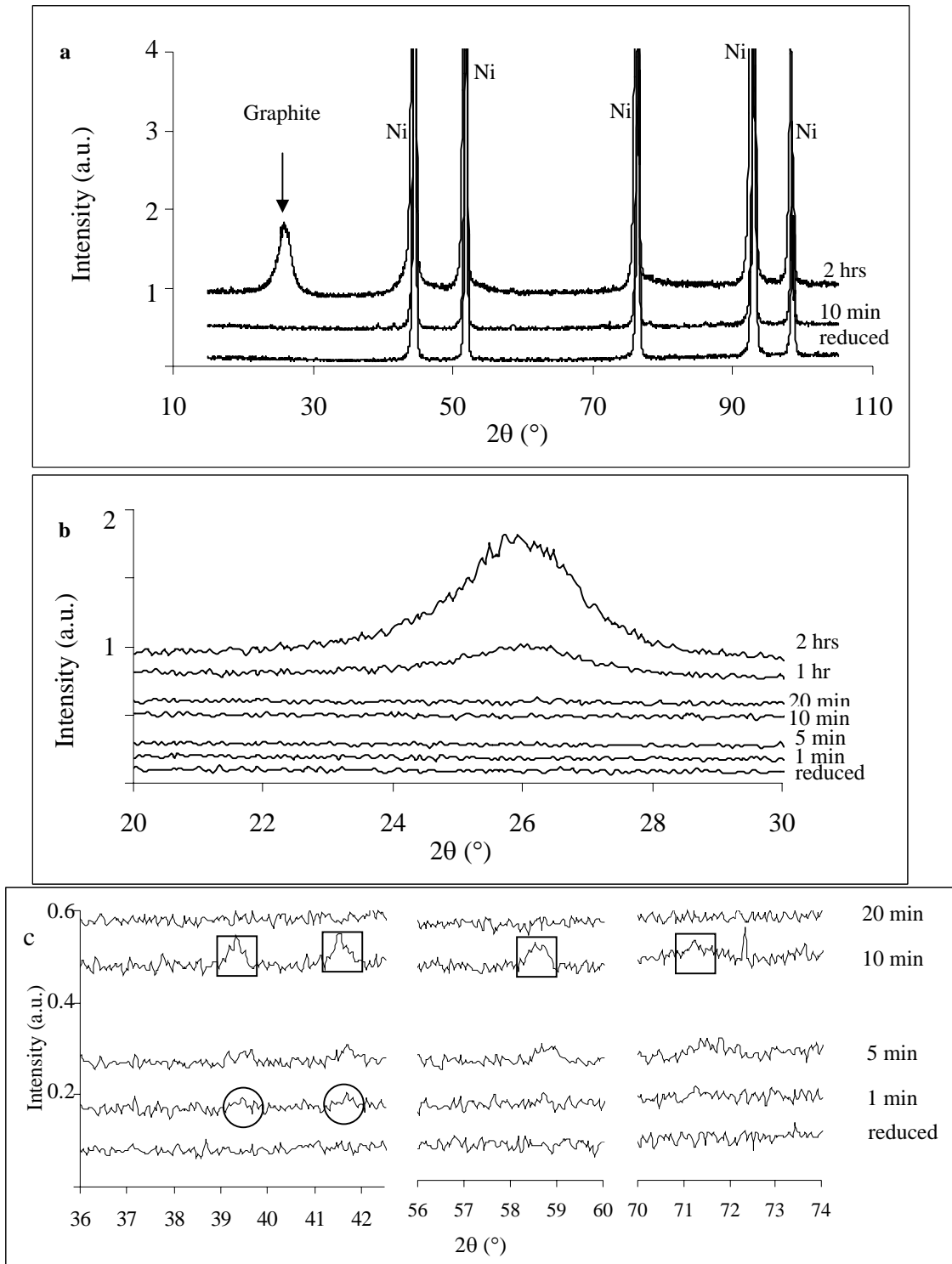


Figure 9: X-ray diffraction patterns on Ni foams after formation of CNFs after different formation time. (a) Full pattern, (b) Graphite peak and (c) Ni₃C peaks.

4. Discussion

First we will discuss the effect of the pre-treatment conditions on the morphology of the Ni surface. Then we will discuss the development of CNFs formation by following the change in the morphology of Ni with time. Finally, the effect of surface morphology of the Ni foam on the structure and the yield of the synthesized CNFs will be discussed.

4.1. Effect of the pre-treatment on the morphology of the Ni foam surface

Reduction of the Ni foam did not influence the size of Ni grains (typically 1 to 10 μm , Figure 1). However, reduction resulted in smoothening the surface of the Ni and removing most of the carbon on the surface as we discussed in Chapter 4. The carbon is probably a remainder of the polymer used to prepare the foam.

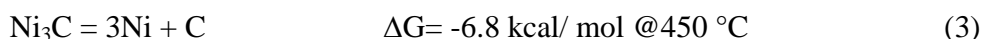
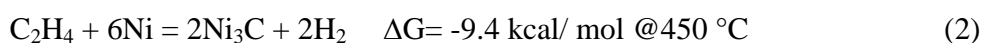
Oxidation of the Ni foam resulted in the formation of a NiO layer on the surface of the Ni foam (Figure 2). Micrograph 2a illustrates that NiO nucleates on the Ni surface, followed by crystal growth [15]. It is clear that the NiO wt% and the size of NiO crystals increased with temperature (Table 1). Obviously, the ratio between the nucleation rate and the growth rate determines the final sizes of the NiO crystals.

Similarly, reduction of a polycrystalline NiO layer proceeds *via* nucleation followed by Ni crystal growth. Again, it is obvious that the ratio between the nucleation rate and growth rate determines the final size of the Ni crystals. Reduction of the NiO formed at 700°C resulted in formation of grains, sized between 0.5 and 3 μm (Figure 4). The creation of holes filled with carbon shows that the original carbon spots (micrograph 1a) were not totally removed from the (oxid- 700°C- red- 700°C) sample.

In summary, the pre-treatments applied here resulted in three types of morphologies of the Ni foam: reduced Ni foam with grain sizes in the range between 1 and 10 μm (Figure 1), reduced Ni foam with grain sizes in the range between 0.5 and 3 μm (Figure 4) and oxidized Ni foam covered with varying amounts of NiO grains, sized in the range from 20 to 70 nm (Table 1).

4.2. Effect of time of CNFs formation on the structure of the Ni-CNFs composites

The initial morphology of the Ni foam reduced at 700°C represents a relatively smooth surface as shown in micrograph 1c. Some features in the range of 100-200 nm were formed when the Ni surface reacted with ethene at 450°C for 1 minute (micrograph 8a). The formation of Ni₃C after 1 min of reaction is indicated from the XRD results (Figure 9c). Therefore, the features formed on the Ni surface (micrograph 8a) consist of Ni₃C. Thermodynamically, the formation of CNFs can take place directly *via* reaction 1 or *via* reaction 2 followed by reaction 3. It is clear that thermodynamically Ni₃C can indeed be formed from the decomposition of ethene over Ni surface at 450°C (reaction 2) [16,17], although Ni₃C is meta-stable compared to Ni and C. Therefore, directly after the reaction, all the samples were analysed using XRD and SEM.



The amount of Ni₃C formed was maximal after 10 minutes (Figure 9c), whereas it was not detectable after 20 and 30 minutes. This agrees with the observation that the specific surface structure in micrographs 8a and 8b have disappeared and a much rougher surface morphology is observed in micrographs 8c and 8d. Both SEM results (micrographs 8a,b and c) as well as the kinetic data in Figure 5 clearly show that up to 20 minutes the formation of CNFs was very limited. Figure 8d as well as Figure 5 also show that both the fragmentation of the Ni grains and the formation of CNFs became significant after 30 minutes, thus after the decomposition of the Ni₃C.

Two factors enabled the detection of Ni₃C on polycrystalline Ni in this study, in contrast to other [18-20] studies. First, the surface area of the Ni foam was two orders of magnitude higher than the surface area of polycrystalline Ni used in literature [18-20]. The amount of Ni₃C formed increases with the surface area of the metal, as it is obvious that Ni₃C is formed on the surface of metal [20,21]. In agreement, it is generally accepted that the formation of CNFs out of pre-shaped, supported Ni nano particles is indeed preceded by the formation of Ni₃C [16,21-24]. In these studies, Ni₃C was easily detected because of the fact that the Ni surface area is very high.

Second, the time window in which Ni₃C can be observed is maximized in this work *via* minimization of the rate of CNFs formation. This was achieved by selecting a suitable pre-treatment of the foam as well as by using a low formation temperature (i.e. 450°C). Similarly, Goodman et al. [25] studied the kinetics of Ni₃C formation on Ni(100) using Auger electron spectroscopy (AES) and found that the decomposition of Ni₃C and formation of graphite started after less than 10 sec at 527°C, while it took 4 minutes to start the formation of graphite at 427°C. This is in fair agreement with our SEM results showing formation of a limited amount of CNFs after 5 minutes of reaction at 450°C (micrograph 8b). Renshaw et al. [26] and Chun et al. [27] used TEM to study the formation of CNFs on polycrystalline Ni and suggested that the observed hexagonal close-packed structures on the Ni surface were Ni₃C. Nakano et al [28] also found proof for the formation of Ni₃C using Scanning Tunneling Microscopy (STM), (AES) and Low Energy Electron Diffraction (LEED) although at much lower temperatures, between 227 and 327°C. These results are in line with our observations. The results in this study directly prove that formation of CNFs is initiated *via* the formation of Ni₃C at 450°C on polycrystalline Ni.

The formation of Ni₃C is expected to start with nucleation, followed by growth of Ni₃C crystals. These crystals decompose when the size of the crystal surpasses the window that allows the formation of CNFs. As a result, Ni particles are formed *via* the decomposition of the Ni₃C particles, thus initiating the formation of CNFs. The rate of formation increases in time (Figure 5a) because of an increasing number of active Ni nano particles. The synthesized CNFs are graphitic according to the XRD results (Figure 9b). The CNFs consist of graphite layers with an interlayer spacing similar to that of bulk graphite (i.e. 0.34 nm) [29,30], although the peak shape in Figure 6 is rather broad, which indicates that the crystallinity of the CNFs is poor [31].

In summary, we conclude that CNFs formation starts with the formation of Ni₃C *via* reaction 2, where after Ni₃C decomposes *via* reaction 3. As a result, Ni particles are created with dimensions suitable for the formation of CNFs.

4.3. Effect of surface morphology of the Ni foam on the texture of CNFs

The mean diameter of the CNFs was calculated using the BET surface area per gram CNFs (Figure 7), assuming the density of the CNFs equals the density of graphite 2.3 g/cm³ [3,32]. The mean diameter of the CNFs was 22 ± 2 nm independent on the original morphology of the Ni foam. This indicates that the mean size of the Ni fragments was

independent on the initial morphology of the Ni foam, as it is well known that the diameter of each CNF is controlled by the size of the Ni particle from which the CNF is formed [33-35]. On the other hand, SEM results show mainly CNFs with diameters between 40 and 70 nm when the foam did not collapse (micrograph 6a), while thin CNFs with a diameter of 20 nm or less were also observed, intertwining between the thick CNFs when the foam had collapsed (micrograph 6b). The fact the BET surface areas per gram CNFs were identical on all the samples implies that the CNFs layer shown in micrograph 6a must contain also thin CNFs. The observation of the thin CNFs (micrograph 7b), which cannot be observed with SEM if the foam remains intact, is evidence that thin CNFs are located deep in the CNFs layer, as we hypothesized in Chapter 4.

Huang et. al. [31] reported that only thick CNFs, between 100 and 300 nm, were formed on the surface of a Ni foam using acetylene and high temperature (550- 700°C). The fact that we synthesized thinner CNFs might be attributed to the difference in the formation conditions and different structure of the Ni foam.

4.4. Effect of surface morphology of the Ni foam on the yield of CNFs

The rate of formation of CNFs on polycrystalline Ni is determined by two factors: first, the number of Ni particles that allow CNFs formation and second, the intrinsic rate of CNFs formation for each Ni particle. The intrinsic rate of CNFs formation depends on the size of the Ni particle as well as on the formation temperature and the carbon containing gas, which were identical in this study (i.e. 450°C, C₂H₄). Moreover, the average diameter of the Ni particles formed was constant (section 4.3). Therefore the intrinsic rate of CNFs formation per Ni particle can be assumed identical on all the Ni foam samples. Thus, the difference in the observed rate of CNFs formation must be due to the number of Ni particles present, allowing CNFs formation.

Figure 5a shows that the rate of CNFs formation on polycrystalline Ni with large grain sizes (Red-700°C) is higher than the rate on the Ni with small grain sizes (Oxid-700°C-Red-700°C). Apparently, the formation rate of Ni nano particles, allowing the formation of CNFs, decreases with the increasing grain size. It is known that carbon dissolves in Ni and segregates in the grain boundaries [18]. Therefore, the carbon concentration will be relatively high in the grain boundaries, thus facilitating the formation of Ni₃C nuclei at the grain boundaries. As a result, the number of Ni nano particles formed *via* the carbide decomposition decreases with increasing grain size.

However, it is not clear why the rate of formation of CNFs decreased when the reduction temperature was increased (Figure 5a), as the size of the grains in both cases was identical. This may be because of the low carbon content of the Ni foam reduced at high temperature, according to the XPS results. It is may be possible that the carbon present originally in the foam contributed to the initiation and formation of CNFs.

Unexpectedly, the rate of formation of CNFs on the foam covered with a NiO layer, formed at 700°C (micrograph 2d) was one order of magnitude higher than the maximum rate of CNFs formation on pre-reduced Ni (micrograph 4b). In contrast, some studies indicated that metal oxides inhibit the formation of CNFs [7,8]. Apparently, ethene was able to reduce NiO under the conditions in the present work, thus initiating CNFs formation. Thermodynamically, NiO can indeed be reduced by C₂H₄ *via* reaction (4) [36].



As described before, the difference in the observed rates of CNFs formation is attributed to the difference in the number of the Ni particles present that allowing the formation of CNFs. The reduction of NiO into Ni proceeds *via* formation of Ni nuclei, which may be immediately converted in the presence of C₂H₄ to Ni₃C *via* reaction (2). The carbide crystals grow and start to decompose when the size surpasses the window that allows the formation of CNFs. We suggest that the formation of small Ni₃C particles directly from Ni nano particles, freshly formed from NiO, is much faster than the formation of Ni₃C particles from large Ni crystals, where nucleation of Ni₃C has to compete with diffusion and dilution of carbon through the Ni crystal. In agreement, Baker et al. [12] showed that the formation rate of CNFs using ethane and acetylene on FeO was one order of magnitude higher than that on Fe. The authors attributed that to the high surface area of the Fe that formed during reduction of FeO. Moreover, the likely formation of H₂O during the decomposition of C₂H₄ on NiO would shift the decomposition rate into the direction of carbon formation [37]. Unfortunately, this study could not confirm the positive effect of water, since the formation of water was not investigated.

The maximum rate of CNFs formation increases with oxidation temperature (Figure 5b) because of the increase in the NiO amount (Table 1). Obviously, the total number of Ni nuclei increases with the amount of NiO. Thus, the rate of formation of Ni₃C increased, resulting in the increase in the formation rate of CNFs. However, the rates of CNFs formation cannot be compared quantitatively because of high conversion of C₂H₄ (e.g. the conversion was 65 and 90% on the samples with 4 and 18wt% NiO, respectively).

5. Conclusions

In this study we discussed how the formation of CNFs from ethene initiates on polycrystalline Ni. The effect of the morphology and surface properties, i.e. the Ni grain size, the coverage with NiO as well as the grain size of the NiO, on the formation of CNFs was studied in detail.

The formation of CNFs on polycrystalline Ni starts with the formation of meta-stable Ni₃C, which later decomposes into Ni and C. As a result, nano Ni particles are created with dimensions suitable for CNFs formation. Therefore, the rate of formation of CNFs on polycrystalline Ni becomes significant after the decomposition of the Ni₃C, thus formatting the Ni nano particles.

The rate of formation of small Ni₃C particles from Ni nuclei, freshly produced *via* in-situ reduction of NiO, is one order of magnitude higher than the rate of Ni₃C formation from large Ni crystals, sized in microns. Therefore, the rate of CNFs formation on NiO simultaneously reduced is one order of magnitude higher than the rate on pre-reduced Ni.

References

1. N. M. Rodriguez, *J. Mater. Res.*, 8, 12, 1993.
2. R. T. Baker, P. S. Harris, R. B. Thomas and R. J. Waite, *J. Catal.*, 30, 86, 1973.
3. K. P. De Jong and J. W. Geus, *Catal. Rev.-Sci. Eng.*, 42(4), 481-510, 2000.
4. T. Ros, *Rhodium Complexes and particles on Carbon nanofibers*, PhD thesis, Utrecht, 2002.
5. F. Bonnet, F. Ropital, Y. Berthier and P. Marcus, *Materials and Corrosion*, 54(11), 870-880, 2003.
6. D. L. Trimm, *Catal. Rev.-Sci. Eng.*, 16, 155, 1977
7. C. H. Bartholomew, *Catal. Rev.-Sci. Eng.*, 24, 67, 1982
8. M. P. Manning, J. E. Garmlrlan and R. C. Reid, *Ind. Eng. Chem. Res.* 21, 404-409 (1982).
9. W. L. Holstein, *Ind. Eng. Chem. Res.*, 33, 1363-1372, 1994.
10. W. L. Holstein and M. Bodart, *Fuel*, 62, 162-166, 1982.
11. I. Wolf and H. J. Grabke, *Solid State Commun.*, 54, 5-10, 1985.
12. R. T. Baker, J. R. Alonzo, J. A. Dumesic and D. J. Yates, *J. Catal.*, 77, 74-84, 1982.
13. N. A. Jarrah, F. Li, J. G. van Ommen and L. Lefferts, *J. Mat. Chem.*, to be communicated.

14. R. Jenkins and R. L. Snyder, Introduction to X-Ray powder diffractometry, vol. 138, Wiley, New York 1996, p. 370-374.
15. M. A. Langel and M. H. Nassir, *J. Phys. Chem.*, 99, 4162-4169, 1995.
16. P. K. Bokx, A. J. Kock, E. Boellaard, W. Klop, J. W. Geus, *J. Catal.* 96, 454-467 (1985).
17. J. Rostrup-Nielsen and D. L. Trimm, *J. Catal.*, 48, 155-165, 1977.
18. A. Sacco, F. W. Geurts, G. A. Jablonski, S. Lee and R. A. Gately, *J. Catal.* 119, 322-341 (1989).
19. Z. Zeng and K. Natesan, *Chem. Mater.* 15, 872-878 (2003).
20. R. Schneider, E. Pippel, J. Woltersdorf, S. Strauß and H. Grabke, *Steel Research* 68(7), 326-332 (1997)
21. N. C. Triantafyllopoulos and S. G. Neophytides, *J. Catal.*, 217, 324-333, 2003.
22. J. Kock, P. K. Bokx, A., E. Boellaard, W. Klop, J. W. Geus, *J. Catal.* 96, 468-480 (1985).
23. M. S. Hoogenraad, Ph.D. thesis, Utrecht University (1995)
24. A. Barrier, E. B. Pereira and G. A. Martin, *Cat. Lett.*, 45, 221-226, 1997.
25. D. W. Goodman, R. D. Kelley, T. E. Madey and J. M. White, *J. Catal.* ,64, 479-481 (1980)
26. G. D. Renshaw, C. Roscoe and P. L. Walker, *J. Catal.*22, 394-410 (1971)
27. C. M. Chun, J. D. Mumford and T. A. Ramanarayanan, *Journal of The Electrochemical Society* 147(10), 3680-3686 (2000).
28. H. Nakano, J. Ogawa and J. Nakamura, *Surface Science*, 514, 256-260, 2002.
29. W. Teunissen, Tailoring of carbon fiber and carbon-coated ferromagnetic catalyst supports, Utrecht, 2000.
30. M. Endo, Y. Kim, T. Takeda, S. Hong, T. Matusita, T. Hayashi and M. Dresselhaus, *Carbon*, 39, 2003-2010, 2001.
31. W. Huang, X. Zhang, J. Tu, F. Kong, Y. Ning, J. Xu and G. van Tendeloo, *Phys. Chem. Chem. Phys.*, 4, 2002, 5325-5329.
32. R. Weast, *CRC Handbook of Chemistry and Physics*, CRC Press, Boca Raton, Florida, 64th edition, 1983.
33. N. Jarrah, J. G. van Ommen and L. Lefferts, *J. Matr. Chem.*, 14(10), 1590-1597, 2004.
34. A. Oberlin, M. Endo and T. Koyama, *J. Cryst. Growth*, 32, 335, 1976.
35. N. M. Rodriguez, A. Chambers and R. T. Baker, *Langmuir*, 11, 3862, 1995
36. Chemical Reaction and Equilibrium Software.
37. W. Qian, T. Liu, F. Wei, Z. Wang and Y. Li, *Applied catalysis A: General*, 258, 121, 2004.

Chapter 6

Formation of carbon nanofibers (CNFs) on Ni –nano particles on Si wafer

Abstract

Scanning Electron Microscopy (SEM) is used to study the catalytic formation of CNFs on Ni nano particles supported on a Si wafer using ethene. The results revealed that the formation of NiSi_x decreased the catalytic activity of the Ni for CNFs formation. Moreover, the rate of CNFs formation decreased with reduction temperature (i.e. when Ni/Si ratio decreased) in the silicide composition.

Lowering of the carbon activity via addition of H₂, resulted in complete fragmentation of the silicide particle into a large number of fragments. This indicates that the distribution of carbon in the particle plays a role in the fragmentation, since the distribution will be more homogeneous in the presence of H₂.

1. Introduction

Carbon nanofibers (CNFs) are graphite materials that can be formed *via* catalytic decomposition of hydrocarbons over small metal particles such as Ni [1]. The mechanism of CNFs formation and the properties of these materials have attracted great interest in different research areas. CNFs display unique electrical properties that have triggered the search for application in electronic devices [2]. As an example, the applications in lithium-ion batteries and in fuel-cell electrodes were studied [3]. From the point of view of catalysis, CNFs are attractive materials because these materials can form aggregates with high surface area (100-200m²/g), high pore volume (0.5-2 cm³/g) without the presence of micropores [4]. These properties are favourable for a catalyst support material because sufficient surface area is provided in combination with high porosity and low tortuosity, thus maximizing the effective diffusion coefficient. This is particularly important in the application of heterogeneous catalysts in liquid phase.

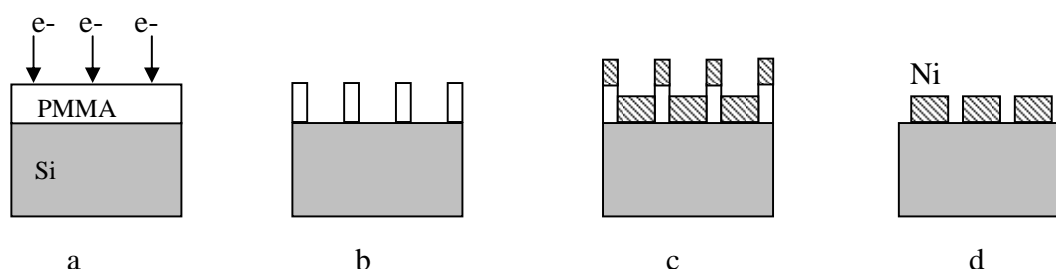
In Chapter 5, we have shown that the formation of CNFs on polycrystalline Ni started with the fragmentation of the Ni grains to Ni nano particles with dimensions suitable for the formation of CNFs. However, it was impossible to correlate the properties of individual CNFs formed to the local morphology of the Ni surface from where the CNF was formed. Obviously, it is impossible to find back a specific position on the polycrystalline Ni surface, e.g. Ni foam, with nm resolution. In this study, we have formed CNFs on well-ordered, perfectly coordinated polycrystalline Ni dots with different dimensions supported on a silicon wafer. The goal of this work is to correlate the properties of individual CNFs to the morphology of the Ni dot from which the CNF was formed. Moreover, we explored the effects of pre-treatments and formation conditions on the morphology of the Ni dots as well as the properties of the CNF formed.

2. Experimental

2.1. Materials

The substrates consisted of well-ordered Ni dots with different sizes supported on a Si wafer (provided by Delft Institute of Microelectronics and Submicron Technology). Figure 1 shows a scheme representing the preparation method of these Ni dots on the wafer. First, a mask of polymethylmethacrylate (PMMA) is deposited on the surface of a clean Si wafer (1a). The key of the process is the formation of holes with appropriate

geometry in the mask, which can be obtained using electron beams (1b). Then, Ni metal is deposited as a top layer on the mask and in the holes (1c). Finally, the mask with the nickel on top is removed using acetone. As a result, the Ni on the top of the mask is lifted off and the Ni particles on the Si wafer remain. Thus, the size of the holes in the PMMA mask determines the size of the final Ni particles (1d) [5,6].



Scheme 1: Preparation of well-ordered arrays of Ni dots on the surface of a Si wafer. (a) Preparing a mask of PMMA on the surface of the Si, (b) holes etched in the mask, (c) Ni metal deposited *via* evaporation and (d) Ni dots left after lifting-off the mask.

The thickness of the dots was 30 nm, independent on the size. The top view of the dots has a square shape. Varying the size of the hole in PMMA controlled the dimensions of the square. Specifically, the squares were sized 50, 75, 100, 125, 150, 200, and 250 nm. These dots were designated as 50, 75, 100, 125, 200 and 250 nm Ni dots, respectively. On each substrate, the nickel dots are deposited in a pattern that could be easily recognized in the microscope. Each sample contained 100 dots of each size mentioned above, arranged in a 10×10 matrix. The matrices are separated by 1 mm.

Micrograph 2a is a typical micrograph of 100 nm Ni dots. Micrograph 2b shows the surface morphology of a fresh 100 nm Ni dot, suggesting that the dot is polycrystalline independent of the size of the dot. The size of the crystallites is in the order of 15 nm, which is in the same order of magnitude as the thickness of the dot.

Hydrogen and nitrogen (99.999%, INDUGAS), and ethene (99.95%, PRAXAIR) were used for CNFs formation without further purification.

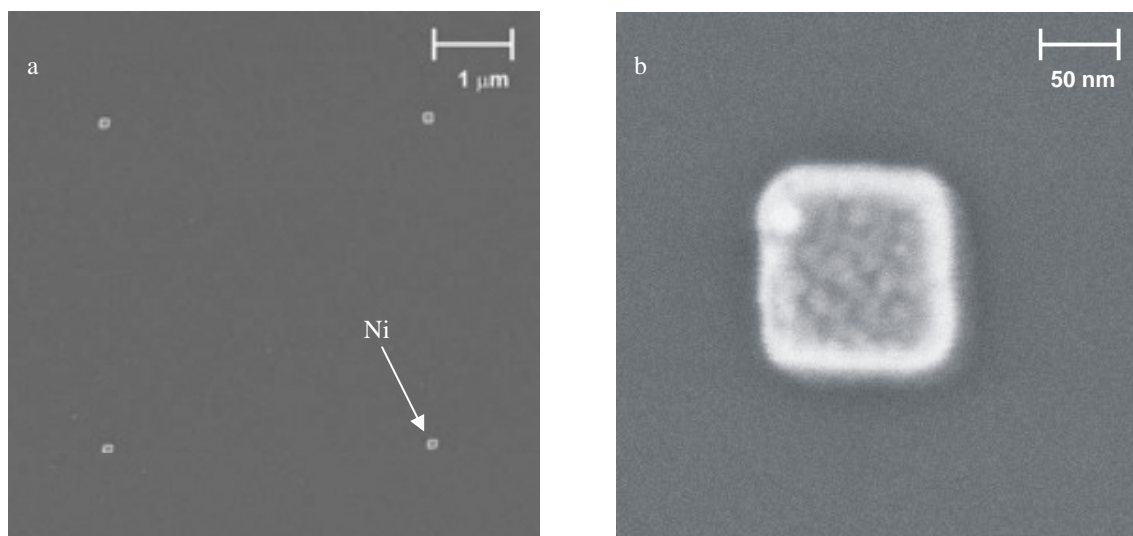


Figure 2: SEM micrograph of 100 nm Ni particles supported on silicon wafer as received. (a) low magnification and (b) high magnification.

2.2. Carbon nanofibers formation

CNFs formation was carried out in a quartz reactor with a porous quartz plate at the bottom to support the sample. The sample was reduced in 20 % H_2 in N_2 with a total flow rate of 100ml/min. The temperature was raised ($5.5^\circ C/min$) from room temperature to 500 or $700^\circ C$ (two hours dwell time), where after temperature was decreased ($5^\circ C/min$) to the desired temperature to form CNFs. CNFs were synthesized using different mixtures containing C_2H_4 , H_2 in N_2 (total flow rate 100 ml/min) at two temperatures, 500 and $550^\circ C$. The maximum conversion of ethene in all cases was well below 5%. Therefore concentration gradients in the reactor can be excluded. Then, the sample was cooled down in N_2 to room temperature. Finally, the sample was removed from the reactor and individual Ni dots were studied with Scanning Electron Microscopy (SEM) (LEO 1550 FEG SEM) equipped with EDX.

After characterization, the sample was reduced again followed by additional formation of CNFs following the same procedure as described above. Then, The change in the morphology of the individual Ni dots as a result of the repeated treatment was again studied with SEM. Table 1 provides an overview of the details of the experimental conditions.

Table 1: Experimental conditions of the CNFs formation on Ni dots on silicon wafer.

Exp. No.	Reduction temperature (°C)	Formation temperature (°C)	Gas composition
1.	500	500	10% C ₂ H ₄ -20% H ₂ -70% N ₂
2.	500	500	20% C ₂ H ₄ -80% N ₂
3.	700	500	20% C ₂ H ₄ -80% N ₂
4.	700	550	20% C ₂ H ₄ -80% N ₂

3. Results

The changes in the morphology of the dots and the structure of the CNFs formed were independent on the size of the dot. Therefore, we present here only the results on 100 nm Ni dots. Figure 3 shows the changes in the morphologies of 100 nm Ni dots and the structure of CNFs formed, resulting from different pre-treatments as well as different formation conditions.

3.1. Effect of reduction on the structure of the Ni particle

Micrographs 3a and 3b show the typical structure of a 100 nm Ni dot after reduction at 500 and 700°C, respectively. Micrograph 3b shows that the domains in the fresh Ni dot (micrograph 2b) disappeared when the dot was reduced at 700°C. The dot became less regular, but it is not clear if the domains totally disappeared after reduction at 500°C (micrograph 3a). However, it is obvious that the crystallinity of the Ni particle increases with reduction temperature.

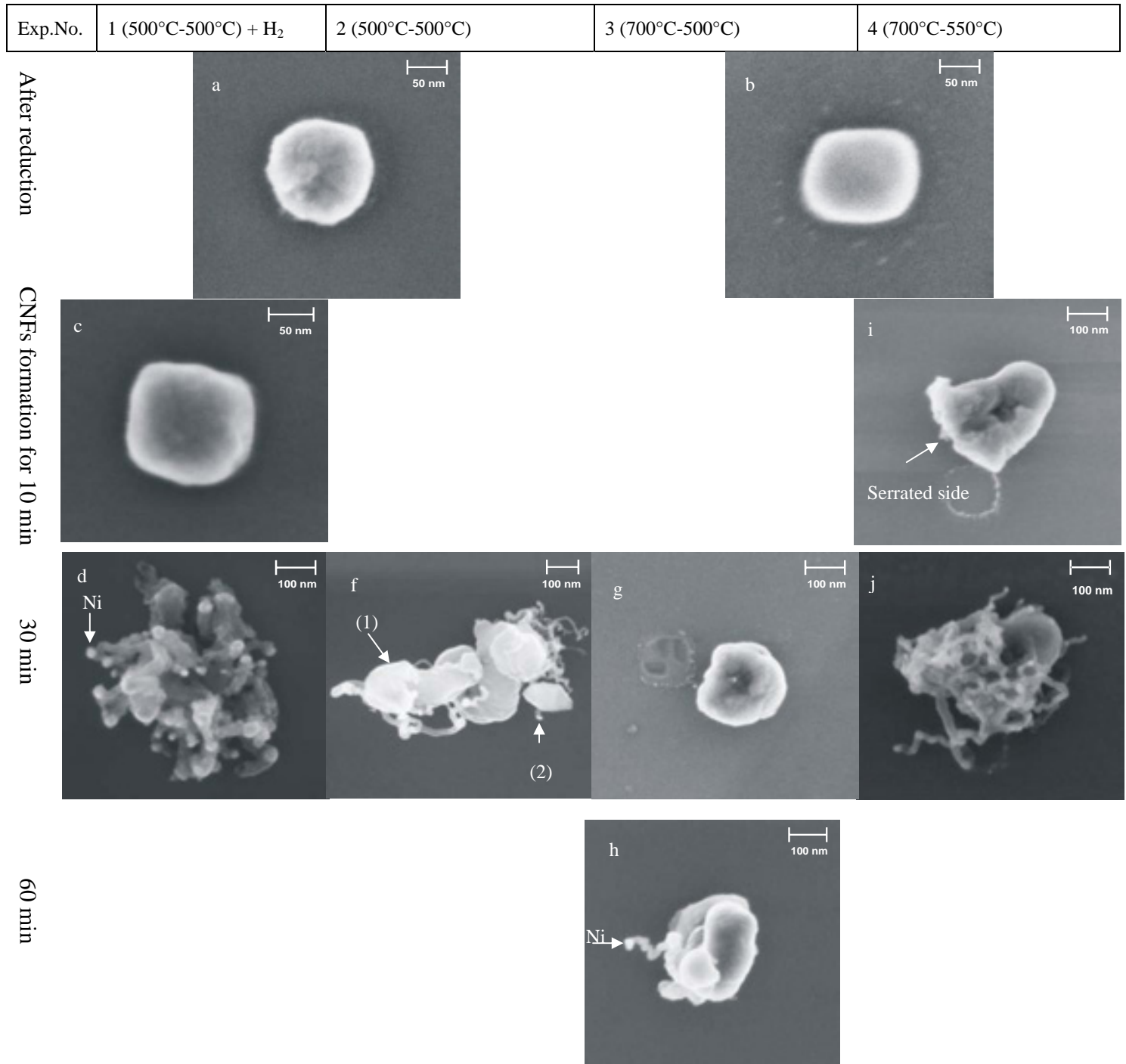


Figure 3: SEM results of CNFs formation on Ni dots supported on Si wafer

3.2. Effect of reduction temperature on the CNFs formation

Micrograph 3f shows the presence of CNFs after 30 minutes of reaction on a Ni dot reduced at 500°C. The Ni dot was fragmented into four relatively large Ni pieces (1), as identified by EDX, whereas small Ni particles (2) were found at the tip of the CNFs formed with diameters between 10 and 20 nm.

Micrographs 3g and 3h show the morphology of a Ni dot reduced at 700°C after formation of CNFs during 30 and 60 minutes, respectively. The shape of the dot became less regular and the size increased significantly to 175 nm. Furthermore, the dot seemed to have been displaced from its original position on the Si wafer, whereas neither fragmentation nor formation of CNFs is obvious after 30 minutes of reaction (micrograph 3g). However, Micrograph 3h shows that fragmentation occurred after 60 minutes of reaction, forming one CNF containing a small Ni particle in its tip, as detected with EDX.

3.3. Effect of the gas composition on the CNFs formation

Micrograph 3f shows the CNFs formed using C₂H₄ in N₂, whereas micrographs 3c and 3d show the results of the reaction when H₂ was added to the gas mixture and C₂H₄ concentration was reduced from 20% to 10%. Micrograph 3c shows that the size of the Ni dot increased to 150 nm, but neither fragmentation of the Ni particle nor formation of CNFs is obvious after 10 minutes of the reaction. However, micrograph 3d shows that the Ni particle fragmented completely to particles with sizes between 10 and 40 nm after 30 minutes of reaction. The fibers are actually shaped like worms. On the other hand, the sizes of the Ni fragments varied, as discussed in 3.2, when H₂ was absent (micrograph 3f) and the CNFs formed were relatively more crystalline.

3.4. Effect of the formation temperature on the CNFs formation

The comparison of micrographs 3g and 3h with micrographs 3i and 3j illustrates the effect of the formation temperature on the formation of CNFs. Micrograph 3i shows the Ni dot was serrated at one side after 10 minutes of reaction at 550°C. Moreover, the dot seemed to have been displaced from its original position on the Si wafer, whereas neither fragmentation nor formation of CNFs is obvious. However, micrograph 3j shows that fragmentation occurred and that CNFs formed at the serrated side after 30 minutes of the reaction. At 500°C, however the extent of CNFs formation is much less (micrographs 3g and 3h) whereas the size of the Ni particle seems to increase first, as described in 3.2.

4. Discussion

The presence of domains in the Ni particles before reduction indicates that the original dots were polycrystalline Ni (micrograph 2b). However, the disappearance of the domains during reduction indicates that the crystallinity of the particle increased probably *via* sintering (micrographs 3a and 3b).

As a rule of thumb, surface diffusion can take place at temperatures above the Huttig temperature (for Ni, 300°C) whereas bulk diffusion becomes significant at the Tamman temperature (for Ni, 590°C) [7,8]. Although one may debate whether the Huttig or Tamman temperatures are the correct numbers to use for these nano-sized particles sintering is indeed to be expected at 500°C and 700°C. Also, increased degree of sintering at 700°C as compared to 500°C is in agreement with these considerations. However, the changes in the morphology might also be due to conversion of Ni to NiSi_x, as will be discussed below.

It is known that CNFs can be formed from Ni particles with sizes between 3 and 100 nm [1,4]. Surprisingly, all Ni particles fragmented during CNFs formation and a single CNF on one particle was never observed, even the 50 nm Ni particle (not shown). Moreover, no CNFs were formed after 30 minutes of reaction at 500°C on the Ni particle reduced at 700°C (micrograph 3g). On the other hand, the rate of formation of CNFs on polycrystalline Ni with grains sized between 1 and 10µm took off after 10 minutes of reaction under identical conditions (Figure 3, Chapter 4). The relatively low formation rate of CNFs on the dots can be attributed to the formation of nickel silicide (NiSi_x), as it is known that Ni diffuses into the Si and forms NiSi_x at temperatures above 300°C [9]. Apparently, nickel silicide is less active in the formation of CNFs. Similarly, De los Arcos et al [10] have found that iron deposited on Si was less active to form CNFs compared to iron deposited on Si covered with a TiN barrier. The authors concluded that the formation of iron silicide limits the formation rate of CNFs. The effect of the silicide composition on the formation of CNFs will be discussed in the next section.

4.1. Effect of the reduction temperature on the CNFs formation

The size of the particle increased after the reaction of the particle with ethene during 10 minutes (micrographs 3c), whereas the size of the particle did not increase during reduction. Thus, the increase in the size of the particle should be due to the reaction of the particle with ethene.

In Chapter 5, we have shown that the formation of CNFs on polycrystalline Ni starts with the formation of Ni_3C . Here, NiSi_x has to be converted to Ni_3C in order to form CNFs. This conversion might be the reason for the expansion of the NiSi_x particle during the first 10 minutes of the reaction (micrograph 3c vs. micrograph 3a). However, it is not clear at this stage whether changes in the thickness of the particles have contributed to changes in the size in top view.

Both the fragmentation rate of the nickel silicide particles and the formation rate of CNFs decreased with reduction temperature (micrograph 3f vs. micrograph 3g). Zhao et. al.[11] studied the formation of nickel silicide *via* annealing of 20 nm Ni films deposited on Si substrates. The authors concluded that the Ni film was completely converted to NiSi during 30 seconds at 450°C . Thermodynamic data indeed confirmed that NiSi could be formed between 400 and 700°C [12]. However, above 700°C , NiSi starts to convert to a new phase of silicide (NiSi_2) [11]. Therefore, it is expected that NiSi is formed during reduction at 500°C , whereas at least part of the silicide formed at 700°C is NiSi_2 (Figure 4). The decrease in the Ni/Si ratio might be the reason for the decrease in the rate of CNFs formation.

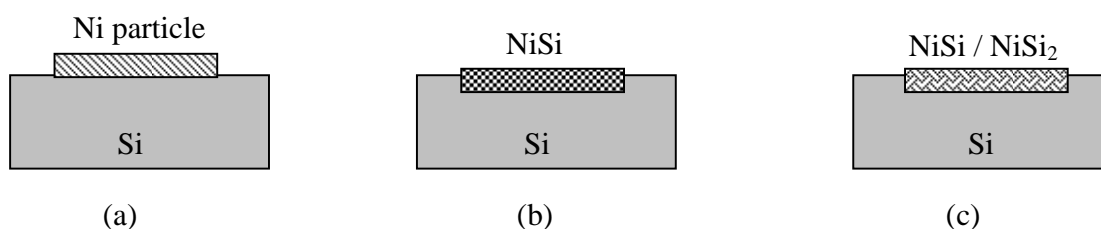


Figure 4: Scheme of formation of Ni silicide phases on a Ni particle on a Si wafer. (a) as received sample, (b) after reduction at 500°C for 2 hrs and (c) after reduction at 700°C for 2 hrs.

4.2. Effect of the conditions on the CNFs formation

Micrograph 3d shows that the number of Ni fragments is much larger at lower ethene concentration and in the presence of H_2 as compared to micrograph 3f. We conclude that lowering of the carbon activity, *via* decreasing the ethene concentration and addition of H_2 , significantly influences the balance between the rate of carbon supply to the surface of the particle *via* the decomposition of ethene and the rate of carbon diffusion into the particle.

Obviously, the concentration gradient of carbon through the particle increases with the rate of ethene decomposition. As a result, a thin layer of carbide will be formed on the surface of the particle (Figure 5a). It is obvious that carbide is formed simultaneously with the segregation of Si out of the silicide. Decomposition of the thin carbide layer results in the formation of Ni nano particles that would form thin CNFs in all directions, whereas the core of the particle remains intact. This is in agreement with the observations in micrograph 3f, although the core of the particle seems to fragmentize into a few large pieces. On the other hand, a homogenous distribution of C in the particle would result when the rate of ethene decomposition is low compared to the rate of carbon diffusion into the particle. As a result, the whole particle might be converted to carbide (Figure 5b). Therefore, the particle would fragmentize completely into small particles when the carbide decomposes (micrograph 3d).

The formation rate of CNFs increases with temperature (micrograph 3g and 3h vs. 3j), as CNFs formation is an activated process [13-15]. However, the structure of the CNFs formed did not change with temperature. On the other hand, we do not understand why the crystallinity of the CNFs decreased with lowering of the carbon activity (micrograph 3d vs. 3f).



Figure 5: Possible profiles of the carbon distribution through the particle, resulting from different gas composition. (a) 20% C₂H₄-80% N₂ and (b) 10% C₂H₄-20% H₂-70% N₂.

5. Conclusions

Scanning Electron Microscopy (SEM) is used to study the catalytic formation of CNFs on Ni nano particles supported on a Si wafer using ethene. The results revealed that the formation of NiSi_x decreased the catalytic activity of the Ni for CNFs formation. Moreover, the rate of CNFs formation decreased with reduction temperature (i.e. when Ni/Si ratio decreased) in the silicide composition.

Lowering of the carbon activity via addition of H₂, resulted in complete fragmentation of the silicide particle into a large number of fragments. This indicates that the distribution

of carbon in the particle plays a role in the fragmentation, since the distribution will be more homogeneous in the presence of H₂.

References:

1. N. M. Rodriguez, *J. Mater. Res.*, 8, 12, 3233, 1993.
2. C. Niu, E. Sichel, R. Hoch, D. Moy and H. Tennent, *Appl. Phys. Lett.*, 70, 1480, 1997.
3. G. Che, B. Lakshmi, E. Fisher and C. Martin, *Nature*, 393, 346, 1998.
4. K. P. De Jong and J. W. Geus, *Catal. Rev.-Sci. Eng.*, 42(4), 481-510, 2000
5. M. Montero, K. Liu, O. Stoll, A. Hoffmann, J. Akerman, J. Martin, J. Vicent, S. Baker, T. Russell, C. Leighton, J. Nogues and I. Schuller, *J. Phys. D: Appl. Phys.*, 35, 2002, 2398-2402
6. J. Rybczynski, U. Ebels and M. Giersig, *Colloids and surfaces A: Physicochem. Eng. Aspects*, 219, 2003, 1-6.
7. G. Ertl, H. Knozinger and J. Weitkamp, *Handbook of heterogeneous catalysis*, volume 1, Wiley-VCH, 1997.
8. R. Weast, *CRC Handbook of Chemistry and Physics*, CRC Press, Boca Raton, Florida, 64th edn., 1983.
9. M. Chhowalla, K. B. Teo, C. Ducati, N. L. Rupesinghe, G. A. Amaratunga, A. C. Ferrari, D. Roy, J. Robertson and W. I. Milne, *Journal of applied physics*, 90(10), 2001, 5308-5317.
10. T. de los Acros, F. Vonau, M. G. Garnier, V. Thommen, H.-G. Boyen, P. Oelhafen, M. Duggelin, D. Mathis and R. Guggenheim, *Applied physics letters*, 80(13), 2002, 2383-2385.
11. F. Zhao, J. Zheng, Z. Shen, T. Osipowicz, W. Gao and L. Chan, *Microelectronics Engineering*, 71, 104-111, 2004.
12. K. Tu, G. Ottaviani, U. Gosele and H. Foll, *J. Appl. Phys.*, 54(2), 758-763, 1983.
13. H. Grabke, *Materials and Corrosion*, 49, 1998, 303-308.
14. H. Grabke, *Materials at high temperatures*, 17(4), 2000, 483-487.
15. C. Chun, J. Mumford and T. Ramanarayanan, *Journal of the electrical society*, 147(10), 2000, 3680-3686.

Chapter 7

Conclusions and recommendations

1.1. The formation of CNFs on macro-structured supports

The work described in this thesis has provided information about the preparation of micro-structured materials based on carbon nano-fibers (CNFs), which were immobilized on macro-structured supports. The CNFs were catalytically produced *via* the decomposition of hydrocarbons (i.e. CH₄ and C₂H₄) over nickel. Two macro-structured materials were used as examples i.e. **ceramic monolith** and **metal foam**. From the perspective of the use of monoliths as structured materials to support catalysts, this work aims on the preparation of improved washcoats based on CNFs, competing the well known relatively dense inorganic washcoats. Metal foams are much less explored as structured catalyst supports and in this case the preparation of stable and uniform washcoats is still a challenge.

Detailed microscopic evaluation of the **monolith** revealed that at the outer surface of the washcoat a hairy layer is formed with a typical thickness of 1 μm containing CNFs exclusively. The structure of this layer is similar to the inverse structure of a traditional alumina washcoat, although much thinner. The hairy layer is supported on a composite layer containing both CNFs and fragments of the alumina washcoat. It turns out that the thickness of the CNFs layer at the outermost surface as well as the diameter of the fibers increases with mean Ni-particle size.

Formation of CNFs on the monolith using methane leads to immediate fragmentation and doubling of the thickness of the washcoat, independent on the amount of CNFs. Thus, a macro-porous composite layer of entangled alumina particles and CNFs is formed. The pore size in the washcoat was 5-20 nm, whereas the typical diameter of the CNFs was 10-30 nm. It is obvious that the formation of a CNF with a diameter larger than that of the pore would result in an immediate fragmentation of the washcoat. The total porosity decreases with the amount of CNF whereas the surface area per gram monolith increases.

Excessive formation of CNFs out of the washcoat results in detachment of the washcoat from the cordierite because a hairy layer of CNFs is formed on the interface between the washcoat and the cordierite, resembling the hairy layer on the outer surface of the

washcoat. Furthermore, extended formation of CNFs inside the cordierite body causes disintegration of the monolith body when macro-pores are locally overfilled with CNFs. Methane is preferred over ethene for the formation of CNFs because ethene forms CNFs rapidly even on relatively large Ni particles, resulting in thick fibers up to 70 nm in the macro-porous cordierite, destroying the monolith.

A rough and hairy layer of entangled CNFs was formed on the surface of the **nickel foam**. The surface area of the Ni foam increased from less than 1 m²/g to about 30 m²/g. The pore volume of the synthesized CNFs layer is 1 cm³/g. Moreover, the voids between the CNFs are macropores and thus significantly larger than the typical mesopores in conventional inorganic catalyst supports.

The formation of CNFs on polycrystalline Ni started with formation of Ni₃C, which then decomposes into Ni and carbon. As a result, a rough surface with small Ni particles (10-100 nm) is formed when the polycrystalline Ni surface was exposed to ethene at 450°C for 0.5 hour. Some of the Ni particles started to synthesize CNFs with diameters between 10 and 70 nm. The size of the Ni particles is significantly smaller than the size of the grains in the Ni foam (1-10 μm). Thus, fragmentation of the Ni grains into small Ni particles occurs before CNFs start to form.

Well-ordered, perfectly coordinated polycrystalline Ni particles with different sizes supported on silicon wafer were used to form CNFs. This study allowed us to correlate the properties of individual CNFs formed with the local morphology of the Ni surface. However, the formation of nickel silicide resulted in decreasing the formation rate of CNFs compared to the formation rate on Ni foam. We suggested that lowering of the carbon activity *via* addition of H₂ resulted in homogenous distribution of carbon in the particle. This can explain why the particle fragmented completely into smaller particles.

The formation rate of CNFs on oxidized Ni foam was one order of magnitude higher than the rate on reduced Ni foam. It is concluded that C₂H₄ was able to reduce NiO under the formation conditions forming Ni nuclei. It is suggested that these nuclei are directly converted to small Ni₃C particles, which grow and then decomposes when the size surpasses the window that allow the formation of CNFs. Obviously, the formation of small Ni₃C particles from Ni nano particles, produced by in-situ reduction of NiO will be faster than the Ni₃C formation from large (microns) Ni crystals.

The formation rate of CNFs on pre-shaped small Ni particles supported on monolith takes off with a high rate followed by deactivation exclusively. In contrast, formation rate of CNFs on polycrystalline Ni foam at constant temperature initially increased, reached a maximum value and then decreased. The initial increase in the formation rate of CNFs on polycrystalline Ni is caused by the necessity of fragmentation of Ni grains into small Ni particles.

1.2. Application of the composite materials as structured catalyst support

The integrity of the samples and strong attachment of the CNFs to the Ni foam surface or to monolith are necessary for application of the final composite materials as structured catalyst supports. The monoliths can easily disintegrate when CNFs formation is excessive, either in the cordierite or on the interface between the cordierite and the washcoat. Thus, having a high Ni concentration at the outer surface of the washcoat and no Ni in the cordierite as well as choosing a low activity of the carbon containing gas (i.e. CH₄) are essential to form CNFs without excessive formation of CNFs in the cordierite.

The integrity of the Ni foam was lost after synthesizing 138 wt% CNFs at 500°C in 3 hours. On the other hand, the foams were stable after synthesizing 50 wt% CNFs at 450°C in 6 hours. The Ni foam collapsed at high temperature because of the increase in the rate of corrosive metal dusting with temperature. As opposed to metal dusting, it seems that dissolution of small amounts of carbon from ethene dissociation in the Ni foam increases the mechanical strength of the foam. In both cases, the CNFs layer can withstand shear forces caused by flowing water (1 m/s) through the composite sample.

1.3. Catalyst preparations and future outlook

It is expected that the use of these composite materials as structured catalyst support will result in better controlling of the concentration of reactants and products at the active sites by diminishing diffusion resistance. This will allow us to optimise the concentration on all the active sites, resulting in the optimisation of the activity and selectivity as well as the size of the reactor. Moreover, it is reported that the activity and selectivity toward a product can be altered when the active phase is dispersed on CNFs compared to the performance obtained with traditional catalyst supports [1,3-5]. These studies suggested that this performance is due to the modification of the morphological properties of the active phase (e.g. electronic properties) *via* the interaction with the CNFs. Obviously, this will add to the CNFs an additional property that can be used to manipulate the activity

and selectivity in order to increase the profitability of the chemical industries (e.g. examples mentioned in Chapter 1).

On the other hand, the hydrophobicity of the CNFs is a drawback for the use of these composite materials as catalyst support [1]. Teunissen [2] and Ros [1] studied the surface structure of the CNFs and concluded that CNFs have a defect-rich graphitic surface structure. These defects lead to the presence of CH_2/CH_3 groups as well as aromatic C-H groups on the surface of the CNFs. Due to the hydrophobicity, not only anchoring of an active phase on the CNFs is difficult to achieve, but also the application of these materials in aqueous solutions is hindered because of poor wetting.

For catalyst preparation, one option would be the use of organic catalyst precursor solutions [4,6]. Figure 1 shows a typical SEM micrograph of (0.7wt%) Pd supported on CNFs-Ni composite. The size of the Pd particles (white spots) varied between 5 and 30 nm. The average size of Pd particles was 8 nm estimated using 200 particles from 10 micrographs on different locations in the sample. This demonstrates that the catalyst preparation problem, due to poor wetting, can be solved, although the loading and dispersion of Pd are rather low. The Pd catalyst (0.7wt%) was prepared by adsorption of a Pd precursor in toluene. Palladium (II) acetylacetonate (75 mg, Aldrich, 99%) was dissolved in toluene (10 ml, Merck, $\geq 99\%$) [6]. The foam was impregnated for 2 minutes in the solution and the free solution was blown out. Then, the sample was dried at 120°C under vacuum for 3 hours.

However, it is obvious that selective anchoring of the active phase on the CNFs, immobilized on the monolith support is difficult due to the high surface area of γ -alumina. A possible solution for this problem would be the preparation of Ni catalyst on α -alumina *via* co-precipitation and using that to washcoat the cordierite. Using such a washcoat would not only solve the problem of the high surface γ -alumina, but would also allow the oxidation of the CNFs as we will discuss below.

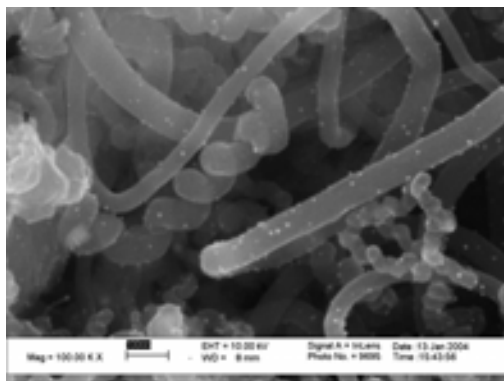


Figure 1: HRSEM micrograph of palladium catalyst supported on CNFs-Ni foam.

For the application of these catalyst supports in aqueous solutions, it is important to be able to increase the hydrophilicity of the surface of the CNFs (e.g. *via* introducing oxygen containing groups). The surface of CNFs can be oxidized with gas-phase O₂ or with liquid phase (e.g. HNO₃, HNO₃/H₂SO₄ and H₂O₂) [1]. The most effective mixture to oxidize the CNFs is HNO₃/H₂SO₄, which is impossible to be used in our materials because Ni and γ -alumina would dissolve and as a result the structure would collapse. However, CNFs could be oxidized using H₂O₂, although the oxidized CNFs with H₂O₂ shows only a weak C=O band [1].

In conclusion, the use of the composite materials synthesized, as structured catalyst support is expected to enhance the activity and selectivity in liquid phase reactions. However, the modification of the surface hydrophobicity of the CNFs is essential in the application of these materials in aqueous phase. Application in organic phase reactions might well be possible without surface modifications.

1.4. Recommendations on the preparation of these composite materials

Optimisation of the activity and the selectivity of a catalyst per unit volume of the reactor implies maximization of the surface area per unit volume and maximization of the effective diffusion coefficient. Based on the composite materials produced, the surface area of the CNFs layer can be maximized by minimizing the diameter of the CNFs as well as maximizing the number and the length of the CNFs. On the other hand, these properties would increase the concentration gradient over the active sites because the thickness of the CNFs layer is maximized and the porosity is minimized as we discussed in Chapter 1. Therefore, the diameter, length and porosity of CNFs layer should be optimised in order to optimise the properties of the composites.

Moreover, the CNFs should be attached to macro-structures with low surface area. Thus, a catalyst can be prepared *via* the deposition of the active phase on the CNFs exclusively. In **monolith**, the disadvantage of the composites formed is the high surface area of the γ -alumina washcoat. This results in the deposition of most of the active phase on the γ -alumina rather than CNFs. The solution for this problem would be maximizing the ratio between the surface area of the CNFs and the surface area of the alumina. This can be achieved by using α -alumina as the monolith washcoat as recommended above.

Another possibility in monolith composites would be immobilization of γ -alumina powders (< 1 μ m) in a macroporous network of CNFs. One possible way of making this is

synthesizing CNFs on a thin ($< 1\mu\text{m}$) γ -alumina washcoat. It is possible that the thin alumina washcoat will completely fragmentize into small particles during the formation of CNFs. These small alumina fragments will be occluded within the CNFs network, as described in Chapter 2. These alumina particles can be used, as a fixed-slurry catalyst support, which would perform better in liquid solid mass transfer than typical fixed catalyst support.

In **Ni foam**, the disadvantage of the composites synthesized is the thick layer of CNFs ($45\ \mu\text{m}$). However, decreasing the thickness of the CNFs layer would decrease the surface area of the composites. Obviously, the preferred structure would be a thin layer of CNFs with a maximized surface area. This can be achieved if only thin CNFs (less than $20\ \text{nm}$) are synthesized. As we have shown in Chapter 3, only thin CNFs were synthesized when less reactive hydrocarbon (i.e. CH_4) was used. However, the reactivity of CH_4 is too low to start the formation of CNFs from polycrystalline Ni. Therefore, a possible solution is to start the formation of CNFs using C_2H_4 in order to create Ni particles on the surface of the foam. Then, the hydrocarbon is replaced by CH_4 , which is expected to synthesize only thin CNFs from small Ni particles.

The application of the CNFs foam composite is a challenge because of the presence of the remaining Ni, especially in hydrogenation reactions. Moreover, the deposition of an active metal (e.g. Pd or Pt) exclusively on the CNFs in the foam composite is a challenge in the presence of Ni. The active metal will be reduced and deposited on the Ni surface *via* electrochemical reaction. However, the oxidation of the Ni would minimize the deposition rate of the active metal on the Ni, which might solve this problem.

The high activity of the NiO for the production of CNFs suggests that oxidized Ni foam may be an alternative catalyst for industrial scale production of CNFs. However, this would result in formation of fluffy CNFs.

References

1. T. Ros, PhD thesis, Utrecht University, 2002
2. W. Teunissen, PhD Thesis, Utrecht University, 2000.
3. M. L. Toebes, PhD Thesis, Utrecht University, 2004.
4. A. Chambers, T. Nemes, N. Rodriguez and R. Baker, *J. Phys. Chem. B*, 102, 1998, 2251-2258.

5. R. Vieira, C. Pham-Huu, N. Keller and M. J. Ledoux, *ChemComm*, 2002, 954-955.
6. J. M. Planeix, N. Coustel, B. Coq, V. Brotons, P. S. Kumbhar, R. Dutartre, P. Genesete, P. Bernier and P. M. Ajayan, *J. Am. Chem. Soc.* 116, 1994, 7935-7936.

Publications

1. Development of monolith with a carbon nanofiber washcoat as a structured catalyst support in liquid phase
N. Jarrah, J. G. van Ommen and L. Lefferts
Catal. Today 79-80, 29 (2003)
2. Growing a carbon nano-fiber layer on a monolith support; Effect of nickel loading and growth conditions
N. Jarrah, J. G. van Ommen and L. Lefferts
J. Mater. Chem. 14, 1590 (2004)
3. Immobilization of carbon nanofibers on a surface of Ni foam for use as catalyst support.
N. Jarrah, F. Li, J. G. van Ommen and L. Lefferts
J. Mater. Chem. To be communicated
4. Effect of the surface state of Ni foam on CNFs formation.
N. Jarrah, J. G. van Ommen and L. Lefferts
In preparation.

Oral Presentations in conferences

1. Growing a carbon nano-fiber layer on a monolith support; Effect of nickel loading and growth conditions
N. Jarrah, J. G. van Ommen and L. Lefferts
NIOK Symposium - the Future of the Dutch Catalyst Institute, Utrecht, The Netherlands, September 2003.
2. Development of monolith with a carbon nanofiber washcoat as a structured catalyst support **N. Jarrah**, J. G. van Ommen and L. Lefferts
4th Netherlands' Catalysis and Chemistry Conference, Noordwijkerhout, The Netherlands, March 2003.
3. Immobilization of carbon nanofibers on macrostructured support
N. Jarrah, J. G. van Ommen and L. Lefferts
228th American Chemical Society (ACS) National meeting and exposition, Philadelphia, USA, August 2004.

Acknowledgments

Looking back on the last four years during my PhD, I have met many people who in a way or another have provided help and support. First of all, I would like to thank Prof. L. Lefferts, who offered me the PhD position at the University of Twente, even though I had little experience in catalysis before coming here. Thank you, Leon, for your guidance and your eagerness to propel me towards new ideas. Leon, without your supervision and patience, it would not have been possible or would have been very difficult to finish this work. I want to thank my assistant promoter Dr. Jan G. van Ommen for his unconditional help in daily discussions.

I deem it pleasure to thank Dr. K. Seshan for his willing to discuss any difficulty any time, Dr. Barbara L. Mojet for invaluable help during reviewing some of my articles and for being smiling most of the time, Bert for technical help and translating many Dutch forms, Karin for changing the gas cylinders, Louise for XRF and some BET results, Vilmos for the BET results, Jeroen, Lianne for being the most helpful and wonderful secretary, and to Cis (the former secretary) for her kindness and help.

I owe a special thank to all my present colleges: Cristiano for being my room mate, Khalid for having the same heritage and discussing the issues in our home, Kazu for nice times we have spent during conferences, Fahong for running some experiments, Salim, Zhu, Igor, Sune, Xu, Valer, Dejan, Daryl, Patrick for the nice time during coffee breaks.

When I started this project, I received help from my former colleges, Laszlo D., who was my room mate for some time, Laszlo L. for his help in CSW and for Marco for various discussions.

I should not forget to thank the students worked with me, Olga, Anna, Chintan and Kumar.

The contribution of the promotion committee constituted probably the most feedback from the outside. I would like to thank everyone who has been part of the committee for his valuable comments.

Outside work, I would like to thank my Jordanian, Egyptian and Indonesian friends at the University of Twente for the good times we have spent together.

I would like to express my deep gratitude for my parents, sisters and brothers for their unconditional support and love. I know that you were not too happy to see me going far away to The Netherlands, so I am grateful for your patience and understanding.

And last, but the most important, there are no words that can express my feeling for my wife Wijdan and my beloved daughter Bana. Without you, your support and understanding, this work not only could not have been fulfilled properly, but it would also not make sense for me.

Resume

Nabeel Jarah was born on 12 March 1972 in Irbid, Jordan. He has completed his high school in 1990. Afterwards, he studied chemical engineering at Jordan University of Science and Technology, which he finished with distinction in 1995. Then, he started a master in the same department for two years. During that time, he was teaching assistant. The graduation project was “Investigation of thermal enhanced oil recovery of Jordanian oil using steam injection”.

In 1998, he started his work at Arab Potash Company as a chemical engineer in production department. During his work, he was assisting in solving daily problems (troubleshooting) in production, training operators, coordinating with maintenance engineer to solve equipment problems in order to maintain continuous operation, preparing report and making plans for preventive action.

From the mid of 2000, he started working as a PhD student in the catalytic processes and materials laboratory of Prof. L. Lefferts, university of Twente. His projects aims to develop structured catalyst supports with superior mass transfer properties for liquid phase application. On October 2004, he will defense his work

ISBN 903652109-2



9 789036 521093